Caveolin-3: Structural and functional insights into its role in murine airway smooth muscle constriction

Inaugural Dissertation
submitted to the
Faculty of Medicine
in partial fulfillment of the requirements
for the PhD-Degree
of the Faculty of Medicine
of the Justus Liebig University Giessen

by
Maryam Keshavarz
from
Shiraz, Iran

Giessen (2016)

From the Institute of Anatomy and Cell Biology
Cardiopulmonary Neurobiology
Head: Prof. Wolfgang Kummer
of the Faculty of Medicine of the Justus Liebig University Giessen

First Supervisor and Committee Member: Prof. Dr. Wolfgang Kummer/Prof. Dr. Gabriela Krasteva-Christ
Second Supervisor and Committee Member: Prof. Dr. Norbert Weißmann
Committee Members: Prof. Dr. Kurt Racké and Prof. Dr. Klaus-Dieter Schlüter

Date of Doctoral Defense: 22.12.2016

To my family

تقدیم به خانواده ام

Table of Contents

List of abbreviations

AR	Adrenergic receptor
α-SMA	α-Smooth muscle actin
5-HT	5-Hydroxytryptamine, serotonin
Ab	Antibody
ACh	Acetylcholine
APS	Ammonium persulfate
ASM	Airway smooth muscle
BHR	Bronchial hyperresponsiveness
bp	Base pair
BSA	Bovine serum albumin
cAMP	Cyclic adenosine monophosphate
Cav	Caveolin
Cav-1	Caveolin-1
Cav-2	Caveolin-2
Cav-3	Caveolin-3
cDNA	Complementary DNA
COPD	Chronic obstructive pulmonary disease
Δ	Delta
DAG	Diacylglycerol
DMEM	Dulbecco's Modified Eagle's Medium
DNA	Deoxyribonucleic acid
DNase	Deoxyribonuclease
dNTPs	Desoxyribonucleosidtriphosphate
DR	Disordered regions
DTT	Dithiolthreitol
EDTA	Ethylene diamine tetra acetic acid
EHDs	Eps15 homology domain-containing protein family
eNOS	Endothelial nitric oxide synthase
ERK	Extracellular signal-regulated kinases
ESC	Embryonic stem cell
FCS	Fetal calf serum
FITC	Fluorescein isothiocyanate
GPCR	G-protein-coupled receptors
HEPES	4-(2-hydroxyethyl)-1-piperazineethanesulfonic acid
HR	Helical region
Ig	Immunoglobulin
IHC	Immunohistochemistry
Ins(1,4,5)P3	Inositol-1,4,5-triphosphate
kDa	Kilodalton
KO	Knock-out
MAPK	Mitogen-activated protein kinase
MCD	Methyl-β-cyclodextrin
MR	Muscarinic receptors
MURC	Muscle-restricted coiled-coil protein (cavin-4)
nNOS	Nitric oxide synthase isoform
ns	Not significant

PBS	Phosphate-buffered saline
PCR	Polymerase chain reaction
PKC	Protein kinase C
PLC	Phospholipase C
PFA	Paraformaldehyde
PP	Phosphate buffer
PTRF	Polymerase transcript release factor (cavin-1)
PVDF	Polyvinylidine difluoride
RNA	Ribonucleic acid
RNase	Ribonuclease
ROCK	Rho-associated kinase
RT	Reverse transcriptase
RT-PCR	Reverse transcription polymerase chain reaction
SD	Standard deviation
SDHA	Succinate dehydrogenase A
SDPR	Serum deprivation protein response (cavin-2)
SDS	Sodium-dodecyl-sulfate
SEM	Standard error of the mean
SM	Smooth muscle
SMC	Smooth muscle cells
SPF	Specific pathogen free
SRBC	Srd-related gene product that binds to c-kinase (cavin-3)
TAE	Tris acetate EDTA buffer
TBS	TRIS-buffered saline
TE	Tris-EDTA
TEMED	N,N,N´,N´-Tetramethylethylemediamine
Tris	Tris(hydroxymethyl)-amino-methane
Vol	Volume
WT	Wild type

1 Introduction

1.1 Lipid raft

Lipid rafts organize the plasma membrane into specialized microdomains which act as platforms for the conduction of different cell functions including vesicular trafficking and signal transduction [1]. Classic lipid rafts are enriched in cholesterol, glycosphingolipid and raft markers such as flotillin (Fig. 1.1A-B) [2, 3].

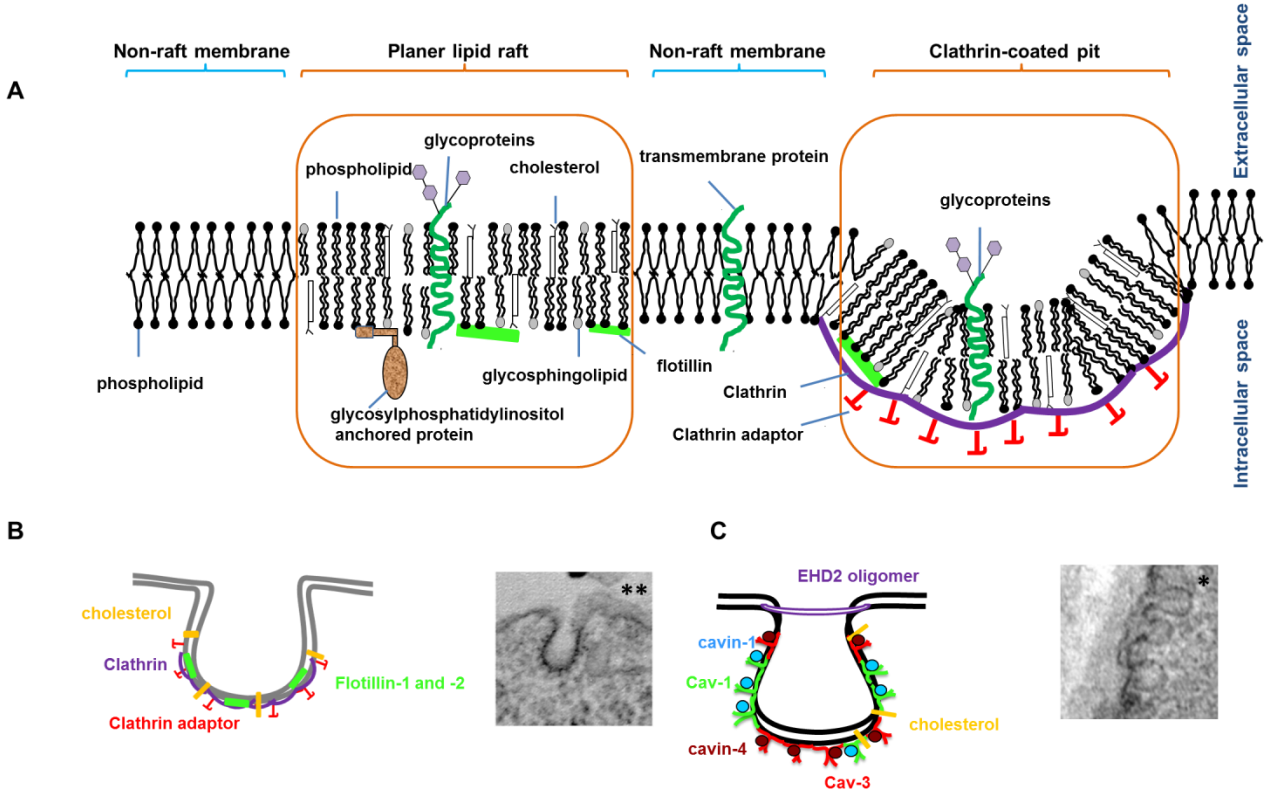

Fig. 1.1 Lipid raft microdomains can be classified by the ultrastructure of the membrane intermediates. (A) Clathrin-coated pit as vesicular lipid raft and planar lipid raft, (B) clathrin-coated pit and (C) caveolae structures. The electron micrographs shown is own unpublished image from tracheal muscle of Cav-3$^{-/-}$ mice (*) or from the COS-1 cell line [4] with permission (**). Cav-1, caveolin-1; Cav-3, caveolin-3.

1.2 Caveolae

1.2.1 Structural and functional role

Caveolae are flask-shaped invaginations of the plasma membrane (50-100 nm in diameter) with a high content of cholesterol and glycosphingolipids; they can be viewed as a subset of lipid rafts (Fig. 1.2). Caveolae are distinguished from other lipid rafts by the presence of caveolins as structural proteins that appear to be responsible for stabilizing the caveolae

structure (Fig. 1.1B) [2, 5-7]. There is a remarkable variation in caveolar density in different tissues [8]. Each caveolae consists of 140-150 caveolin molecules [9]. Caveolae are anchored to the plasma membrane via the cytoskeleton and are abundant in mature smooth muscle cells (SMC) [10, 11]. Caveolae concentrate numerous structural proteins, ion channels, G-protein-coupled receptors (GPCR) and receptor kinases and play a key role in pathways associated with cell proliferation, calcium homeostasis, migration, mechanosensing, cholinergic signaling via muscarinic receptors (MR) and airway smooth muscle cell (ASM) constriction [11-19]. The importance of caveolae is highlighted by links between their dysfunction and human diseases including lipodystrophy, muscular dystrophies, cardiac disease, infection, osteoporosis and cancer [8, 20, 21].

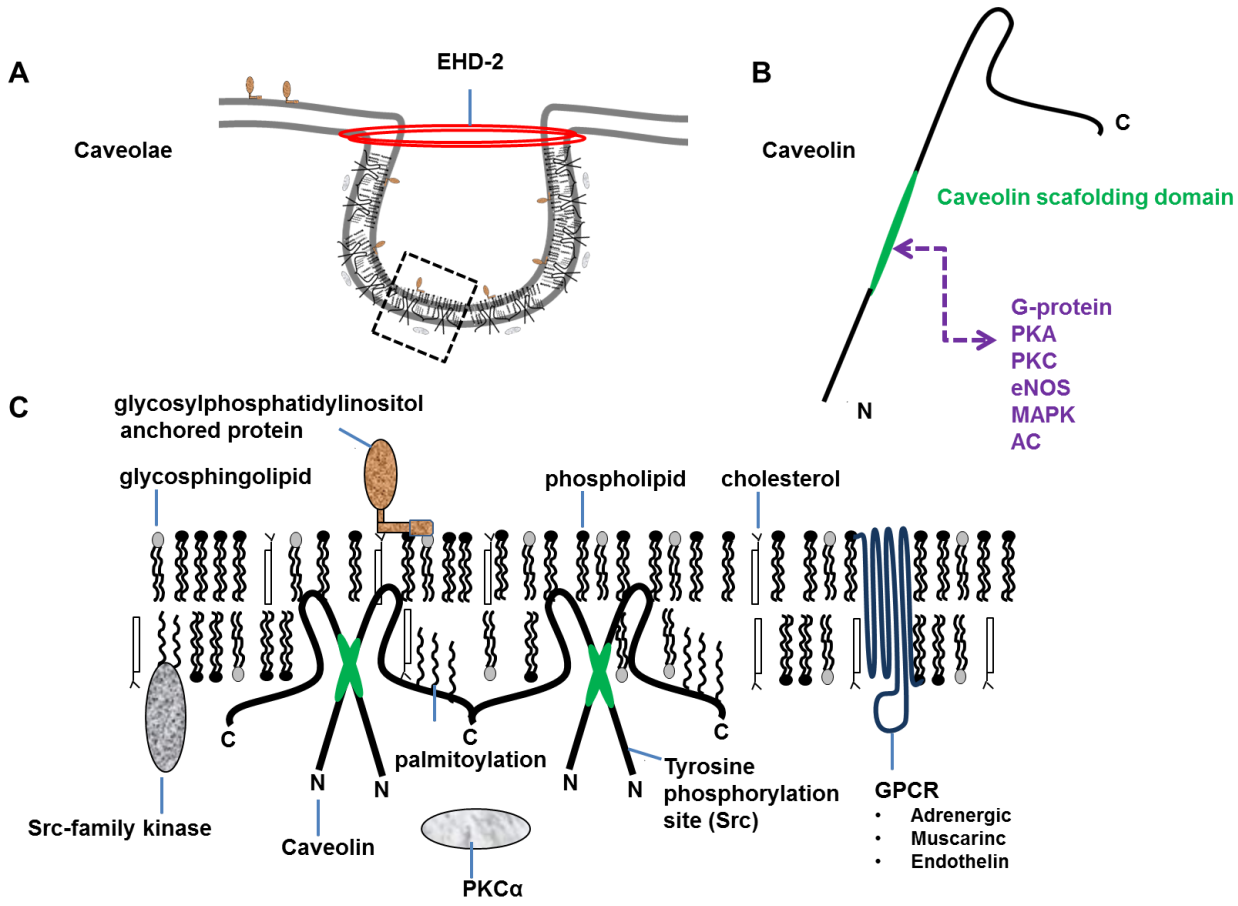

Fig. 1.2 Caveolae are specialized lipid rafts enriched in cholesterol and sphingolipids, characterised by the presence of caveolins. (A) A structural cartoon of a caveola depicting the organisation of caveolins, signaling and EHD-2 proteins. (B) Caveolin protein structure showing the amino-terminus, carboxy-terminus and scaffolding domain which interact with cholesterol and signaling molecules. (C) Selected area of a caveolae structure indicated by the boxed area in (A) that presents the association of the caveolin oligomer, the lipid bilayer, glycosphingolipids, phospholipid, cholesterol and signaling molecules. AC, adenylyl cyclase; C, protein carboxy-terminus; eNOS, endothelial nitric oxide synthase; GPCR, G-protein coupled receptor; MAPK, mitogen-activated protein kinase; N, protein amino-terminus; PKA, protein kinase A; PKC, protein kinase C.

1.2.2 Caveolins

1.2.2.1 Caveolin structure

Caveolins (Cav-1, -2, and -3) are acylated 22-24 kDa proteins embedded in the cytosolic leaflet of cell membranes with both amino (N-) and carboxyl (C-) termini residing in the cytosol (Fig. 1.2) [22, 23]. Cav interact with themselves to oligomerize (~14-16 Cav monomers per oligomer) and can bind to additional proteins via the caveolin scaffolding domain (residues 82 to 101 in Cav-1) or carboxyl tail (Fig. 1.2) [3, 24, 25]. Cav-1 and Cav-3 are essential for caveolae formation and serve as binding partners for receptors and enzymes [14]. Some cell types including smooth muscle and cardiomyocytes express all types of caveolins [26-28]. Caveolin levels show dramatic differences from tissue to tissue [8].

1.2.2.2 Cav-1

Cav-1 is widely expressed in type I pneumocytes, endothelial cells, adipocytes, fibroblasts and SMC [14, 29]. Cav-1 and Cav-2 are generally expressed together [14].

Cav-1 has emerged as a critical regulator of signaling pathways involved in lung fibrosis, inflammation, NO production by endothelial nitric oxide synthase (eNOS), microvascular permeability, Ca^{2+} entry into endothelial cells, vascular remodeling and angiogenesis [24, 30-34].

1.2.2.3 Cav-3

Cav-3 is expressed highly in striated muscle cells (skeletal and cardiac muscle) and certain SMC and is critical for caveolae formation in the same manner as Cav-1 elsewhere [29, 35, 36]. Cav-3 is 60% homologous to Cav-1 with the major differences occurring in the N-terminal portion of the protein. Cav-3 expression is detectable at embryonic day 10 in a mouse heart, and it has been shown to associate with the developing T-tubule system in skeletal myoblasts [37, 38]. Cav-3 expression and caveolae formation are required to generate a highly organized/fully mature T-tubule system in vivo [3]. In prior studies, we have shown that both Cav-1 and Cav-3 are present and interact in murine ASM [16]. Cav-1/Cav-3 hetero-oligomeric complexes were also observed in rat and mouse myocytes from mice overexpressing Cav-1 [39, 40]. Furthermore, Cav-3 regulates the switch from synthetic to contractile phenotype in vascular SMC [41].

Cav-3 has been shown to interact with a variety of signaling molecules including Gi2α, Gβγ, c-Src, and Src-like kinases in C2C12 cells, suggesting a role for Cav-3 in the transduction events mediated by these molecules [29]. Cav-3 has also been reported to directly interact

with the neuronal nitric oxide synthase isoform (nNOS) expressed in skeletal muscle and causes the inhibition of nNOS enzymatic activity [35, 36]. Cav-3 is a negative regulator of p42/44 MAPK, and loss of Cav-3 expression is sufficient to induce cardiomyopathy [24].

1.2.2.4 Cav deficiency

Phenotypes of caveolin knockout mice (Cav KO) include metabolic disorders associated with adipose tissue abnormalities, airway hyperresponsiveness, urogenital alterations, deregulation of the eNOS signaling pathway, pulmonary hypercellularity, cardiac disease, altered susceptibility to tumorigenesis and skeletal muscle myopathy [42, 43]. Specific phenotypes were described in Cav KO animals reflecting the importance of Cav expression in particular tissues. Surprisingly, all transgenic animals were viable and fertile despite a loss of muscle-caveolae in Cav-3 KO animals or non-muscle-caveolae in the absence of Cav-1 [42].

Most of the abnormalities observed in Cav-1 KO are localized within the lungs, adipose tissue, and vascular compartment [14]. Interestingly, an immunohistochemical analysis of endobronchial biopsies of asthmatic patients revealed a remarkable loss of Cav-1 compared to the control group [44]. The major vascular, cardiac, and pulmonary phenotypes in Cav-1 KO are largely caused by the loss of caveolae in the endothelium of these organs, supporting the concept that endothelial Cav-1 can regulate remodeling of cardiac and pulmonary tissues [32].

Cav-3 deficiency, in line with its muscle-specific expression, leads to skeletal muscle pathology and cardiomyopathy through multiple pathogenic mechanisms in mice [3, 45]. Interestingly, skeletal muscle fibers from Cav-3 KO mice show a number of myopathic changes, consistent with a mild-to-moderate muscular dystrophy phenotype [46]. Similar to Cav-1 KO mice, the p42/44 MAP kinase cascade is hyperactivated in the hearts of Cav-3 KO mice and may partly account for cardiac defects [46]. In case of a heart failure, there is an extensive remodeling of the T-tubule network and this change may contribute to abnormal calcium handling [47]. Furthermore, a mutation in Cav-3 has been found in familial hypertrophic cardiomyopathy [48] and the skeletal muscles of patients with limb girdle muscular dystrophy [49]. These effects can be due to a dominant-negative effect of the mutated Cav-3 and its retention in the Golgi apparatus, disorganization of skeletal muscle T-tubule network or disruption of distinct cell-signaling pathways.

The genetic loss of both Cav-1 and Cav-3 results in severe cardiomyopathy and a dramatic increase in the left ventricular wall thickness. These effects can be due to the alteration of caveolin levels as a negative regulator of proliferation, hypertrophy, or remodeling by

modulating signal transduction (such as β-adrenergic signaling, NO, and the MAPK cascade), or by structural disarrangement of the T-tubule system or impaired calcium homeostasis [50-52].

1.2.3 EHD

Proteins within the Eps15 homology domain-containing protein family (EHDs) have been shown to participate in the remodeling of membranes in the endosomal system [53]. The mammalian genome encodes four EHDs, EHD1-4 [53]. EHD-2 oligomers (ATPase) as ring structures are bound and localized to the caveolae neck to stabilize and control the dynamics of such invaginations at the cell surface [53, 54]. Intriguingly, EHD-2 is not required for the caveolae formation but acts as a negative regulator of endocytosis and its depletion results in an increased caveolin mobility and caveolae budding [55, 56]. The expression of EHD-2 is also reduced In Cav-$1^{-/-}$ and cavin-$1^{-/-}$ mice, thereby providing direct evidence for its link to the caveolar abundance and function [57].

1.2.4 Cavin

Over the past few years, a new family of cytoplasmic proteins, termed cavins, has also been shown to have the potential to dynamically transmit signals from caveolae to various cellular destinations [8]. The cavin family includes cavin-1 to -4 and stabilizes the mature classical flask-shaped caveolae (Fig. 1.3) [58]. All cavins share conserved α-helical secondary structure elements within two clearly delineated regions called helical region (HR) which are separated by three disordered regions as proteolytic and phosphorylation sites (DR) (Fig. 1.3). Cavins possess the ability to associate into higher ordered homo- and hetero-oligomers [59]. Additionally, all of the cavins through their N-terminal domains can bind phosphatidylserine which is abundant on the cytoplasmic face of the plasma membrane, particularly in areas that are rich in caveolae [60, 61]. The ratio of cavin-1 to Cav-1 was estimated to be 1 to 4 and is independent of other cavins [59].

Cavin-1 (synonym: PTRF, polymerase I and transcript release factor) acts as a nuclear protein [62]. Cavin-2 (synonym: SDPR, serum deprivation response protein) and cavin-3 (synonym: SRBC, srd-related gene product that binds to c-kinase) are identified as protein kinase C (PKC) substrates and have been suggested to target PKC to caveolae [63, 64]. Cavin-4 (synonym: MURC, muscle-restricted coiled-coil protein) is predominantly expressed in cardiac and skeletal muscle and links to myogenesis and muscle hypertrophy via the Rho-associated kinase (ROCK), ERK1 and ERK2 [65-67].

The change in the recruitment of cavins to caveolins might change the architecture of caveolae and contributes to the disassembly of the entire structure. The high cholesterol content of the caveolar domain is also crucial for the Cav-cavin integrity [68, 69] and dissociation of Cav-1-cavin-1 flattens the caveolar structure [70]. The fact that cavins show tissue-specific expression profiles implies that the cavin proteins could generate differences between caveolae in diverse tissues or cell types [57, 58].

Cavin-1 is required for the formation of caveolae, and the absence of cavin-1 in both cultured cells and animal systems causes a loss of caveolae [68, 71]. Early studies showed that cavin-1 co-localizes with Cav-1 in adipose tissues and cavin-1 over-expression increases the Cav-1 level and its knockdown reduces the Cav-1 level [71, 72]. Importantly, the tissue distribution of cavin-1 is broader than that of Cav-1 and is dominant in both muscle and non-muscle tissues [73]. It is not surprising that the phenotypes of cavin-1 KO mice are similar to those of Cav-1/Cav-3 double knockouts [49, 71, 74-77]. Indeed, the absence of cavin-1 leads to a suppressed protein expression of all three caveolin isoforms [73].

Cavin-2 has been linked to determining the size or stability of cavin complexes for caveolae generation in lung and fat endothelia, as the deletion of cavin-2 actually increases the apparent size of cavin complexes and reduces the depth of caveolae in lung endothelium [57]. Cavin-3 does not appear to be needed for generating endothelial caveolae but has the properties to link caveolae to signal transduction pathways [57, 78]. Cavin-4 was shown to be associated with muscle biogenesis [66] and its knocking down or over-expression has been shown to impair or improve the differentiation of mouse C2C12 myoblasts through decreased or increased ERK1/2 activation in the differentiation stages [79]. Cavin-4 expression is perturbed in human muscle diseases associated with a Cav-3 dysfunction [21].

Most clinical features of cavin mutated patients are then likely to be explained by the secondary reduction of a caveolae and/or caveolin deficiency. For example, the missense mutations of cavin-1 are associated with deficiency and mislocalization of all three caveolin family members [21]. It seems that cavin-1 mutation affects its interaction with Cav-3 and reduces the caveolae structures in skeletal muscle biopsies [21]. Both Cav-3 and cavin-4 mutations have been linked to dysregulation of hypertrophy and hypertrophic signaling pathways in cardiac and skeletal muscle [8]. Mutations in human Cav-3 or cavin-1 result in human cardiomyopathies such as the long-QT syndrome [20, 80].

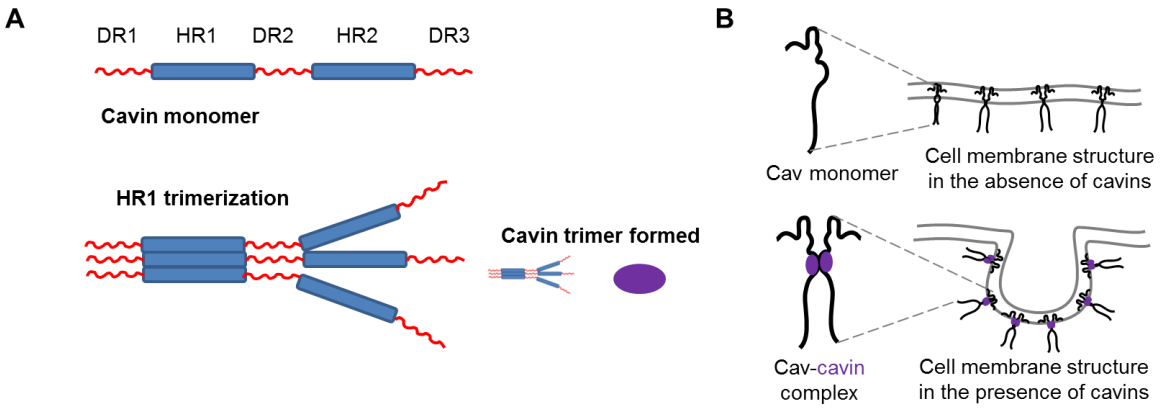

Fig. 1.3 Caveolin and cavin complex. (A) Cavin structure. (B) Caveolin oligomers embed in the cell membrane but do not form caveolae structure. The presence of cavin allows caveolins to form a caveolae structure. Cav, caveolin; DR, disordered regions; HR, helical region.

1.3 Regulation of airway smooth muscle tone

1.3.1 Structure of the airway tree

The respiratory system is composed of a tree-like structure of branched tubes that carry air to and from the alveoli. This basic design is conserved among vertebrates, but there are important differences between mouse and human airways due to the very large differences in body size. Transgenic mouse models are very largely used for studying the respiratory function, and the trachea, being the largest airway, is equivalent to the diameter of the small peripheral airways in the human lung. In mice, cartilage rings are only present in the extrapulmonary airways, but cartilage extends for several bronchial generations into the human lung. Since the cartilage amount differs along the airway tree, we expected that the SM constriction would also differ because of differences in the stiffness of the airway wall. Submucosal glands which produce mucins and other factors are restricted to the proximal trachea in the mouse but reach deep into the human lung [81]. Striking interspecies differences are also found with respect to the cellular composition and receptors in the airways [81]. The cellular composition and organization of the mouse trachea is much more similar to human small airways, whereas the mouse intrapulmonary airway resembles only the most distal portions of the human conducting airways [81]. From this, we conceive that it is important to know the agonist-induced airway SM constriction of different parts of the murine airways. Here we show that all compartments of the airway (extra- and intrapulmonary) have different impact on their response to contractile stimuli such as muscarine and serotonin (synonym: 5-HT, 5-Hydroxytryptamine).

1.3.2 G-protein-coupled receptors

GPCR, also known as seven-transmembrane domain receptors, constitute the largest superfamily of cell-surface receptors [82]. Several GPCR are not randomly distributed along the cell surface but aggregate at caveolae structures [14]. Members of this GPCR family include for example 5-HT, β2-adrenergic receptor (β2-AR) and MR [82]. Despite their diversity, all GPCR mediate their effects at least in part through coupling to heterotrimeric G-proteins comprising α-, β- and γ-subunits. The α-subunit is responsible for GTP and GDP binding and GTP hydrolysis, whereas the β- and γ-subunits are associated in a tightly linked complex as βγ-dimer. The activated heterotrimer dissociates into an α-subunit and a βγ-dimer, both of which have an independent capacity to regulate separate effectors (Tab. 1.1) [83]. Upon agonist activation of receptors, a rapid attenuation of receptor responsiveness occurs through feedback mechanisms, which involve phosphorylation of activated GPCR by kinases and/or second messenger dependent kinases [82].

G-protein subunit	function
$G\alpha_s$	↑ Adenyl cyclase, increase in cAMP level
$G\alpha_i$	↓ Adenyl cyclase, decrease in cAMP level
$G\alpha_q$, $G\alpha_{11}$	↑ Phospholipase C, increase in Ins(1,4,5)P_3 and DAG levels
$G\alpha_{12}$, $G\alpha_{13}$	↑ Rho-GEF, ↑ Rho, induction of stress-fiber formation
$G_{\beta\gamma}$	↑ Adenyl cyclase, ↑ Phospholipase C, increase in cAMP and Ins(1,4,5)P3 levels

Tab. 1.1 Examples of heterotrimeric G-protein mediated effector functions based on Ref. [83]. Receptors are classified by operational, structural and transductional criteria. ↑ Denotes increase, ↓ decrease in cellular levels of second messenger. cAMP, cyclic adenosine monophosphate; Ins(1,4,5)P_3, inositol-1,4,5-triphosphate; DAG, diacylglycerol; GEF, guanine nucleotide exchange factor.

1.3.2.1 Muscarinic receptors

Release of acetylcholine (ACh) from parasympathetic nerve fibers causes ASM constriction by acting through MR [84]. Five molecularly distinct MR subtypes (M1R-M5R) are known (Tab 1.2). We previously identified M2R and M3R as being essential for murine ACh-induced constriction in bronchial SMC [85]. Within the SM, the highest MR density is in the lower trachea, while the upper trachea and bronchi contain significantly less receptors [86, 87]. In most animal species, there are many more M2R than M3R in the conducting airways. Depending on the species, 50 to 80% of the receptors can be M2R [88]. With quantitative receptor binding analysis, Ikeda and coworkers reported a significantly higher density of M3R

than M2R in human bronchi at different levels [89]. Functional studies indicate that the M3R mediates ASM contraction in animals [88] and in humans [90], like in ileal, uterine, and bladder SM [91]. The M3R is thought to be coupled primarily via $G\alpha_q$ to phospholipase C (PLC) signaling pathways and calcium release mechanisms that support SM contraction. Activation of PLC catalyzes the formation of inositol triphosphate and diacylglycerol from the membrane phospholipid phosphatidylinositol 4,5-bisphosphate, and coupling of M3R to inositol triphosphate has been demonstrated in all studied species including in human bronchial SM [92, 93]. The M2R couples to $G\alpha_i$, thereby inhibiting adenylate cyclase, activating nonselective cation channels, and sensitizing the contractile system to calcium [94, 95]. It seems that M2R do not play a direct role in SM contraction, but inhibit SM relaxation through inhibition of adenylyl cyclase (Fig. 1.4) [96, 97]. Furthermore, we previously observed a considerable decrease, but not a complete loss of the muscarine-induced bronchoconstriction response of $M3R^{-/-}$ mice compared with wild-type mice in precision cut lung slice (PCLS). In addition, we used $M2R^{-/-}$ mice to test the contribution of M2R to cholinergic constriction of peripheral airways. Interestingly, $M2R^{-/-}$ bronchi showed similar muscarine-induced bronchoconstriction compared with wild-type bronchi. Strikingly, muscarine-mediated bronchoconstriction was completely abolished in PCLS preparations from $M2/3R^{-/-}$ mice [85].

These results together with earlier findings confirmed that the remaining cholinergic bronchoconstriction in $M3R^{-/-}$ mice was mediated by the M2R [16, 85]. Likewise, in the murine tracheal SM, M3R and M2R importantly contributed to the muscarinic induced contraction [98, 99].

MR subtypes are functionally coupled to Cav-isoforms in the heart, urinary bladder SM and tracheal SM [18, 100, 101]. We previously observed a decrease in the response to muscarine in PCLS after disruption of caveolae with the cholesterol depleting agent, methyl-β-cyclodextrin (MCD), pointing to an association of either Cav-1 or Cav-3 with airway MR [16]. Moreover, disruption of caveolae or knockdown of Cav-1 reduced the MR-mediated calcium mobilization in airway SMC [18]. Cav-1 was found to be co-localized with M3R as intracellular Ca^{2+} regulatory protein, and the downregulation of Cav-1 expression considerably decreased the Ca^{2+} responses to ACh [102].

Indeed, the contractile response to the MR agonist carbachol is decreased in the urinary bladder of $Cav\text{-}1^{-/-}$ mice [100] but the ASM response to methacholine remains unchanged [103]. In support of this, own recent data also showed that the airway response to muscarine is

unchanged in Cav-1$^{-/-}$ mice [submitted]. M2R are targeted to plasmalemmal caveolae upon agonist stimulation in adult rat ventricular myocytes and co-purified with Cav-3 and eNOS [104]. In addition, eNOS/Cav-3 interactions hold a key role in the cholinergic modulation of cardiac myocyte function [105]. However, functional consequences of the receptor-Cav-3 interactions in ASM remained poorly defined. We previously showed a direct association between M2R and Cav-3 in murine bronchial SMC which suggests that anchoring of M2R to caveolae via Cav-3 is important for initiation of M2R-mediated signaling [16].

Receptor type	Signal transduction pathway	Mechanism of action
M1R	$G\alpha_q/G\alpha_s$ protein coupled	↑ $Ins(1,4,5)P_3$ and DAG
M2R	$G\alpha_i$-protein coupled	↓ cAMP
M3R	$G\alpha_q$-protein coupled	↑ $Ins(1,4,5)P_3$ and DAG
M4R	$G\alpha_i$-protein coupled	↓ cAMP
M5R	$G\alpha_q$-protein coupled	↑ $Ins(1,4,5)P_3$ and DAG

Tab. 1.2 Characteristics of muscarinic receptors (MR). Receptors are classified by operational, structural and transductional criteria. ↑ Denotes increase, ↓ decrease in cellular levels of second messenger. cAMP, cyclic adenosine monophosphate; $Ins(1,4,5)P_3$, inositol-1,4,5-triphosphate; DAG, diacylglycerol.

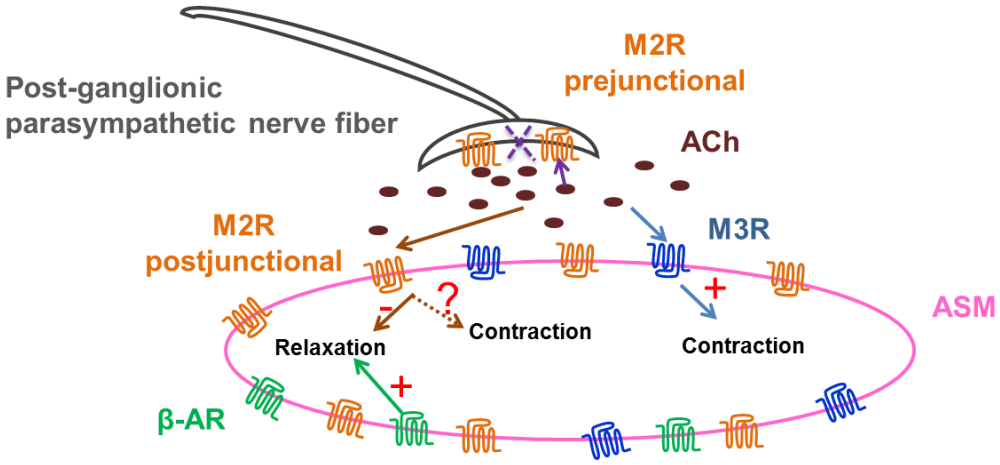

Fig. 1.4 Airway smooth muscle contraction. M3R mediate acetylcholine (ACh)-induced contraction of airway smooth muscle (ASM). Prejunctional M2R limit the amount of ACh released from stimulated cholinergic axons, thereby limiting the level of bronchoconstriction. In contrast, activation of postjunctional M2R can enhance the overall level of bronchoconstriction by opposing ASM relaxation, which might occur through activation of β2-adrenergic receptors (β-AR). MR, muscarinic receptor.

1.3.2.2 5-HT receptors

5-HT, a secretory product of mast cells, leads to contraction of airway SMC *in situ* and *in vitro* acting on a wide variety of G-protein-coupled 5-HT receptor subtypes (Tab. 1.3) [106-108].

There is a discrepancy between the effects of 5-HT *in vivo* and *in vitro*. Although 5-HT can activate human and rat ASM *in vitro* [109, 110], 5-HT inhalation does not lead to airway constriction *in vivo* [111]. As the 5-HT constrictor pathway involves the direct stimulation of bronchial SMC [107], 5-HT inhalation may not reach directly SMC to elicit a constrictor effect. It has been shown that increased levels of free 5-HT are present in the plasma of symptomatic asthmatic patients compared with levels in asymptomatic patients [112, 113]. We showed previously that the MCD treatment completely abolished the bronchoconstrictor response to 5-HT, thereby providing evidence for involvement of caveolae-coupled signaling pathways [16]. Likewise, this dependency was previously reported in bovine airway and rat arterial SMC [114, 115]. Interestingly, the responses to 5-HT were not affected in the absence of caveolae in ileal smooth muscle from Cav-1 KO mice [116]. These discrepant findings in the response to 5-HT between different tissues highlight the unique regulation of smooth muscle function, depending on organ and/or agonist. Generally, 5-HT contraction is mediated by i) an increase in calcium influx, and ii) the sustained contraction by calcium sensitization process [117, 118] which is regulated by the shift of rhoA, rho kinase and/or PKC from caveolar to noncaveolar lipid rafts [119]. A shift of 5-HT2A receptor subtype between caveolar and planar lipid raft membrane compartments was observed in cardiomyocytes and bovine tracheal SMC [114, 120]. Bhatnagar et al. showed that Cav-1 associates with the 5-HT2A receptors in HEK-293 and C6 cells and in rat brain synaptic membranes [121]. Mialet-Perez also demonstrated that 5-HT2A receptors interact with Cav-3 upon 5-HT stimulation, and Cav-3 silencing enhances the myocyte hypertrophic response [120]. Moreover, we recently showed a complete dependency of the 5-HT response to Cav-1 in murine extrapulmonary and a partial dependency in the intrapulmonary airway [submitted].

The different actions of 5-HT on airways might partly be attributed to the involvement of different receptor subtypes and effector systems to which the receptors are linked. The receptor subtypes present in airway SMC appear to be species-dependent [122]. In the guinea pig, 5-HT2 receptors have been found to play a direct role in airway contraction [123], whereas other 5-HT receptor subtypes including 5-HT1 and 5-HT3, 5-HT4 and 5-HT7 have a modulatory role [124-126]. Rat tracheal SMC contraction involves the 5-HT2C subtype [127].

Receptors from the 5-HT1 group have also been shown to mediate sheep tracheal contraction, whereas 5-HT2 receptors do not seem to be involved in bronchoconstriction [128]. Our RT-PCR analysis revealed the expression of 5-HT1B, 5-HT2A, 5-HT6 and 5-HT7 receptors as the most prevalent subunits in the airways of C57BL/6J mice [submitted]. Ketanserin, as pharmacological inhibitor of the 5-HT2A receptors, concentration-dependently abolished 5-HT-induced constriction in murine PCLS [submitted].

Receptor type	Signal transduction pathway	Mechanism of action
5-HT1A, B, D, E, F	$G\alpha_i/G\alpha_o$ protein coupled	↓ cAMP
5-HT2A, B, C	$G\alpha_q/G\alpha_{11}$ protein coupled	↑ $Ins(1,4,5)P_3$ and DAG
5-HT3A, B	Ligand-gated Na^+ and K^+ ion channel	Depolarization of plasma membrane
5-HT4	$G\alpha_s$-protein coupled	↑ cAMP
5-HT5A	$G\alpha_i/G\alpha_o$ protein coupled	↓ cAMP
5-HT6	$G\alpha_s$-protein coupled	↑ cAMP
5-HT7	$G\alpha_s$-protein coupled	↑ cAMP

Tab. 1.3 Characteristics of 5-HT receptors. Receptors are classified by operational, structural and transductional criteria. ↑ Denotes increase, ↓ decrease in cellular levels of second messenger. cAMP, cyclic adenosine monophosphate; $Ins(1,4,5)P_3$, inositol-1,4,5-triphosphate; DAG, diacylglycerol.

1.3.3 Caveolae/caveolins and smooth muscle contraction

Caveolae harbor a number of signaling proteins to facilitate GPCR-mediated contraction in vascular SM [115, 129], SM from the gastrointestinal tract [130], from the urogenital tract [100], and from the myometrium [131].

Concepts of the role of caveolae in governing muscle contraction include regulation of i) calcium entry and homeostasis, and ii) formation of the transverse (T)-tubule system during muscle development [12, 13]. Both, Cav-1 and Cav-3 are important for the regulation of calcium mediated responses and metabolism [102, 132, 133]. Cav-3 may specifically play a role in the formation of the muscular T-tubule system [38, 134].

Caveolae and Cav-1 appear to be most important in regulating the sensitivity of the airway SMC responses to ACh [14, 102, 132]. In human airway SM, Cav-1 was identified as a marker of the contractile airway SM phenotype [102, 132].

Cav-3 also co-localizes with the nAChR and promoted proper clustering of the nAChR in myotubes [135]. The presence of Cav-3 in ASM has been described in the rat tracheal muscle [105]. We identified both Cav-1 and Cav-3 in mouse and human ASM on mRNA and protein level [16], whereas other groups reported an absence of Cav-3 in isolated human ASM [18, 102, 136].

When myoblasts fuse to form myotubes driving skeletal muscle development, the expression of Cav-1 starts to decrease and the expression of the Cav-3, the dominant caveolin of differentiated muscle fibers, dramatically increase [38, 137, 138]. In arterial SMC, Cav-3 regulates the switch between contractile and synthetic phenotypes [41].

Vascular SMC co-express either Cav-1 and -2 (in veins) or Cav-1, -2, and -3 (in arteries), whereas differentiated cardiac and skeletal muscle cells express only the Cav-3 isoform [139]. It seems that, in arteries Cav-1 and -3 are co-expressed or there are different sub-populations of SMC which express different caveolin proteins [140]. In addition, Cav-3 may have two distinct functions in vascular SMC including regulation of signaling pathways at the plasma membrane or regulation of SMC contraction through association with the cytoskeletal network [41]. Studies in Cav-1/Cav-3 double knockout mice have indicated that Cav-1 is responsible for the formation of the majority of caveolae in bladder SMC while Cav-3 has an as-yet unidentified role in this cell type [75]. These discrepant findings regarding the role of Cav-3 in SMC contraction might illustrate important tissue-dependent differences in the role of Cav-3 in contraction.

1.3.4 Hyperreactivity and airway diseases

Bronchial hyperresponsiveness (BHR) is defined by an excessive contraction of ASM leading to bronchial narrowing in response to various inhaled stimuli, and is considered as a hallmark in asthma and COPD [141, 142]. In the course of inflammation, a wide range of additional contractile stimuli are released acting either directly on bronchial SMC or indirectly through neural pathways leading to BHR [84]. In the animal models of hyperresponsiveness, the release of ACh from the nerves is considerably increased, while there is no change in the sensitivity or expression of M3R on ASM [143]. According to a common concept, M2R are dysfunctional and do not control release of ACh in the hyperresponsiveness animal models [143]. Moreover, it is suggested that caveolins (Cav-2 and -3) have a functional role in the overactivity of the rat urinary bladder SM that occurs in association with hormonal alteration [144].

However, the lack of Cav-1 induces ASM hyperresponsiveness in mice and guinea pigs [18, 43, 145]. Furthermore, Cav-3 directs β2-AR-cAMP signaling to the T-tubular compartment in rat cardiomyocytes [146, 147]. cAMP compartmentation is a fundamental strategy which cells can orchestrate complex receptor signaling with a single second messenger [147]. The ASM is unable to relax when the β-AR is impaired [143]. The ASM hyperresponsiveness may be mediated by M2R since activation of these receptors inhibits β-AR-mediated relaxation [143]. A cross-talk between M2R and β2-AR and Cav-3 is likely to be present in ASM.

1.4 Aim of the study

There is evidence that the mechanisms of ASM constriction involve caveolae and their structural protein Cav-3, and dysregulation may be involved in pathogenesis of airway hyperreactivity. Thus, the present study aimed to assess the distribution of this caveolar structural protein, its interaction with binding partners (cavins), and its functional role in cholinergic and serotonergic airway constriction. To this end, immunohistochemical localization and co-immunoprecipitation studies were conducted, and Cav-3 deficient mice were generated for functional analyses. Given the known regional differences in airway responsiveness and underlying mechanisms along the airway tree, murine tracheal segments (cranial, middle and caudal) and extra- and intrapulmonary bronchi were separately investigated in organ bath experiments (extrapulmonary airways) and by videomorphometry in PCLS.

2 Materials and methods

2.1 Mouse genetics and husbandry

2.1.1 Cav-3 knock-out strategy

To generate Cav-3 knock-out mice, embryonic stem cells (ESC) were transfected with targeting vector and screened for homologous recombination by the PolyGene Company (Zurich, Switzerland). Furthermore, they produced the floxed germline within the knock-out mouse project 8053. Briefly, the targeting vector expressing neomycin resistance gene (neo^R) flanked by two *FRT* sites was placed in an upstream of exon-2 which itself was flanked by two *Lox*P sites (Fig. 2.1). ESC were electroporated with the *Not* I linearized targeting vector and the transfected ESC clones were screened to identify the targeted vector by PCR and Southern blot analysis using probes external to the targeting vector. Resistant colonies that contained neo^R were tested for homologous recombination on the 5'-end of the Cav-3 targeting vector by PCR and Southern blot analysis. These resistant colonies of transfected ESC were used to produce a chimeric mouse.

The resultant chimeric male mouse was mated with C57Bl6/J *FLIP* deleter females and germline transmission of the mutant allele was verified by a PCR analysis of genomic DNA from pigmented F1 offspring. Genotyping with 8053 primers flanking the *FRT* cassette indicated one male pup (8052.1007) which shows *FLIP* mediated deletion of the *FRT*-flanked neo^R cassette.

We used these Cav-3-*loxP* (floxed) male mice which were produced by the PolyGene Company further on to establish a conditional Cav-3 knock-out mouse colony. Moreover, we backcrossed the resulting floxed chimeric animals to the C57Bl6/J *Cre* deleter mouse strain from Jackson to obtain Cav-3 knock-out and Cre negative homozygous mice. The loss of the genomic locus of interest was confirmed by genotyping, immunohistochemistry and Western blot. Genotyping was carried out by a multiplex PCR with primers shown in (Tab. 2.1).

2.1.2 Animals

The Cav-3-deficient mice and the corresponding wild-type mice used in all experiments were sex and age matched, kept in individually ventilated cages in specific pathogen free (SPF) conditions and fed with a standard chow. The animals were held according to the German guidelines for care and use of laboratory animals (registration code: 491). They were killed

either by inhalation of an overdose of isoflurane (Abbott, Wiesbaden, Germany) or cervical dislocation for organ bath recording and videomorphometry experiments, respectively.

2.2 Genotyping

2.2.1 DNA extraction

Tail cuts (0.5-1 cm) were taken and stored at -20°C until use. Total DNA was isolated by using the DNeasy blood and tissue kit according to the manufacturer's protocol (Qiagen, Hilden, Germany). Briefly, tail cuts were incubated overnight with 180 µl ATL lysis buffer and 20 µl proteinase K at 56°C. Then they were mixed vigorously by vortexing, 400 µl AL-ethanol mixture buffer were added and the solution pipetted to mini column. After two steps of washing with AW wash buffer, we placed the column in a clean tube and pipetted 150 µl water onto the DNeasy membrane and used a centrifuge to solve the extracted DNA and to elute it.

2.2.2 Polymerase chain reaction (PCR)

PCR was performed by adding 1 µl cDNA, 0.5 µl of each gene-specific intron-spanning primer pair for Cav-3-8053-6f-5r or Cre (20 pM; MWG Biotech, Ebersberg, Germany) shown in (Tab. 2.1), 2.5 µl 10X PCR buffer II (100 mM Tris-HCl, 500 mM KCl, pH 8.3), 2 µl $MgCl_2$ (15 mM), 0.75 µl dNTP (10 mM each), 0.25 µl AmpliTaq Gold polymerase (5 U/µl; all reagents from Applied Biosystems, Darmstadt, Germany) and 18 µl H_2O. The cycling conditions were 12 min at 95°C, for 40 cycles: 30 s at 95°C, 30 s at 62°C - 0.5°C per cycle, 25 s at 72°C, and a final extension at 72°C for 7 min. The control reaction included the absence of DNA template. The PCR products were separated by electrophoresis on a 2% TRIS-acetate-EDTA agarose (Biozym GmbH, Wien, Austria) gel.

The PCR for Cav-3-8053-12f-5r was performed by adding 5 µl diluted cDNA (1/10), 2.5 µl of gene-specific intron-spanning primer pair for Cav-3-8053-6f-12r (20 pM; MWG Biotech, Ebersberg, Germany) shown in (Tab. 2.1), 2.5 µl 10X PCR buffer II (100 mM Tris-HCl, 500 mM KCl, pH 8.3), 2 µl $MgCl_2$ (15 mM), 0.75 µl dNTP (10 mM each), 0.25 µl AmpliTaq Gold polymerase (5 U/µl; all reagents from Applied Biosystems, Darmstadt, Germany) and 12 µl H_2O. Cycling conditions were 12 min at 95°C, for 45 cycles: 30 s at 95°C, 30 s at 64°C - 0.5°C per cycle, 120 s at 72°C, and a final extension at 72°C for 7 min. Control reaction included the absence of DNA template. The PCR products were separated by electrophoresis on a 1% TRIS-acetate-EDTA agarose gel.

2.3 Human bronchial smooth muscle cells

Primary human bronchial smooth muscle cells (HBSMC) were commercially purchased from Promocell (Heidelberg, Germany, catalog number C-12561) and grown in DMEM (PAA, Cölbe, Germany) supplemented with 10% heat inactivated fetal calf serum (FCS) (PAA, Cölbe, Germany) and penicillin/streptomycin (Sigma-Aldrich Chemie GmbH, München) in humidified 5% CO_2-95% air at 37°C incubator. Once the cells were confluent, they were trypsinized with 0.25% trypsin (PAA, Cölbe, Germany) and 0.02% EDTA in PBS containing 137 mM NaCl, 2.7 mM KCl, 10 mM Na_2HPO_4 and 1.8 mM KH_2PO_4, centrifuged, and the precipitate was used for gene expression and Western blot studies.

2.4 Western blotting

2.4.1 Protein extraction, electrophoresis, protein transfer and protein detection

Different murine organs or HBSMC were immediately frozen on dry ice and either processed the same day or stored at -80°C. The Cav-3-deficient mice and the corresponding wild-type mice were sex and age matched. Samples were homogenized with an homogenizer (Retsch MM300, California, USA) in octylglucoside lysis buffer (10 mM Tris-HCl, pH 7.4, 50 mM NaCl, 60 mM octylglucoside, and 1% triton X100) (Sigma-Aldrich Chemie GmbH, München) supplemented with a concentrated complete mini protease inhibitor cocktail, dilution of 1:200 (Roche Diagnostics, Mannheim, Germany) for 10 min. The homogenate was cleared by centrifugation at 8000 rpm for 5 min. The protein concentration in each tissue was determined using the method by Lowry with a commercially available kit (Bio-Rad, Hercules, CA, USA) using Nanodrop 2000 (Thermo Scientific, USA). Then, 50 µg of each protein lysate supernatant, mixed with 6 µl of 5X reducing sample buffer (320 mM Tris-HCl (pH 6.8), 5% sodium dodecyl sulfate (SDS), 50% glycerol, and 0.25 mg/ml bromophenol blue and 1% β-2-mercaptoethanol), boiled for 5 min at 95°C and were loaded onto reducing 10% or 15% SDS-polyacrylamide gel for electrophoresis. For the caveolin protein with a low molecular weight, a 15% SDS-PAGE separating gel, and for cavins and EHD2 proteins, a 10% SDS-PAGE separating gel was used. For the 15% SDS-PAGE separating gel, 7.5 ml of 30% acrylamide (Roth, Karlsruhe), 2.8 ml of 2 M Tris-HCl, pH 8.8; 75 µl of 20% SDS (Serva, Heidelberg, Germany), 80 µl 10% ammonium persulfate (APS; Merck, Darmstadt, Germany), 7.5 µl TEMED (Roth, Karlsruhe, Germany) and 4.62 ml H_2O were poured. For the 10% SDS-PAGE separating gel, 5 ml of 30% acrylamide, 2.8 ml of 2M Tris-HCl (pH 8.8), 75 µl of 20% SDS, 80 µl 10% APS, 7.5 µl TEMED and 7.12 ml H_2O were mixed. After the complete polymerization of the 10% or 15% separating gel, 1 ml 30% acrylamide, 50 µl

of 20% SDS, 1.25 ml of 1M TRIS-HCl (pH 6.8), 80 µl 10% APS, 10 µl TEMED and 7.7 ml H_2O were poured to make the stacking gel. Electrophoresis was performed under reducing condition. One liter of the electrophoresis buffer contained 0.025 M TRIS, 0.192 M glycine, 2.5 ml of 20% SDS and water. Electrophoresis was carried out for 20 min at 75 V followed by 100 min at 180 V. Subsequently, the proteins were blotted to polyvinylidine difluoride membranes (PVDF; Millipore, Schwalbach, Germany). We kept the PVDF membrane for 30 s in methanol (Sigma-Aldrich Chemie GmbH, München, Germany), 40 s in transfer buffer novex 1X (Thermo Fisher, Darmstadt, Germany) and embedded the membrane between 6 layers of transfer buffer saturated filter papers without bubbles. From the top, there were three layers of filter papers, the electrophoresed gel, the PVDF membrane and another three layers of filter papers. The blotting was carried out for 90 min at 90 mA per gel using a semi-dry blotter (Peqlab GmbH, Erlangen, Germany). Thereafter, the gel was stained for 2 h in 30% methanol (Sigma-Aldrich Chemie GmbH, München, Germany), 10% acetic acid (Merck, Darmstadt, Germany) and 0.2% Coomassie brilliant blue R250 (Sigma-Aldrich Chemie GmbH, München, Germany) and destained with a solution containing 40% methanol and 10% acetic acid. The blotted PVDF membrane was immersed in TTBS (0.01 M Tris-HCl (pH 8.0), 0.2 M NaCl and 0.05% Tween-20) and 10% dried skimmed milk powder (Roth, Karlsruhe, Germany) for 3 h to saturate non-specific protein binding sites. Then it was incubated overnight with the appropriate antibodies (Tab. 2.2) (diluted in TTBS and 5% milk powder; Pierce, Rockford, USA), washed 3 × 10 min with TTBS and incubated with secondary horseradish peroxidase-conjugated antibodies (Tab. 2.3) (diluted in TTBS and 2.5% milk powder; Pierce, Rockford, USA) for 1 h. Immunoreactive bands were visualized by the enhanced chemiluminescence kit (Thermo Scientific, USA) with Fusion FX (Vilber Lourmat, Australia). The PVDF was blocked in TTBS containing 10% dried skimmed milk powder for 5 h. The PVDF membrane was incubated with the primary antibody (β-tubulin or succinate dehydrogenase A (SDHA) antibodies as a reference control) overnight. Then, it was washed and incubated with secondary horseradish peroxidase-conjugated antibodies. Immunoreactive bands were visualized with Fusion FX. Next, the PVDF membrane was stained in Ponceau S solution (Sigma-Aldrich Chemie GmbH, München, Germany) for 1 min. The stained PVDF membrane and the destained gel were scanned. The densitometry data were used to calculate the ratio of the target protein to the reference control protein using the image J software (Bethesda, Maryland, USA).

2.4.2 Statistical analysis

Nonparametric statistical tests were used. The ratio of densitometric data is presented as box plot depicting all quartiles from 0 to 100. We used the Mann-Whitney *U*-test to analyze differences between Cav-$3^{+/+}$ and Cav-$3^{-/-}$ mouse strains using SPSS software version 11.5 (SPSS Software, Munich, Germany). Differences were considered as statistically significant when $P < 0.05$.

2.5 PCR

2.5.1 RNA extraction

Samples from lung, trachea, main bronchus, tracheal muscle, tracheal epithelium and the rest of the trachea (epithelium and muscle were removed) from Cav-$3^{+/+}$ and Cav-$3^{-/-}$ mice were shock-frozen and stored at -80°C until use. In addition, HBSMC were cultured and after confluency, the cells were trypsinized, washed with PBS and centrifuged. There is one more step concerning the RNA isolation of epithelial cells. The epithelial cells were abraded from the trachea using cotton swabs and purified with a QIA shredder column (Qiagen, Hilden, Germany). Total RNA from all tissues was isolated by using the RNeasy method according to the manufacturer's protocol (Qiagen, Hilden, Germany). The amount of RNA was determined by Nanodrop and diluted to 1 µg/µl with water and stored at -80°C for further processing.

2.5.2 DNA digestion and reverse transcription

Contaminating DNA from isolated 8 µl (1 µg/µl) RNA was degraded using 1 µl of DNase I (1 U/µl, Invitrogen, Karlsruhe, Germany), 1 µl 10X DNase I reaction buffer (Invitrogen, Karlsruhe, Germany) and 8 µl of water for 15 min at 25°C. Then, the enzyme was inactivated by the addition of 1 µl ethylene diamine tetra acetic acid (EDTA) (25 mM, pH: 8.0, Invitrogen, Karlsruhe, Germany) for 10 min at 65°C followed by an incubation for 5 min on ice. For the reverse transcription of mRNA into cDNA, 1 µl oligo DTs (500 µg/µl, Perkin Elmer, Ohio, USA), 1 µl dNTP mix (10 mM of each dNTP, Amersham Pharmacia Biotech, Freiburg, Germany), 2 µl dithiolthreitol (DTT) (0.1 M, Invitrogen, Karlsruhe, Germany) and 1 µl Superscript II reverse transcriptase (200 U/µl, Invitrogen, Karlsruhe, Germany) were incubated for 50 min at 42°C following 10 min at 72°C to inactivate the Superscript II enzyme and then stored until further use at -20°C.

2.5.3 RT-PCR

RT-PCR was performed by adding 1 µl cDNA, 0.75 µl of gene-specific intron spanning primer sets for murine target genes as shown in (Tab. 2.4) and human target genes as shown

in (Tab. 2.5) (20 pM; MWG Biotech, Ebersberg, Germany), 2.5 µl 10X PCR buffer II (100 mM Tris-HCl, 500 mM KCl, pH 8.3), 2 µl $MgCl_2$ (15 mM), 0.75 µl dNTP (10 mM each), 0.25 µl AmpliTaq Gold polymerase (5 U/µl; all reagents from Applied Biosystems, Darmstadt, Germany) and 17.75 µl H_2O. Cycling conditions were 12 min at 95°C, for 40 cycles: 30 s at 95°C, 30 s at 59°C, 30 s at 72°C, and a final extension at 72°C for 7 min. The PCR products were separated by electrophoresis on a 2% TRIS-acetate-EDTA agarose gel.

2.5.4 Control reactions

As a control for sample contamination of with genomic DNA, we performed PCR reaction with water instead of cDNA. Additionally, control reactions without adding reverse transcriptase enzyme were carried out. Beta-actin primers were used to check the efficiency of RNA isolation and cDNA synthesis.

2.5.5 Gel electrophoresis

PCR products were separated by electrophoresis in a 2% TRIS-acetate EDTA agarose gel containing 20 g/l agarose (Biozym GmbH, Wien, Austria), 482 g/l TRIS (USB, Cleveland, USA), 104.2 ml/l glacial acetic acid (Merck, Darmstadt, Germany), 200 ml/l of 0.5 M EDTA (Invitrogen, Karlsruhe, Germany) which were solved in 1 l H_2O, pH 8.0 with the addition of 10 µl/l ethidium bromide (1%; Roth GmbH, Karlsruhe, Germany). Twenty-five µl of the PCR products were mixed with 5 µl loading buffer (0.1 g Orange G dye (Sigma-Aldrich Chemie GmbH, München, Germany), 5.88 ml of 87% glycerol (Sigma-Aldrich Chemie GmbH, München, Germany), 250 µl Tris-HCl buffer (pH 8.0), 1 ml EDTA solution (pH 8.0; Sigma-Aldrich Chemie GmbH, München, Germany), and mixed in 10 ml H_2O and applied in the gel. The PCR products were run through a horizontal electrophoresis in a Horizon 11-14 (Gibco, Karlsruhe, Germany). A 100 bp DNA ladder (Invitrogen, Karlsruhe, Germany) was run as marker (6.5 µl). The electrophoresis was carried out at a voltage of 150 V over 45 min. The PCR fragments were separated on the gel and were detected by UV illumination using a spectrophotometer (Ultrospec 2100 Pro, Biochrom, Cambridge, UK).

2.5.6 DNA purification and sequencing

The bands obtained with primers for cavin-1-4 were determined from agarose gel under UV light, cut out and transferred to a 2 ml reaction buffer. DNA extraction from the gel was carried out using the Gel Extraction Kit (Qiagen, Hilden, Germany) according to the instructions of the manufacturer. The absorbance of DNA content was determined by the

Nanodrop. Specificities of the amplified gel-extracted PCR products were verified by sequencing (MWG Biotech, Ebersberg, Germany).

2.5.7 Real-time PCR

Total RNA from lung, trachea, main bronchus, tracheal muscle, tracheal epithelium and the rest of the trachea (epithelium and muscle were removed) were isolated from Cav-$3^{+/+}$ and Cav-$3^{-/-}$ mice using the RNeasy method as explained before. The Cav-3-deficient mice and the corresponding wild-type mice were sex and age matched. Contaminating DNA was degraded using 1 unit of DNase I and reverse transcription was carried out as described above. Real-time PCR was performed in an iCycler (Bio-Rad, Munich, Germany) using QuantiTect SYBR Green PCR Kit (Bio-Rad, Munich, Germany). Characterization of gene-specific intron spanning primer sets for cavin-1, cavin-2, cavin-3, cavin-4, Cav-1, EHD2 and β-actin is given in (Tab. 2.4) The PCR conditions included initial denaturation in one cycle of 10 min at 95°C followed by 40 cycles of 30 s at 95°C, 30 s at 60°C, and 30 s at 72°C.

2.5.8 Calculation of relative expression

All analyses were done in triplicate and the mean cycle thresholds (CT) for all target genes were calculated. The ΔCT of all target genes compared with β-actin was calculated as follows:

ΔCT target gene= CT target gene – CT β-actin

Control reactions included the absence of DNA template and the absence of reverse transcriptase enzyme. The PCR products were separated by electrophoresis on a 2% Tris-acetate-EDTA agarose gel.

2.5.9 Statistical analysis

Nonparametric statistical tests were used. ΔCT values are presented as box plot. Differences between Cav-$3^{+/+}$ and Cav-$3^{-/-}$ groups was analyzed with the Mann-Whitney *U*-test using SPSS software. Differences were considered as statistically significant when $P < 0.05$.

2.6 Immunohistochemistry

2.6.1 Transtracheal filling with OCT compound for immunohistochemistry

The thorax of the mouse was opened and a plastic cannula (1.1 mm diameter; Braun, Melsungen, Germany) was inserted into the trachea. After placing the cannula and fixing it, the lungs were filled with approximately 2 ml of OCT compound (Sakura, Zoeterwoude, Netherlands) diluted with an equal amount of 0.1 M phosphate buffer (pH 7.4). Then, all

thoracic viscera (heart, lungs, trachea, esophagus and thoracic aorta) were removed, frozen on filter paper in melting isopentane, transferred to liquid nitrogen, and finally stored at -80°C.

2.6.2 Paraffin embedding

Lung biopsies from COPD patients and donors (n=4) were provided by the institute of pathology and cytology, Wetzlar (Prof. Ludger Fink). Bronchial samples were fixed in 10% formalin according to the standard method and they were embedded in paraffin. The study was approved by the local ethical committee (Ref. No. 100/07).

2.6.3 Indirect immunofluorescence on cryosections

The tissues to be examined were cut on a cryostat (Microm HM 560, Microm International GmbH, Walldorf, Germany) at a thickness of 10 µm and placed on super frost plus slides (Menzel-glasses, Braunschweig, Germany). The sections were fixed either for 10 min in acetone precooled at -20°C or for 20 min in 4% PFA at room temperature. In case of using PFA as fixative, we washed the slides for 2 × 10 min in PBS and 1 × 10 min in distilled water. All sections were dried for one h at room temperature. The blocking of nonspecific protein binding sites was carried out for one h with one of the following blocking solutions: acetone-treated sections with 50% heat inactivated normal horse serum (NHS; DakoCytomation, Glostrup, Denmark) in PBS, and for PFA-treated sections 10% heat-inactivated NHS, 0.5% Tween-20, 0.1% BSA in PBS, pH 7.4. The primary antibodies (Tab. 2.6) were solved in PBS with addition of 0.01% NaN_3 and 0.05 M NaCl (PBS + NaN_3 + S) in the working dilution and incubated overnight at room temperature. The primary antibodies were applied either singly or in combination for double-labeling immunofluorescence. Primary antibody combinations were as follows: rabbit anti-Cav-1/mouse anti-α-SMA; rabbit anti-cavin-1/mouse anti-α-SMA; rabbit anti-cavin-4/mouse anti-α-SMA; goat anti-Cav-3/ mouse anti-α-SMA. After 3 × 10 min washing with PBS, the corresponding secondary antibody was applied in PBS + NaN_3 + S for one h. After washing 3 × 10 min with PBS, the sections were put for a further 10 min in 4% PFA in 0.1 M phosphate buffer (pH 7.4) to conserve the interaction between the primary and the secondary antibodies. Following the washing step, the slides were cover-slipped with carbonate buffered glycerol (pH 8.6) and stored at a dark place at 4°C.

2.6.4 Indirect immunofluorescence on paraffin sections

The paraffin embedded human lung tissues were cut by a microtome (Tetra Santander, Jung, Heidelberg, Germany) at a thickness of 8 µm and collected on super frost plus slides.

Sections were dried overnight in an incubator (Heraeus, Hanau, Germany) at 37°C, so the tissues could adhere better on the slides. Sections were stored at room temperature until use. Before incubation with the primary antibody, the sections were deparaffinised (2 × 5 min in xylene, absolute, 96%, 80%, 70% and 50% ethanol, respectively, for 5 min). Then the slides were placed in a cuvette filled with PBS containing 10% citric acid, pH 6 (Merck, Darmstadt, Germany). We floated the cuvette containing the slides in a water bath with 700 ml water and put them in a microwave oven for 8 min (800 W). When we saw the first bubble in the bath, we continued this process for another 5 min. After this procedure, we put the bath containing the slides for about 15 min to cool. We proceeded on by 3 × 5 min washing steps with PBS. Next, we incubated the slides with 10% NHS, 0.5% Tween-20, 0.1% BSA in PBS, pH 7.4 for 1 h before applying the appropriate primary antibody (Tab. 2.6). These antibodies were applied either singly or in combination for double-labeling immunofluorescence. Primary antibody combinations were as follows: rabbit anti-Cav-1/mouse anti-α-SMA; rabbit anti-cavin-1/mouse anti-α-SMA; rabbit anti-cavin-4/mouse anti-α-SMA. After 3 × 10 min washing with PBS, the corresponding secondary antibody (Tab. 2.7) was applied for 1 h. After washing 3 × 10 min with PBS, the sections were put for a further 10 min in 4% PFA and they were cover-slipped with carbonate buffered glycerol and stored at 4°C.

2.6.5 Controls for immunohistochemical studies

Cryosections of Cav-3 deficient mice were used for confirming the specificity of Cav-3 antibody labeling. To determine the specificity of the secondary antibody, the primary antibody was omitted and incubation with only PBS + NaN_3 + S on the sections was applied. A monoclonal antibody, isotype IgG_2, raised against neuro-filament-68 (Nf-68) was used as irrelevant antibody isotype control for the monoclonal anti Cav-3 antibody on sections from paraffin embedded specimens.

2.7 Co-Immunoprecipitation

2.7.1 Protein extraction and co-immunoprecipitation

Trachea and lung samples from both Cav-$3^{+/+}$ and Cav-$3^{-/-}$ mice and HBSMC were homogenized with a homogenizer in octylglucoside lysis buffer supplemented with 1X concentrated protease inhibitor cocktail for 10 min. Skeletal muscle or heart tissue from Cav-$3^{+/+}$ mice were used as positive control. The homogenate was cleared by centrifugation as described in chapter 2.4 Western blotting. Total tissue homogenate (2 mg) for each reaction was incubated with 1 µg of experimental antibody (Tab. 2.8) in 150 µl PBS + Tween-20

(0.02%) at 4°C and rotated overnight. Then, we added 50 µl dynabeads coated with protein G (Life Technologies GmbH, Darmstadt, Germany) to each immunoprecipitation (IP) tube and rotated them for 4 h at 4°C. Next, we removed the supernatant and froze the samples for further analysis. The dynabeads-antibody-protein complex was washed three times with 200 µl PBS + Tween-20. Then, we added 100 µl PBS + Tween-20 to the dynabeads-antibody-protein complex and transferred it to a fresh Eppendorf tube.

2.7.2 Elution of the proteins from the beads and detection with Western blotting

We put the fresh Eppendorf tube with dynabeads-antibody-protein complex on a magnetic base and removed the PBS. Then, we added 60 µl reducing sample buffer and left it for 5 min to boil at 95 °C, followed by gel electrophoresis on a 12% separating gel including 6 ml of 30% acrylamide, 2.8 ml of 2 M Tris-HCl, pH 8.8, 75 µl of 20% SDS, 80 µl 10% ammonium persulfate, 7.5 µl TEMED, 6.12 ml H_2O for caveolins and 10% separating gel including 5 ml of 30% acrylamide, 2.8 ml of 2 M Tris-HCl pH 8.8, 75 µl of 20% SDS, 80 µl 10% APS, 7.5 µl TEMED and 7.12 ml H_2O for cavins, and electrophoresed the samples in 150 V for 90 min. Western blot analysis was carried out as explained above. The primary and secondary antibodies for Western blot are listed in (Tab. 2.2 and 2.3), respectively. For cavins, we loaded 30 µl and for caveolins 20 µl from the sample diluted in 60 µl reducing sample buffer. Protein-protein interaction provided by co-immunoprecipitation (CO-IP) is schematically diagramed in (Fig. 2.2).

2.8 Videomorphometry

2.8.1 Intrapulmonary bronchi

Precision cut lung slices (PCLS) were prepared using a slightly modified version of the protocol described by Martin et al. [148] and reported in detail earlier [16, 85]. Briefly, the airways were filled via the cannulated trachea with low melting point agarose (Sigma, Taufkirchen, Germany). The lungs and the heart were dissected in HEPES-Ringer containing 110 mM NaCl, 2.6 mM KCl, 1.2 mM KH_2PO_4, 1.2 mM $MgSO_4$, 25 mM HEPES and 11 mM glucose. The dissected lung was cooled in cold HEPES

, and PCLS were cut with a vibratome (VT1000S, Leica, Bensheim, Germany) at a thickness of 200 µm from the left lobe of the lung and incubated in minimal essential medium (MEM, GIBCO, Karlsruhe, Germany) at 37°C for 2-4 h to remove the agarose.

Experiments were performed in a HEPES-Ringer buffer in a lung slice superfusion chamber (Hugo Sachs Elektronik, March, Germany) mounted on an inverted microscope. Images of

the bronchi were recorded with a CCD camera and analyzed with Optimas 6.5 software (Stemmer Imaging, Puchheim, Germany) (Fig. 2.3).

Only those bronchi which responded to a test stimulus of 60 mM KCl with a reduction of luminal area of at least 20% were included in the final data analysis. Muscarine and 5-HT were purchased from Sigma (Taufkirchen, Germany). Muscarine and 5-HT were dissolved in water and diluted in HEPES to the desired experimental concentration immediately before use. The volume of the chamber was 1500 µl. All analyses were done and the EC50 in response to muscarine and 5-HT were calculated. EC50 of muscarine and 5-HT represent the concentration of a compound where 50% of their maximal effects were observed.

2.8.2 Studying the effect of cumulative concentrations of muscarine and 5-HT on bronchial diameter

PCLS from Cav-$3^{+/+}$ and Cav-$3^{-/-}$ mice were first washed for 5 min to reach an equilibrium, then KCl (60 mM) was applied for 5 min as a reference control. The luminal bronchial area was measured in 1 min intervals. At least 20% response to KCl compared to baseline was the inclusion criterion for the experiments. We washed the slices with HEPES for 20 min to remove KCl and to reach the baseline level. Next, muscarine (10^{-8}-10^{-4} M) or 5-HT (10^{-7}-10^{-3} M) were administrated at cumulative concentrations (Fig. 2.4A, 4B), each concentration for 10 min. After administration of the highest concentration we continued washing for 10 min to reach the baseline again and applied KCl (60 mM) as a viability control for another 5 min.

2.8.3 Studying the effect of different application schedules of increasing 5-HT concentrations on bronchial diameter

To test for a desensitizing effect of 5-HT during cumulative application, we additionally used three different schedules of 5-HT application (Fig. 2.4C, D). PCLS from Cav-$3^{+/+}$ and Cav-$3^{-/-}$ mice were first washed for 5 min to reach an equilibrium, then KCl (60 mM) was applied for 5 min as a reference control. The luminal bronchial area was measured in 1 min intervals. We washed the slices with HEPES for 20 min to remove KCl and to reach the baseline level. In the first schedule, we sequentially applied 5-HT at 10^{-6} M, 10^{-5} M and 10^{-4} M as the highest concentration. In the second schedule, we applied 5-HT directly at 10^{-4} M and 10^{-3} M.

2.8.4 Statistical analysis

Data of videomorphometric experiments are presented as means ± SEM of 4 to 12 bronchi obtained from 4 to 6 animals. Because it is principally impossible to test for a normal (Gaussian) distribution at such numbers, nonparametric statistical tests were used. Differences of minimum luminal area between Cav-$3^{+/+}$ and Cav-$3^{-/-}$ were analyzed with the

Kruskal-Wallis test and, in case $P < 0.05$, followed by Mann-Whitney *U*-test using SPSS software. Differences were considered as statistically significant when $P \leq 0.05$. EC50 values of agonist responses were estimated using nonlinear regression sigmoidal curve analysis using Microsoft Excel. We used the Mann-Whitney *U*-test to analyze differences between Cav-$3^{+/+}$ and Cav-$3^{-/-}$ mice strains.

2.9 Organ bath experiment

2.9.1 Force recording

The thorax was opened and the submandibular gland was removed. Tracheal rings (4 cartilages per ring) were isolated from the cranial, middle and caudal parts of the trachea and the left main bronchus was dissected. Isometric contraction was measured in isolated rings that were mounted between two stainless steel clips in vertical 15 ml organ baths of a computerized isolated organ bath system (AD Instruments GmbH, Heidelberg, Germany).

Baths were filled with MEM and penicillin-streptomycin maintained at 37°C and bubbled with a 95% O_2/5% CO_2 gas mixture. The upper stainless clip was connected to an isometric force transducer (Power Lab 8.30; AD Instruments GmbH, Heidelberg, Germany). Tissues were equilibrated against a passive load of 0.5 g for all rings (Fig. 2.5).

At the beginning of each experiment, KCl (60 mM) was administered to each of the rings to elicit a reference control. The force response was measured in 1 min intervals. Rings were then washed with fresh MEM to eliminate the KCl response. Then a cumulative concentration administration of muscarine (10^{-9}- 5×10^{-4} M) and 5-HT (10^{-8}- 10^{-4} M) was performed (Fig. 2.6). Changes in tension were recorded as a force in 1 min intervals and evaluated by software (Lab Chart 7, AD Instruments GmbH, Heidelberg, Germany). All analyses were done and the EC50 in response to muscarine and 5-HT were calculated. EC50 of muscarine and 5-HT represent the concentration of a compound where 50% of their maximal effects were observed. The airway reactivity of the response to muscarine or 5-HT was calculated as follows:

Reactivity [muscarine] = Max force [muscarine] / Max force [KCl] or

Reactivity [5-HT] = Max force [5-HT] / Max force [KCl].

2.9.2 Statistical analysis

Data are presented as means ± SEM of four to seven animals. Differences of maximal force response and reactivity between Cav-$3^{+/+}$ and Cav-$3^{-/-}$ groups and between Cav-$3^{+/+}$ or Cav-$3^{-/-}$ tracheal parts and main bronchi were analyzed with the Kruskal-Wallis test. In case $P < 0.05$,

differences between 2 groups were analyzed by Mann-Whitney *U*-test using SPSS software. Differences were considered as statistically significant when $P \leq 0.05$. EC50 values of agonist responses were estimated using nonlinear regression sigmoidal curve analysis using Microsoft Excel. We used the Mann-Whitney *U*-test to analyze differences between Cav-$3^{+/+}$ and Cav-$3^{-/-}$ groups and between Cav-$3^{+/+}$ or Cav-$3^{-/-}$ mice strains.

Gene	Primer	Product length (bp) Cav-3-*loxP*	Product length (bp) Cav-$3^{+/+}$	Product length (bp) Cav-$3^{-/-}$
Cav-3-8053-6F-5R	fwd ttatgcgcaccatcagtc rev cctaggtgtgctcatttg	368	323	-
Cav-3-8053-12F-5R	fwd aaggaggcaatctgggctac rev cctaggtgtgctcatttg	2000	1700	497
Cre	fwd gacaccaccagcaacacact rev tccttgaagagcaggacgtg	390	390	390

Tab. 2.1 Oligonucleotide primers for Cav-3 genotyping.

Antigen	Host species	Dilution	Catalog number/Clone	Source
Cav-1 (N-20)	Rabbit (p)	1:400	Sc-894	Santa Cruz, USA
Cav-3 (N-18)	Goat (p)	1:300	Sc-7665	Santa Cruz, USA
cavin-1	Rabbit (p)	1:200	Ab48824	Abcam, UK
cavin-4	Goat (p)	1:100	Sc-163021	Santa Cruz, USA
EHD2	Goat (p)	1:500	Ab23935	Abcam, UK
SDHA	Rabbit (p)	1:500	Clone 11a	Own laboratory
β-tubulin IV	Mouse (m)	1:400	Mu178-UC/Clone ONS1A6	Biogenex, USA

Tab. 2.2 Primary antibodies used for Western blots. P = polyclonal, m = monoclonal antibody. N denominates the N-terminus of the protein with 16, 18 and 20 amino acid residues, respectively.

Antigen	Host species	Conjugate	Dilution	Catalog number	Source
Mouse IgG	Goat	Peroxidase	1:10000	M32307	Thermo Fisher, Germany
Rabbit IgG	Goat	Peroxidase	1:10000	31460	Thermo Scientific, USA
Goat IgG	Rabbit	Peroxidase	1:5000	61-1620	Thermo Fisher, Germany

Tab. 2.3 Secondary antibodies used for Western blots.

Gene	Genebank accession No.	Primer	Product length (bp)
cavin-1	NM008986.2	fw dgagcaacaccgtgagcaagt rev ctccgactctttcagcgact	220
cavin-2	NM138741.1	fwd tggaacagcgtcagatcaac rev ctggctccttcacaaacaca	290
cavin-3	NM028444.1	fwd gacaccaccagcaacacact rev tccttgaagagcaggacgtg	172
cavin-4	NM026509.3	fwd gcaacaggttcgtgtaacca rev tgctctttgcctgacttcct	251
EHD2	NM153068.3	fwd tggagagcatcagcatcatc rev gtgggcatcaaagagcaaga	140
β-actin	NM007393.3	fwd gtgggaatgggtcagaagg rev ggcatacagggacagcaca	299
Cav-1	NM001243064.1	fwd gcacaccaaggagattgacc rev agatgagtgccattgggatg	212
Cav-3	NM007617.3	fwd aggacattcactgcaaggag rev gtacttggagacggtgaacg	167

Tab. 2.4 Oligonucleotide primers for PCR analysis of murine samples.

Gene	Genebank accession No.	Primer	Product length (bp)
cavin-1	NM012232.5	fwd gagcaatacggtgagcaagc rev ggcagcttcacttcatcctg	180
cavin-2	NM004657.5	fwd ggtcaaagagcgcatggata rev ggtttcctccagggatttgt	208
cavin-3	NM145040.2	fwd gacaccaccagcaacacctt rev gacttcaccctcctccttga	186
cavin-4	NM001018116.2	fwd gctttcacagtcgcatagca rev aacaacagacagggatgtcg	223
EHD2	NM014601.3	fwd atcctcaaactgcccgtcat rev gcgagtgaaacttggtgaag	127
Cav-1	NM001172897.1	fwd tctctacaccgttcccatcc rev caaagagggcagacagcaag	287
Cav-3	NM001234.4	fwd cgtgtggaaggtgagctaca rev tgcggatgcagagtgagtag	212

Tab. 2.5 Oligonucleotide primers for PCR analysis of human samples.

Antigen	Host species	Dilution	Catalog number/Clone	Source
Cav-1 (N-20)	Rabbit (p)	1:400	Sc-894	Santa Cruz, USA
Cav-3	Mouse (m)	1:300	610421/clone 26	BD Bioccience, Germany
Cav-3 (N-18)	Goat (p)	1:300	Sc-7665	Santa Cruz, USA
Cav-1+Cav-3	Rabbit (p)	1:300	63941	BD Bioscience, Germany
cavin-1	Rabbit (p)	1:200	Ab48824	Abcam, UK
cavin-4	Rabbit (p)	1:100	BP5646a	Abgent, USA
α-SMA	Mouse (m)	1:1000	F3777/clone 1A4	Sigma, Germany
Nf-68	Mouse (m)	1:300	N5139/clone Nr4	Sigma, Germany

Tab. 2.6 Primary antibodies used for immunohistochemistry. p = polyclonal, m = monoclonal antibody. N denominates the N-terminus of the protein with 18 and 20 amino acid residues, respectively.

Antigen	Host species	Conjugate	Dilution	Catalog number	Source
Mouse IgG	Donkey	Cy3	1:1000	715-165-150	Dianova, Germany
Rabbit IgG	Donkey	Cy3	1:2000	AP182C	Chemicon, USA
Goat IgG	Donkey	Cy3	1:800	705-165-003	Dianova, Germany

Tab. 2.7 Secondary antibodies used for immunohistochemistry.

Antigen	Host species	Concentration	Catalog number	Source
cavin-1	Rabbit (p)	1 µg/µl	Ab48824	Abcam, UK
Cav-1 (N-20)	Rabbit (p)	1 µg/µl	Sc-894	Santa Cruz, USA
Cav-3 (N-18)	Goat (p)	1 µg/µl	Sc-7665	Santa Cruz, USA

Tab. 2.8 Antibodies used for precipitation in Co-IP. p = polyclonal, m = monoclonal antibody. N denominates the N-terminus of the protein with 18 and 20 amino acid residues, respectively.

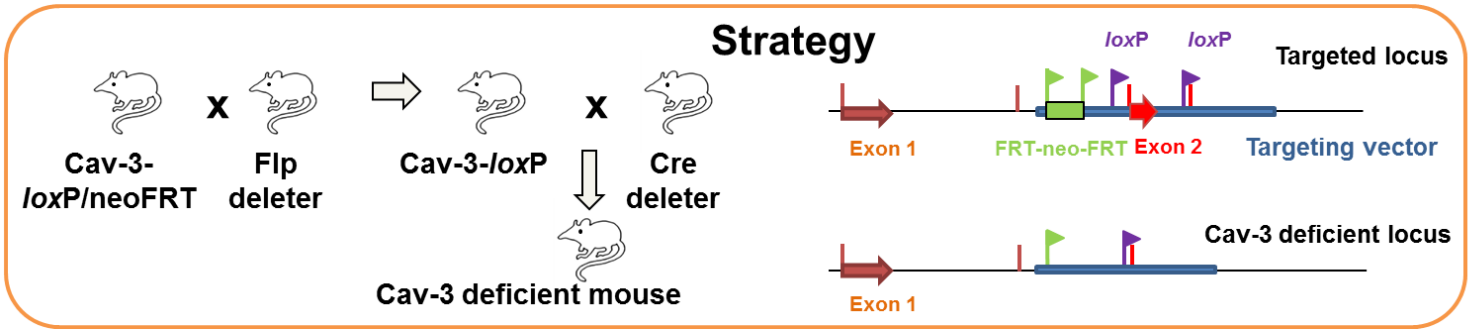

Fig. 2.1 Schematic overview of the generation of Cav-3-*loxP* mouse strain and of general Cav-3 deficient mice. Neo^R flanked by two *FRT* sites was placed in upstream of exon-2 which itself flanked by two *lox*P sites. Mating of *FLIP* deleter mice with Cav-3-*loxP*/neo*FRT* mice caused depletion of neo^R locus and generation of Cav-3-*loxP* mice. Further mating of Cav-3-*loxP* (Flox) mice with Cre deleter mice caused depletion of Cav-3 exon-2 locus and generation of Cav-3 deficient mice.

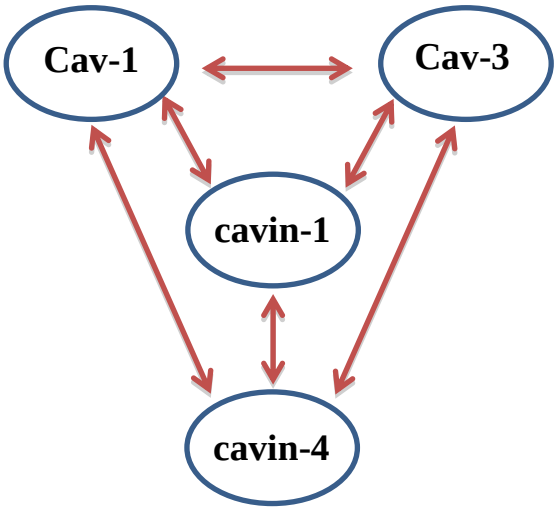

Fig. 2.2 Schematic overview of the protein-protein interaction studies using CO-IP method. The red arrows indicate couples of proteins being analyzed for potential interaction.

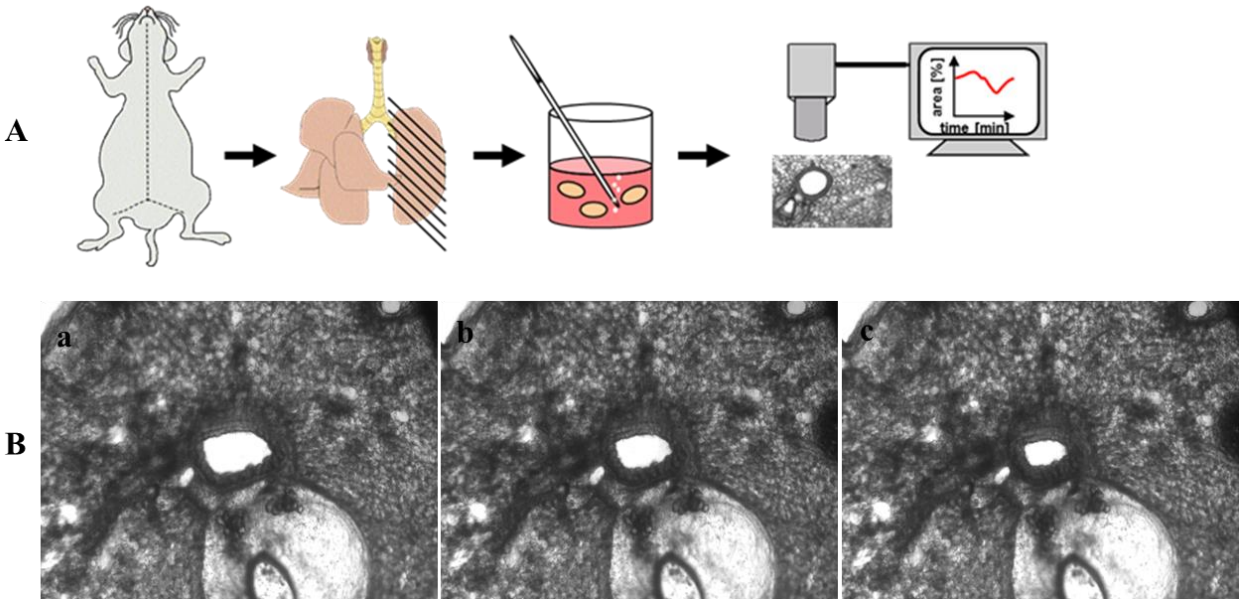

Fig. 2.3 Schematic overview of the videomorphometry method. (A) Briefly, mice are killed by cervical dislocation. After opening of the chest, the lungs are filled with low melting point agarose and after cooling down cut into 200 µm thick PCLS. After removing the agarose at 37°C one PCLS is transferred into the flow-through superfusion chamber in which it is exposed to HEPES at 37°C. Constriction is recorded as changes in the luminal area. (B) Changes in the luminal area are shown in (a-c).

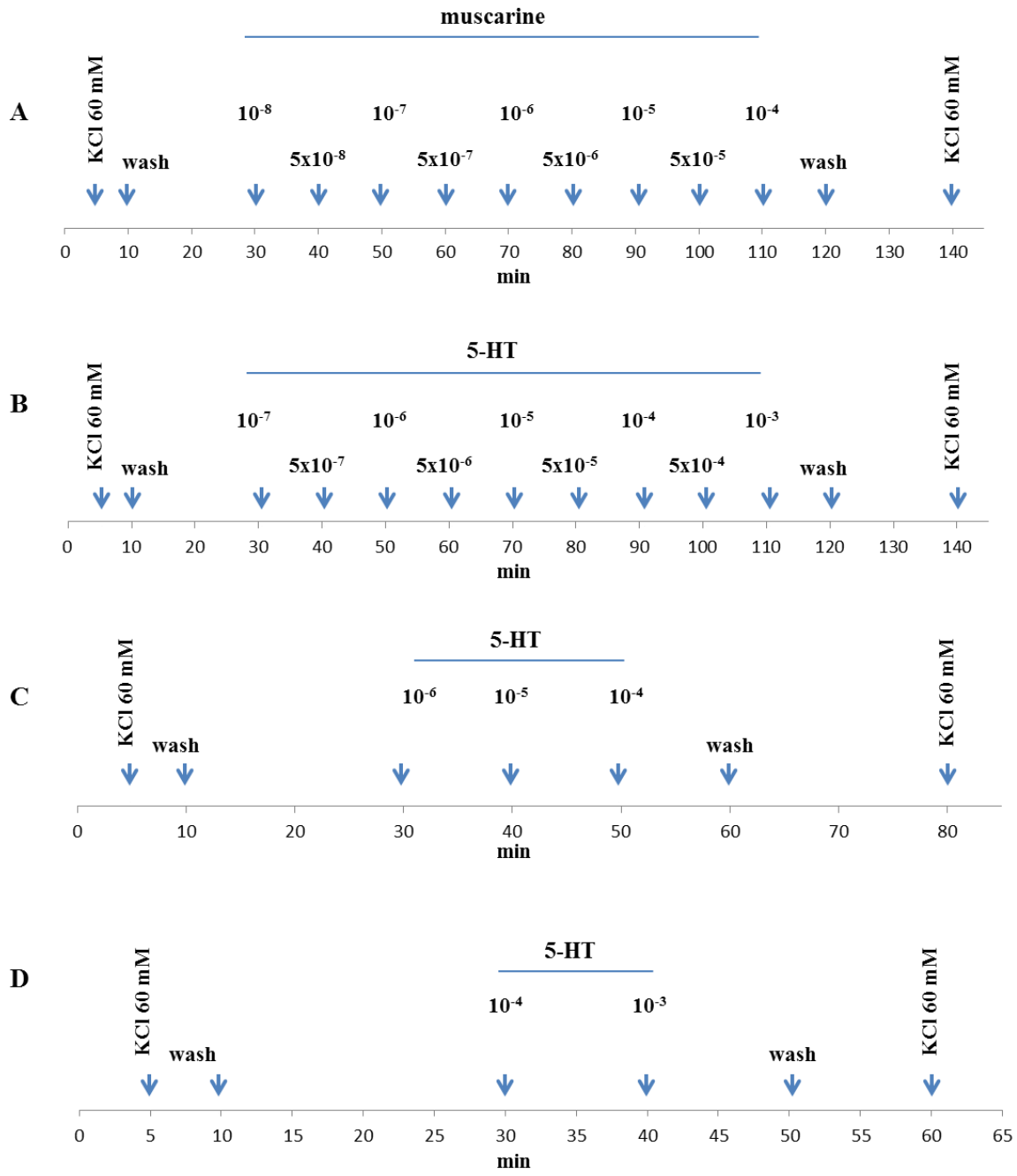

Fig. 2.4 Schematic overview of application schedules of (A) muscarine and (B-D) 5-HT concentrations. The concentrations are indicated in molarity and were used in the flow-through superfusion chamber in which PCLS were exposed to HEPES at 37°C.

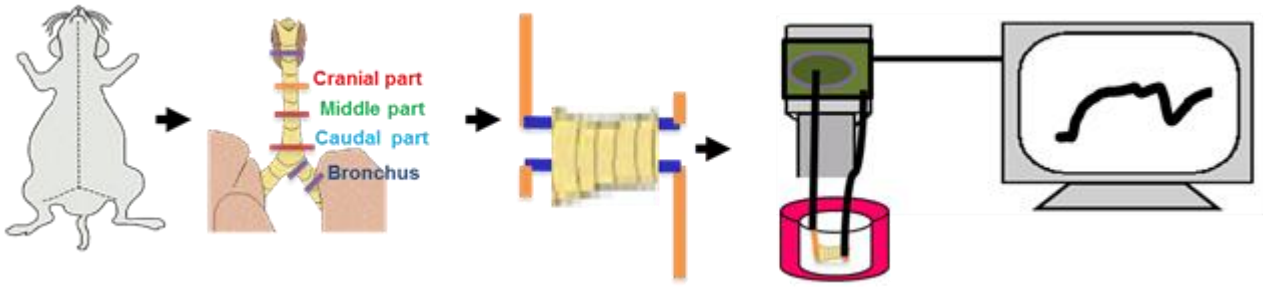

Fig. 2.5 Schematic overview of the organ bath recording method. Briefly, mice are killed by inhalation of an overdose of isoflurane**.** After opening of the chest, the airway was cut as shown to four parts (cranial, middle, caudal trachea and bronchus). Isolated rings were mounted between two stainless steel clips in organ baths exposed to medium gassed with 5% O_2. Constriction is recorded as changes in tension or force**.**

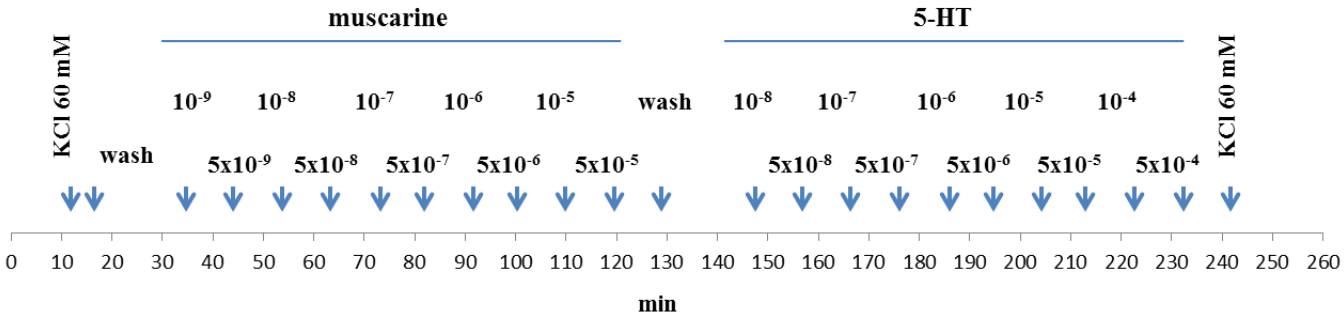

Fig. 2.6 Schematic overview of application schedules of muscarine and 5-HT concentrations. The concentrations are indicated in molarity and were used in the flow-through superfusion chamber in which tracheal or bronchial rings were exposed to medium gassed with 5% O_2

3 Results

3.1 Cavin isoforms expressed in the murine lung and trachea

3.1.1 Expression of cavins (1-4) analyzed by RT-PCR in C57BL/6J mice

The RT-PCR analysis of mRNA isolated from the trachea and lung revealed expression of all cavins and β-actin as a housekeeping gene (Fig. 3.1). The mRNA of cavins was consistently expressed in all trachea and lung preparations. The identity of the amplified products was confirmed by sequencing, and negative controls were run by adding H_2O instead of the DNA template and absence of reverse transcriptase.

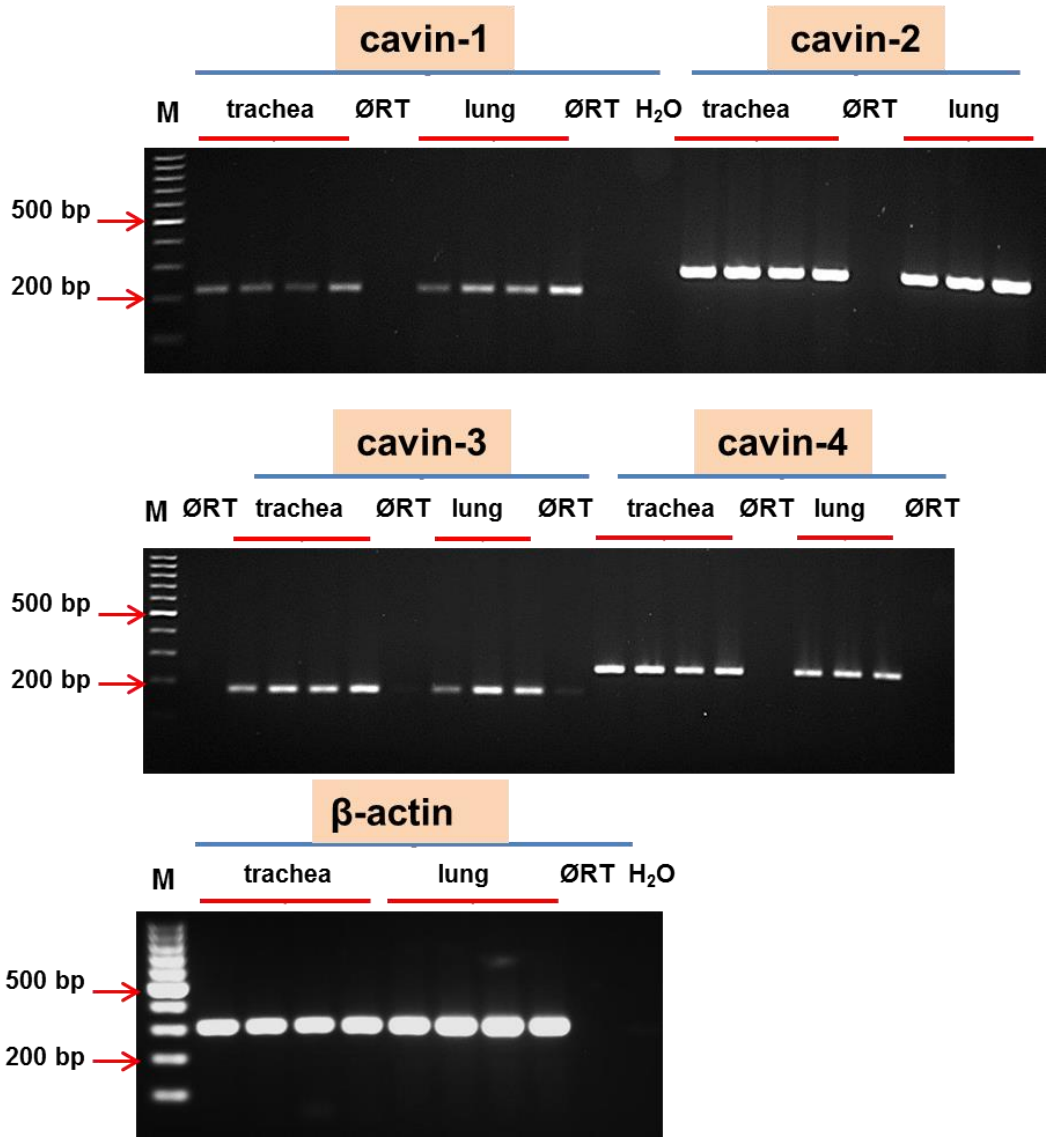

Fig. 3.1 RT-PCR analysis of cavin-1 to -4 in trachea and lung homogenate of C57BL/6J mice. All tested trachea and lung preparations were positive for cavin-1 to -4 mRNAs, as shown in the different mice samples. β-actin as housekeeping gene control was run on all 4 lung and trachea samples. Control reactions included the absence of a template (H_2O) and the absence of reverse transcriptase (ØRT). M = marker.

3.1.2 Expression of cavins analyzed by RT-PCR in tracheal wall compartments

The RT-PCR analysis of mRNA isolated from abraded tracheal epithelium, tracheal muscle and trachea after removing epithelium and muscle revealed expression of cavin-1 and cavin-2. Products corresponding to cavin-3 and cavin-4 were not found in the tracheal epithelium, although they were easily detectable in tracheal muscle and trachea without epithelium and muscle (Fig. 3.2). Negative controls were run by adding H_2O instead of the DNA template and by omission of the RT step and they were indeed negative.

3.1.3 Cavin-1 is more abundantly expressed than cavin-4 in lung and trachea of C57BL/6J mice

Real-time PCR analysis of mRNA isolated from trachea, tracheal different parts and lung revealed a higher expression of cavin-1 compared to cavin-4 gene expression. CT-values are compared to β-actin as a reference gene (Fig. 3.3).

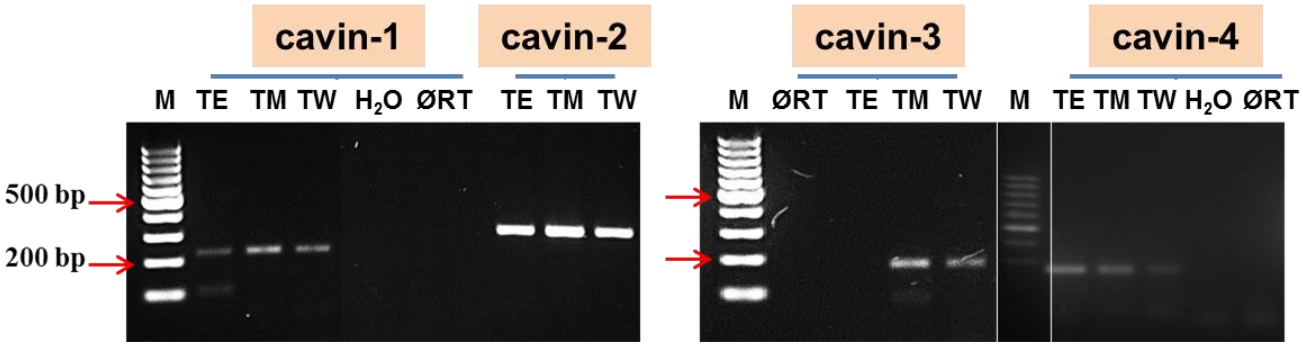

Fig. 3.2 RT-PCR analysis of cavin-1 to -4 in different tracheal wall compartments of C57BL/6J mice. All tested tracheal samples were positive for cavin-1 and -2 mRNAs. The mRNA coding for cavin-3 and -4 was absent in the tracheal epithelium (TE), but it expressed in tracheal muscle (TM) and trachea without epithelium and muscle (TW). Control reactions included the absence of template (H_2O) and the absence of reverse transcriptase in TM sample (Ø RT). M = marker.

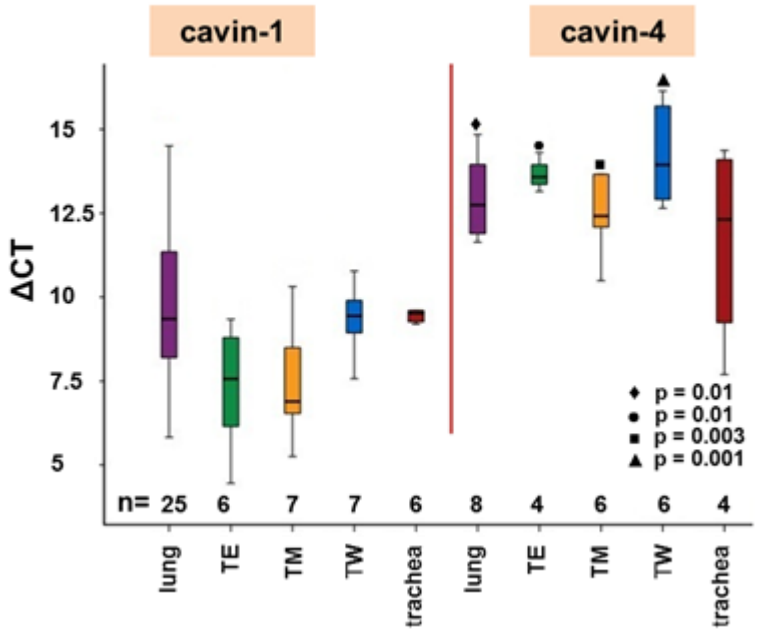

Fig. 3.3 Real-time PCR of cavin-1 and cavin-4 in trachea and lung of C57BL/6J mice. ΔCT of cavin-1 and cavin-4 mRNAs compared to β-actin are shown for trachea, tracheal epithelium (TE), tracheal muscle (TM), trachea without epithelium and muscle (TW) and lung. Lower ΔCT reflects higher expression. As shown for all tissue samples, cavin-1 gene expression is significantly higher than cavin-4 gene expression in the samples from C57BL/6J mice using the Kruskal-Wallis and Mann-Whitney *U*-test, n = number of animals.

3.2 Cavin-1 and cavin-4 tissue distribution parallels that of Cav-1 and Cav-3, respectively

3.2.1 Cavin-1 and Cav-1 tissue distribution in thoracic organs that contain Cav-1-dependent caveolae

The expression of Cav-1 and cavin-1 was assessed by immunohistochemistry. Cardiac capillary and aortic endothelium served as positive control for Cav-1, demonstrating labelling of endothelial cells (Fig. 3.4). Cardiac capillary and aortic endothelial cells were also cavin-1 immunoreactive (Fig. 3.4). The Cav-1- and cavin-1-antibodies clearly stained tracheal basal cells (Fig. 3.4). There was no labelling in the absence of primary antibodies. Similar staining patterns with Cav-1- and cavin-1-antibodies were observed in tracheal and bronchial smooth muscle cells (SMC) (Fig. 3.4).

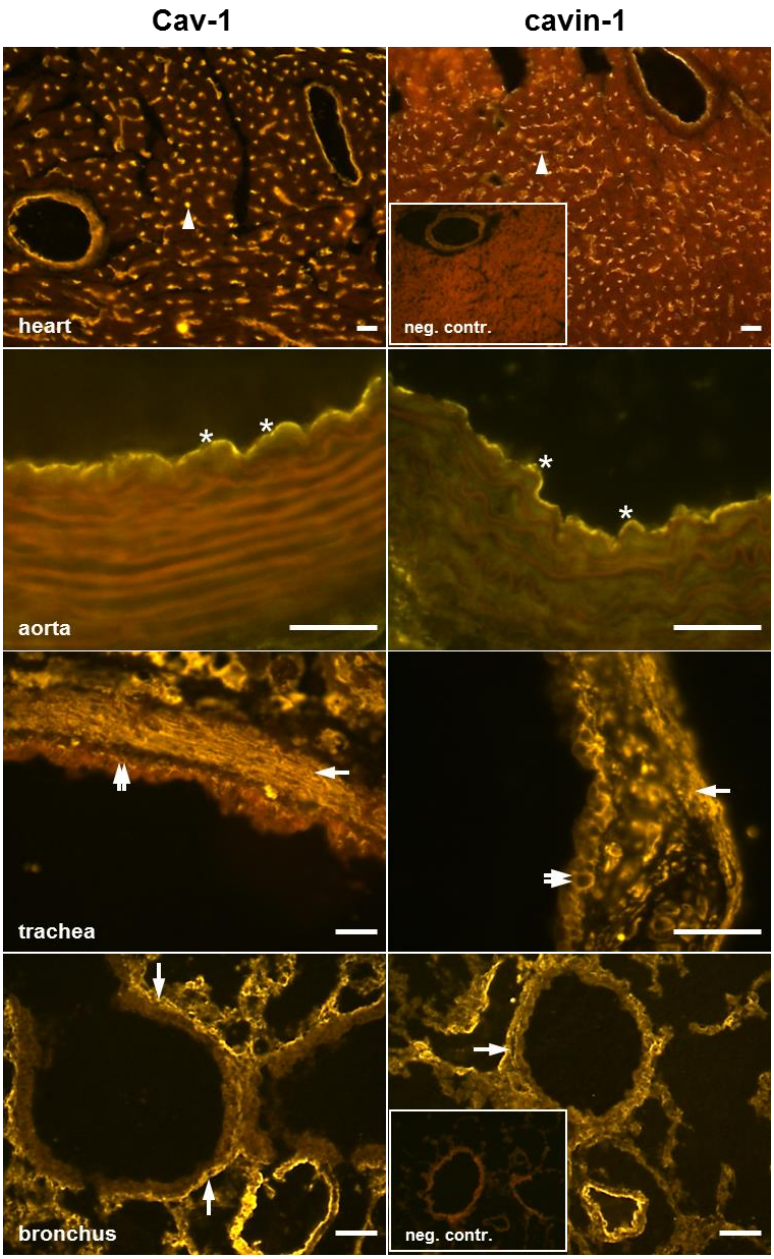

Fig. 3.4 Cavin-1 and Cav-1 tissue distribution in thoracic organs that contain Cav-1-dependent caveolae. Endothelial cells in cardiac capillaries (arrowhead) and aorta (asterisk) are positive for Cav-1 and cavin-1. The antibodies to Cav-1 and cavin-1 label tracheal basal cells (double arrow) and SMC (arrow). The antibodies to Cav-1 and cavin-1 label bronchial SMC (arrow). Negative controls (neg. contr.) were done by omission of the primary antibody. Bar = 50 μm.

3.2.2 Cavin-4 and Cav-3 tissue distribution in thoracic organs containing Cav-3-dependent caveolae

The expression of Cav-3 and cavin-4 was assessed by immunohistochemistry. The heart served as a positive control for Cav-3-immunolabelling, demonstrating labelling of cardiac muscle cells (Fig. 3.5). Cardiac muscle cells were also positive for cavin-4 (Fig. 3.5). Similar staining patterns with Cav-3- and cavin-4-antibodies were observed in tracheal and bronchial SMC (Fig. 3.5). There was no labelling in the absence of primary antibodies.

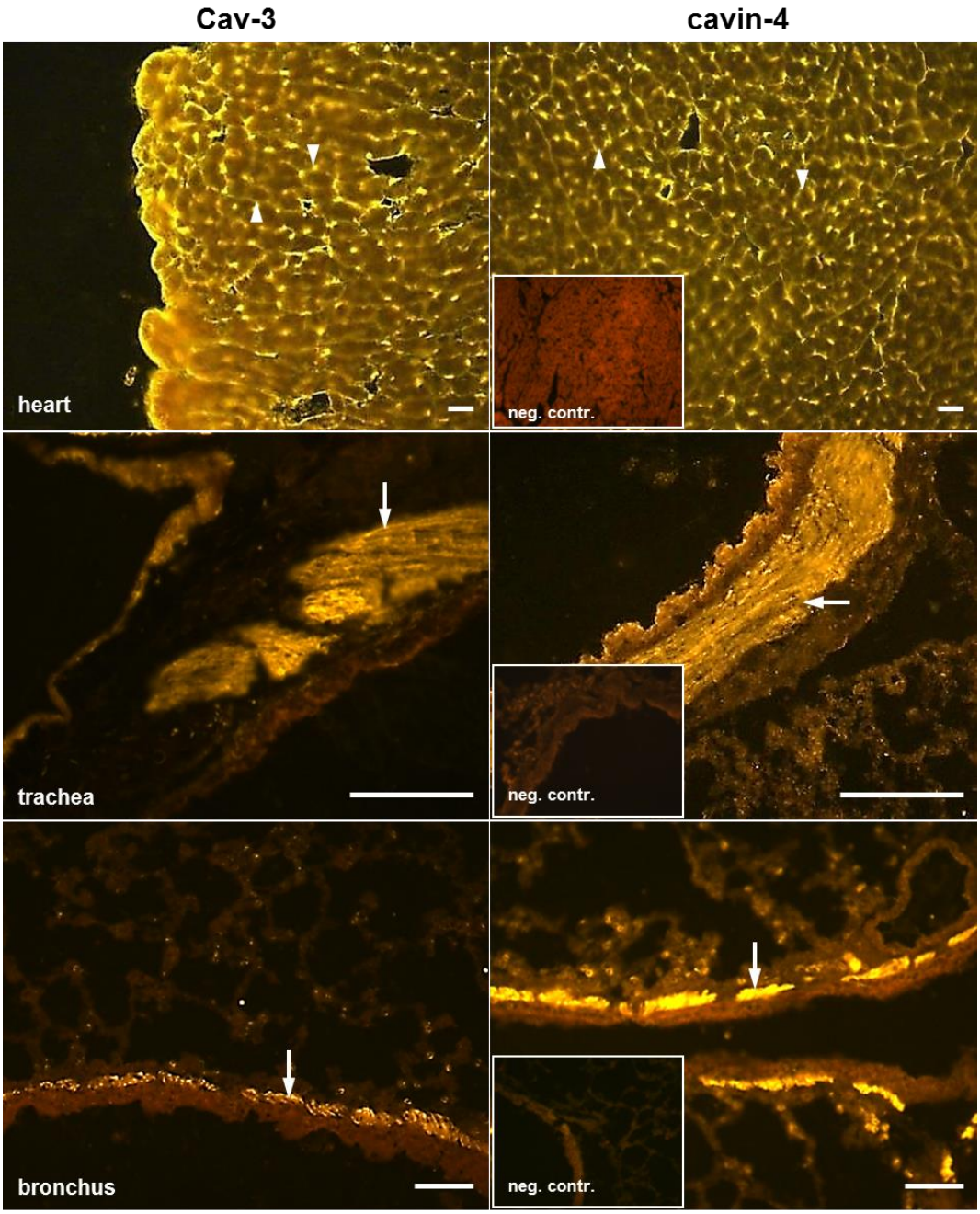

Fig. 3.5 Cavin-4 and Cav-3 tissue distribution in thoracic organs that contain Cav-3-dependent caveolae. The antibodies directed against Cav-3 and cavin-4 label cardiac muscle as a positive control (arrowhead). The

antibodies to cavin-4 and Cav-3 label tracheal and bronchial SMC (arrow). Negative controls (neg. contr.) were done by omission of the primary antibody. Bar = 50 µm.

3.3 Cav-3 and caveolae peripheral components in primary human bronchial smooth muscle cells and human lung

3.3.1 RT-PCR

RT-PCR analysis of mRNA isolated from primary human bronchial SMC revealed expression of Cav-1, Cav-3, cavin-1 and cavin-4. The mRNAs of cavins were consistently expressed in primary human bronchial SMC (Fig. 3.6). The negative controls were done by adding H_2O instead of the DNA template and by omission of the reverse transcription step.

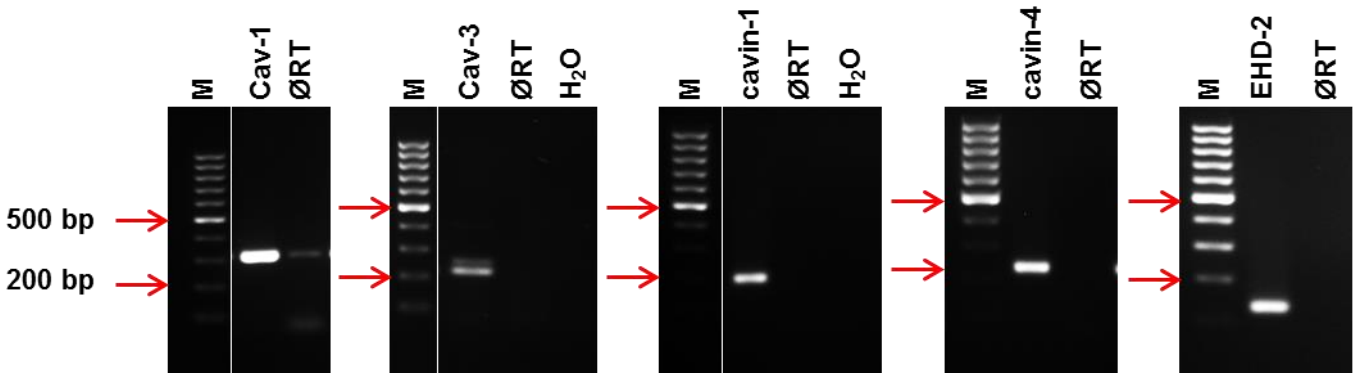

Fig. 3.6 RT-PCR analysis of Cav-1, Cav-3, cavin-1 and cavin-4 in primary human bronchial smooth muscle cells. Positive results were obtained for Cav-1, Cav-3, cavin-1 and cavin-4 mRNAs. Control reactions included the absence of template (H_2O) and absence of reverse transcriptase (Ø RT). M = marker.

3.3.2 Immunohistochemistry

3.3.2.1 Double-labelling immunofluorescence for Cav-1, cavin-1 and cavin-4 with α-SMA in human lung

The protein expression of Cav-1, cavin-1 and cavin-4 was assessed by immunohistochemistry. α-SMA-positive bronchial SMC were immunoreactive for Cav-1, cavin-1 and cavin-4 (Fig. 3.7). Immunofluorescence with antisera directed against Cav-1 showed strong staining of α-SMA-positive cells, while antibodies to the cavins gave a faint staining (Fig. 3.7).

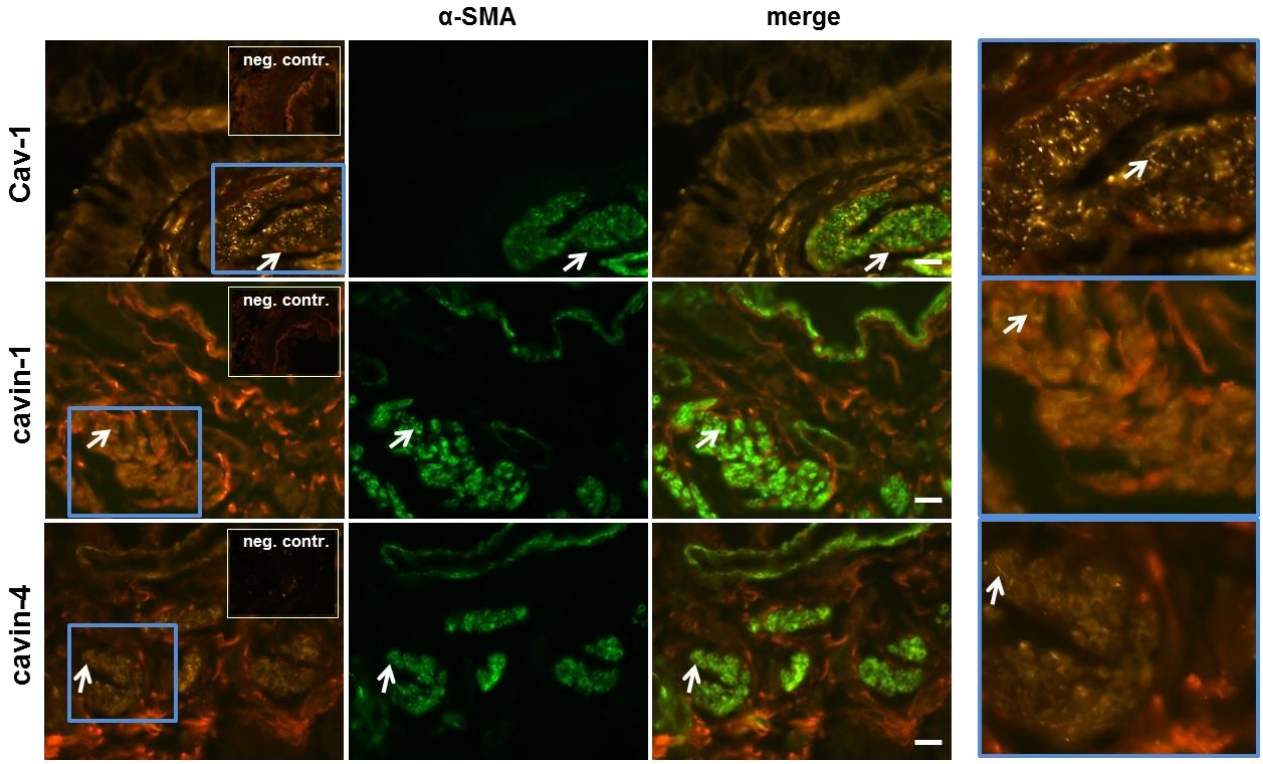

Fig. 3.7 Double-labelling immunofluorescence for Cav-1, cavin-1 and cavin-4 with α-SMA in human bronchi. Immunolabelling for Cav-1, cavin-1 and cavin-4 was found in the bronchial SMC (arrow). α-SMA fluorescence labelling was also demonstrated in the bronchial SMC (arrow, depicted in the green channel). Negative controls (neg. contr.) were done by omission of the primary antibody. In merged images, Cav-1, cavin-1 and cavin-4 are seen in α-SMA-positive SMC. Selected areas of Cav-1-, cavin-1- and cavin-4-staining indicated by blue boxed areas in the left panel are shown at high magnification in the right panel. Bar = 75 µm.

3.3.2.2 Immunoflorescence labelling for Cav-3 in human lung

The protein expression of Cav-3 was assessed by immunohistochemistry using rabbit polyclonal anti-Cav-1+Cav-3 and mouse monoclonal anti-Cav-3-antibodies. Bronchial SMC were immunoreactivite for α-SMA. Immunofluorescence with antisera directed against α-SMA showed strong staining, while antibodies to Cav-3 gave a faint staining (Fig. 3.8). The Nf-68 monoclonal antibody, isotype IgG2, was used as irrelevant antibody isotype control for the monoclonal anti-Cav-3-antibody (Fig. 3.8).

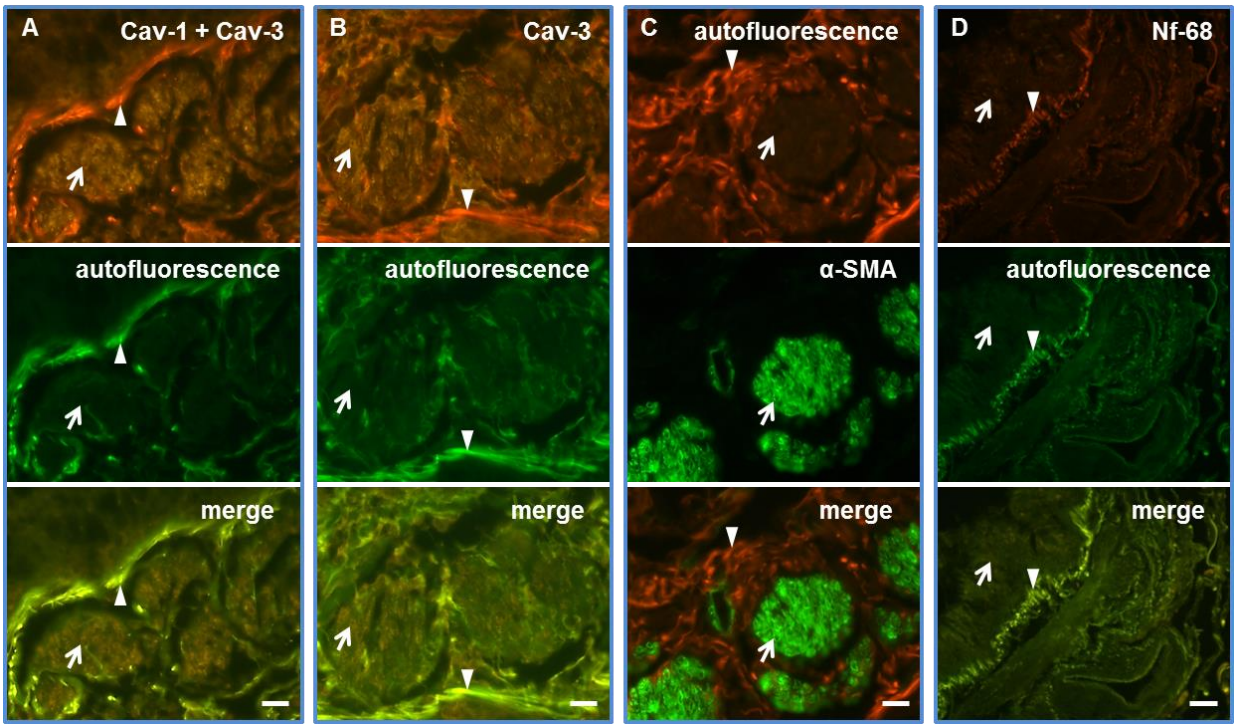

Fig. 3.8 Immunofluorescence labelling for Cav-3 in bronchial smooth muscle cells of human lung. Cav-1- Cav-3- and Cav-3-immunoreactivity were found in bronchial SMC (arrow). α-SMA-immunoreactivity was also observed in the bronchial SMC (arrow). Isotype control was done by incubation with the monoclonal Nf-68-antibody. The autofluorescence of the epithelial basal membrane and of connective tissue fibers is indicated by arrowheads. Bar = 75 µm.

*3.4 Generation of the Cav-3-*loxP*-flanked mouse strain and of general Cav-3 deficient mice*

3.4.1 Genotyping

DNA extracted from tail snips was analyzed by PCR with different primer sets detecting the wild-type and knockout version of the Cav-3 gene as described in section 2.2.2. Samples from animals with the wild-type, heterozygous and *loxP*-flanked Cav-3 gene showed a band of the predicted size, and samples from animals that carried the knockout gene did not present any band (Fig. 3.9A). To confirm the presence of the knockout allele, we did another PCR with a different primer set, and all genotypes of the Cav-3 gene demonstrated a band of the predicted size (Fig. 3.9B). Homozygous Cav-3 knockout and wild-type mice were also checked for Cre transgene and those with deleted Cre were selected for mating and all sets of experiments (Fig. 3.9C). Negative controls were run by adding H_2O instead of the DNA template.

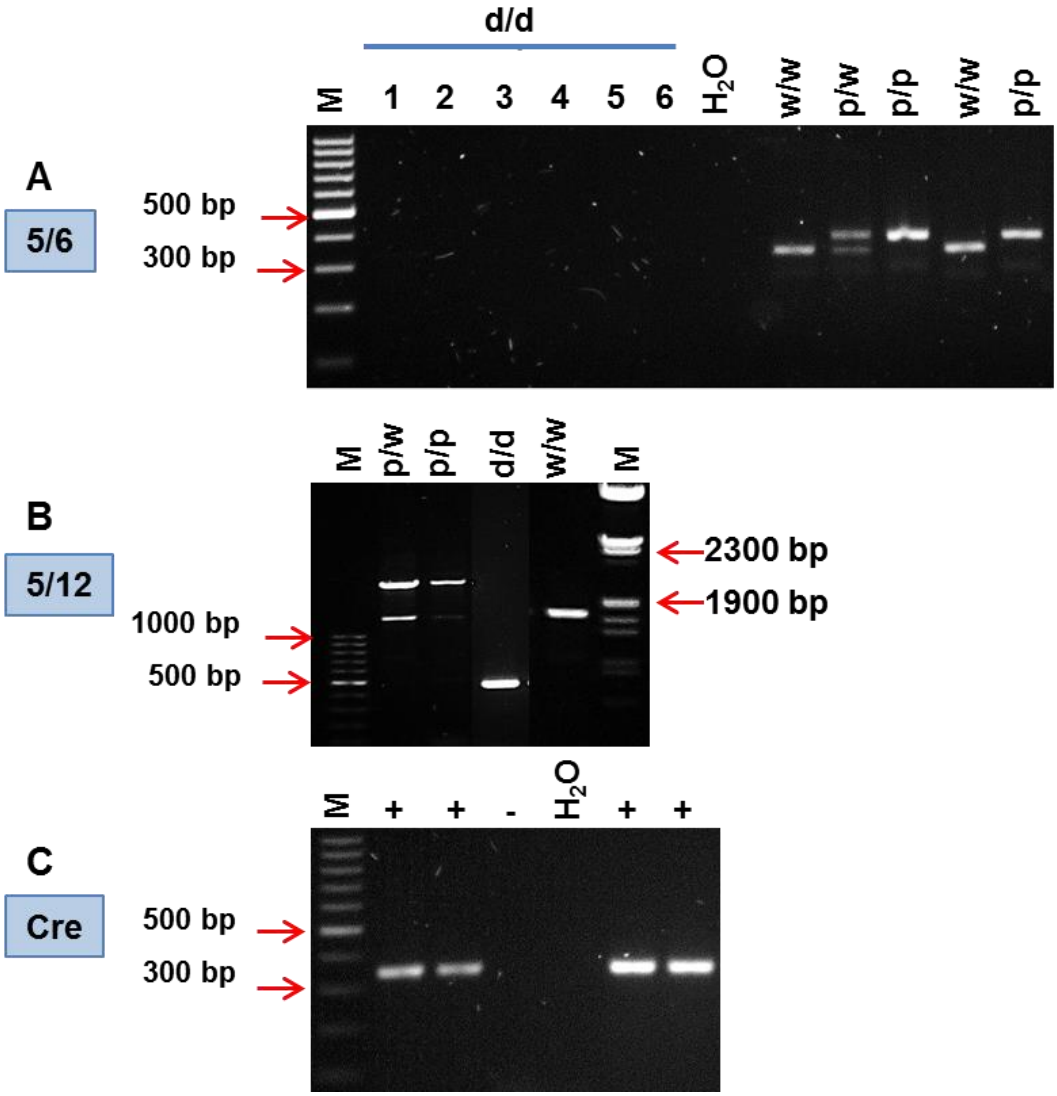

Fig. 3.9 PCR genotyping for Cav-3 deficiency. DNA extracted from tail cuts was analyzed by PCR using different primer sets. (A) 5/6 primers detected wild-type (w/w) and *loxP*-flanked Cav-3 gene (p/p) with amplicons of 323 and 368 base pairs and no amplicon for Cav-$3^{-/-}$ (d/d) mice. (B) Analyses with 5/12 primers detected w/w, p/p and d/d alleles of the Cav-3 gene with 1700, 2000 and 497 bp, respectively. Heterozygous p/w showed bands for wild-type and *loxP*-flanked alleles using both 5/6 and 5/12 primers. (C) PCR analysis with Cre primers showed animals carrying the Cre allele (+). Control reaction included the absence of template (H_2O). M = marker.

3.4.2 Validation by RT-PCR

RT-PCR analysis of mRNA isolated from tracheal wall compartments and lung of Cav-$3^{+/+}$ mice revealed expression of Cav-3 mRNA. Corresponding amplicons were never found in the tracheal wall compartments, bronchus, lung and liver of Cav-$3^{-/-}$ mice (Fig. 3.10). The control runs without template were negative.

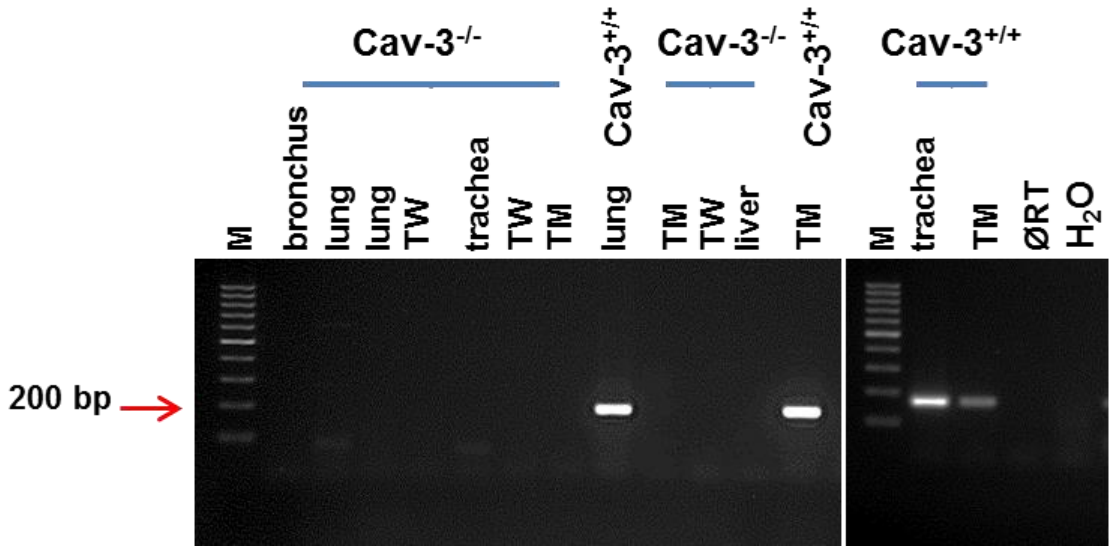

Fig. 3.10 RT-PCR analysis of Cav-3 mRNA in Cav-3$^{+/+}$ and Cav-3$^{-/-}$ mice. Samples from Cav-3$^{+/+}$ mice consistently express mRNA coding for Cav-3, as shown for bronchus, lung, trachea and tracheal muscle (TM). The mRNA coding for Cav-3 is not detected in lung, trachea, liver, TM and trachea without epithelium and muscle (TW) in Cav-3$^{-/-}$ mice. Control reactions included the absence of template (H_2O), and the absence of reverse transcriptase in the trachea (Ø RT). M = marker.

3.4.3 Validation by immunohistochemistry

The Cav-3 localization was assessed by immunohistochemistry. Tracheal epithelium and SMC were immunoreactive for Cav-3 in Cav-3$^{+/+}$ mice (Fig. 3.11). Bronchial and pulmonary arterial SMC were also immunoreactive for Cav-3 in Cav-3$^{+/+}$ mice. Cav-3 staining was predominantly localized near the cell membrane. The polyclonal antibody to Cav-3 did not show any labelling in Cav-3$^{-/-}$ mice (Fig. 3.11). α-SMA-Immunoreactivity was observed in tracheal, bronchial and pulmonary arterial SMC of both strains (Fig. 3.11). The specificity of the Cav-3-antibody was validated by Western blotting (see 3.4.4).

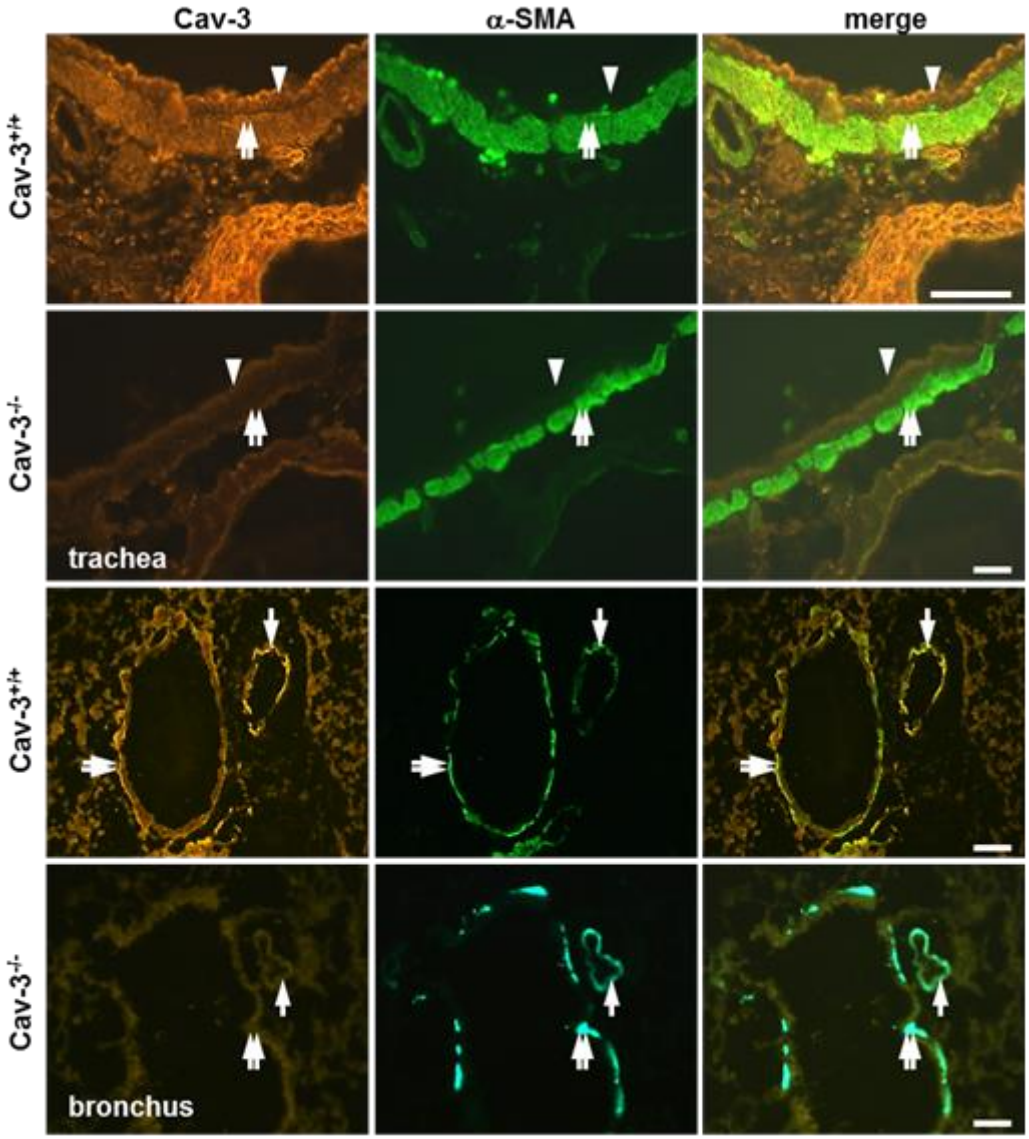

Fig. 3.11 Double-labelling immunofluorescence for Cav-3 and α-SMA in Cav-3$^{+/+}$ and Cav-3$^{-/-}$ mice. Cav-3 immunoreactivity is seen in the tracheal epithelium (arrowhead), both tracheal and bronchial SMC (double arrow) and pulmonary arterial smooth muscle (arrow) in Cav-3$^{+/+}$ mice. α-SMA-immunoreactivity is observed in the SMC of trachea, bronchus and pulmonary artery. No Cav-3 labelling is noted in Cav-3$^{-/-}$ mice, although they show labelling for α-SMA in trachea and bronchial SMC. Bar = 50 µm.

3.4.4 Validation by Western blotting

Crude tissue lysates were loaded onto a 10% polyacrylamide gel in concentrations of 40 µg/µl, 50 µg/µl and 60 µg/µl (Fig. 3.12 A-C). The gels were stained with Coomassie dye to visualize the protein bands. Crude tissue lysate (50 µg/µl) in which all the protein bands were well-separated was selected for all Western blots.

Western blotting supported the immunohistochemical findings since the Cav-3-antibody recognized Cav-3, a ≈20 kDa band, in protein preparations from Cav-3$^{+/+}$ mice while it did not label a band in protein extracts from Cav-3$^{-/-}$ mice. This immunoblot confirmed the

specificity of the Cav-3-antibody (Fig. 3.13). SDH-A was immunolabeled in protein preparations from both Cav-$3^{-/-}$ and Cav-$3^{+/+}$ mice as a reference control.

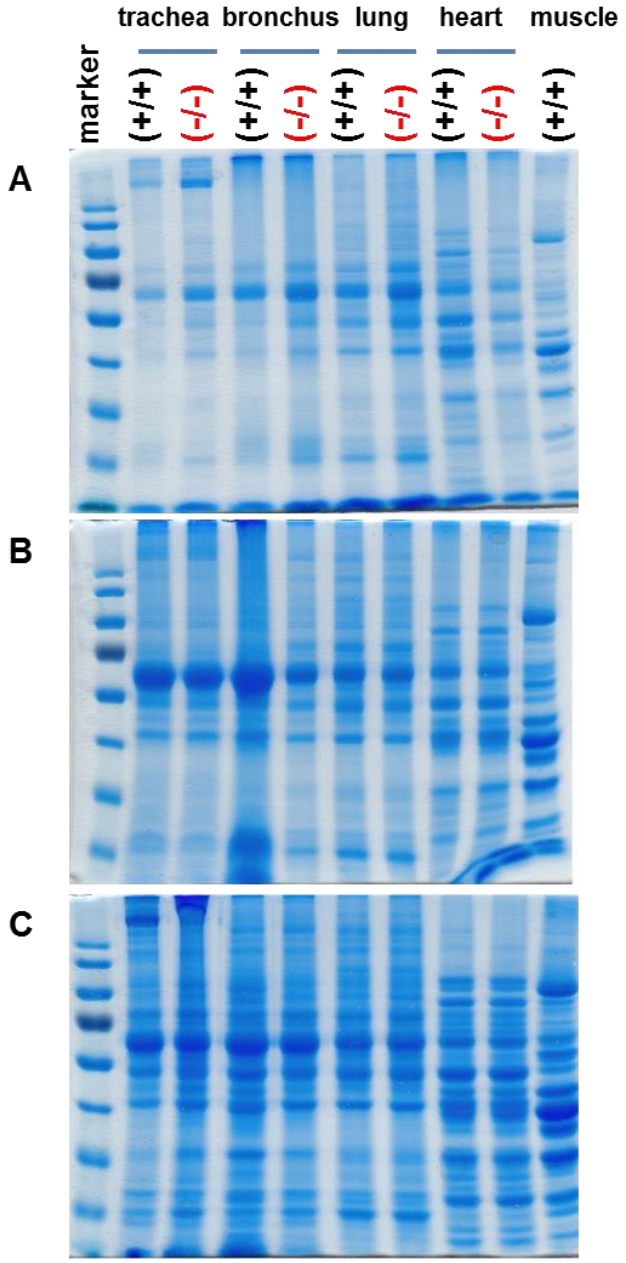

Fig. 3.12 Selection of protein concentration for immunoblots. Crude tissue lysates from trachea, bronchus, lung, heart and skeletal muscle were loaded onto a 10% polyacrylamide gel in (A) 40 µg/µl, (B) 50 µg/µl and (C) 60 µg/µl concentrations. The gels were stained with Coomassie brilliant blue dye. Samples were from Cav-$3^{+/+}$ (+/+) and Cav-$3^{-/-}$ (-/-) mice.

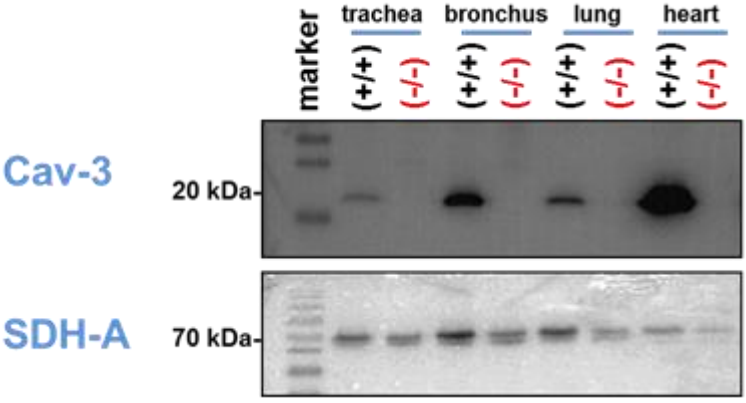

Fig. 3.13 Cav-3 immunoblots. No Cav-3 immunolabelling is present in Cav-$3^{-/-}$ mice samples, while the antibody recognizes a single 20 kDa protein band in protein extracts from Cav-$3^{+/+}$ mice samples. Our own laboratory polyclonal antibody to SDH-A labels a protein band at 70 kDa in all Cav-$3^{-/-}$ and Cav-$3^{+/+}$ mice samples as reference control.

3.5 Cav-3 deficiency: No significant difference in the expression of caveolin and peripheral caveolar components in airways

3.5.1 RT-PCR and real-time PCR

The mRNAs of cavin-1, cavin-4, Cav-1 and EHD2 were consistently expressed in samples from Cav-$3^{+/+}$ and Cav-$3^{-/-}$ mice (Fig. 3.14A). The control runs without template were negative. Quantification of relative expression of Cav-1, cavin-1, cavin-4 and EHD2 was done by real-time PCR. CT-values were compared to β-actin as reference gene. In Cav-$3^{+/+}$ mice, the Cav-1 expression in tracheal muscle was higher than in Cav-$3^{-/-}$ mice. Otherwise, the expression of all tested genes was similar in Cav-$3^{-/-}$ and Cav-$3^{+/+}$ mice (Fig. 3.14B).

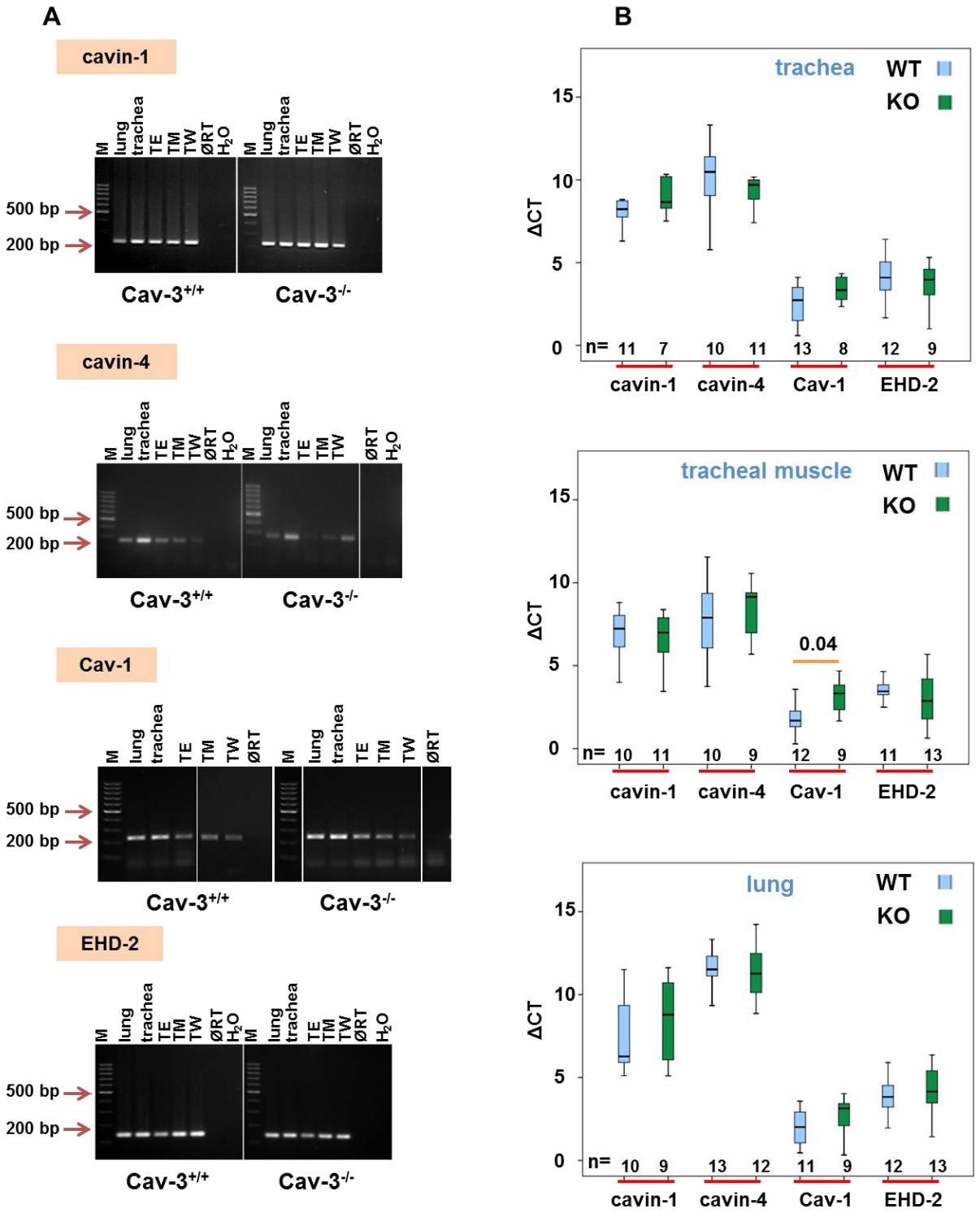

Fig. 3.14 mRNA expression of cavin-1, cavin-4, Cav-1 and EHD-2 in Cav-3$^{+/+}$ and Cav-3$^{-/-}$ mice. (A) Cavin-1, cavin-4, Cav-1 and EHD-2 mRNAs were detected by RT-PCR in abraded tracheal epithelium (TE), tracheal muscle (TM), trachea, lung and trachea without epithelium and muscle (TW) of both Cav-3$^{+/+}$ and Cav-3$^{-/-}$ mouse strains. Control reactions for each primer pair included the absence of template (H_2O) and absence of reverse transcriptase in the lung (Ø RT). (B) Real-time PCR for cavin-1, cavin-4, Cav-1 and EHD-2 in Cav-3$^{+/+}$ and Cav-3$^{-/-}$ mice tissue homogenates, relative expression is presented as ΔCT compared to β-actin. A significant difference (Mann-Whitney *U*-test) between Cav-3$^{-/-}$ and Cav-3$^{+/+}$ mice was seen only for Cav-1 in tracheal muscle. Lower ΔCT reflects higher expression.

3.5.2 Western blotting

Blots for the lung, trachea and main bronchus were processed and exposed simultaneously (Fig. 3.15A, B), such that the intensity of the bands gives information on the relative abundance of Cav-1, cavin-1, cavin-4 and EHD2 compared to β-tubulin in that tissue. There were no significant differences between Cav-$3^{-/-}$ and Cav-$3^{+/+}$ mice in the trachea, bronchus and lung (Fig. 3.15A).

Western blotting supported the immunohistochemical findings that Cav-1, cavin-1 and cavin-4 were detected in the tracheal muscle of both Cav-$3^{+/+}$ and Cav-$3^{-/-}$ mice (Fig. 3.16). In the Western blots of tracheal epithelium homogenates, neither cavin-1 and cavin-4 nor Cav-2 proteins were detected in Cav-$3^{+/+}$ and Cav-$3^{-/-}$ mice (Fig. 3.16). Tubulin as reference control was consistently detected in all trachea and bronchus preparations (Fig. 3.16).

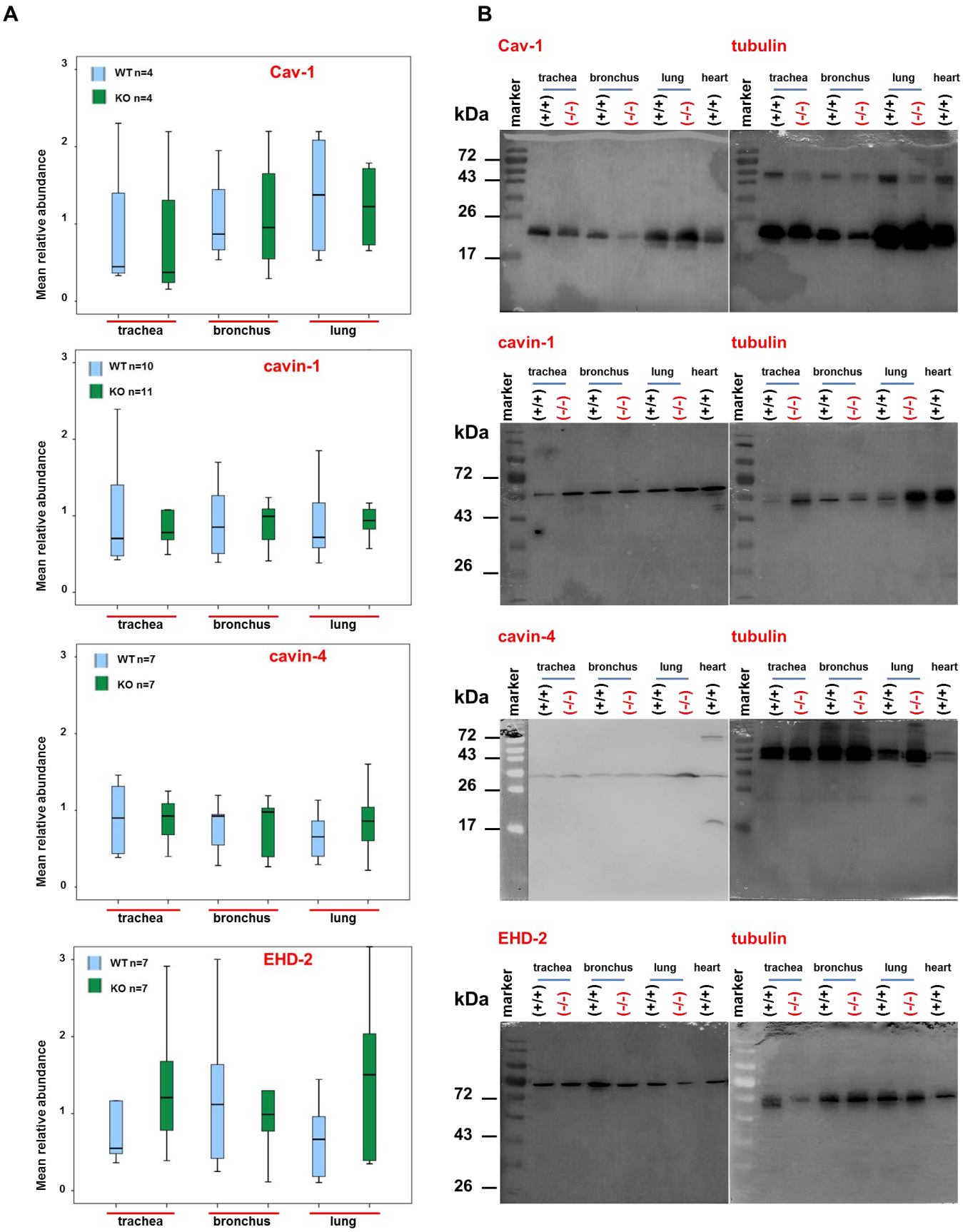
A
WT n=4
KO n=4
Cav-1
Mean relative abundance
trachea
bronchus
lung
WT n=10
KO n=11
cavin-1
WT n=7
KO n=7
cavin-4
EHD-2
B
Cav-1
tubulin
cavin-1
cavin-4
EHD-2
marker
kDa
72
43
26
17
heart
(+/+)
(-/-)

Fig. 3.15 Expression of Cav-1, cavin-1, cavin-4 and EHD-2 proteins in Cav-3$^{+/+}$ and Cav-3$^{-/-}$ mice. (A) The expression of Cav-1, cavin-1, cavin-4 and EHD-2 proteins from Cav-3$^{+/+}$ and Cav-3$^{-/-}$ mice estimated by a densitometric analysis of Western blots is presented in the box plots depicting quartiles from 0 to 100. There was no significant difference in the mean relative abundance of Cav-1, cavin-1, cavin-4 and EHD-2 to tubulin as reference control in the preparations from Cav-3$^{+/+}$ and Cav-3$^{-/-}$ mouse strains using the Mann-Whitney *U*-test. (B) Representative Western blots demonstrating the detection of Cav-1, cavin-1, cavin-4, EHD-2 and tubulin (as reference control) in trachea, bronchus, lung and heart homogenate of both mouse strains.

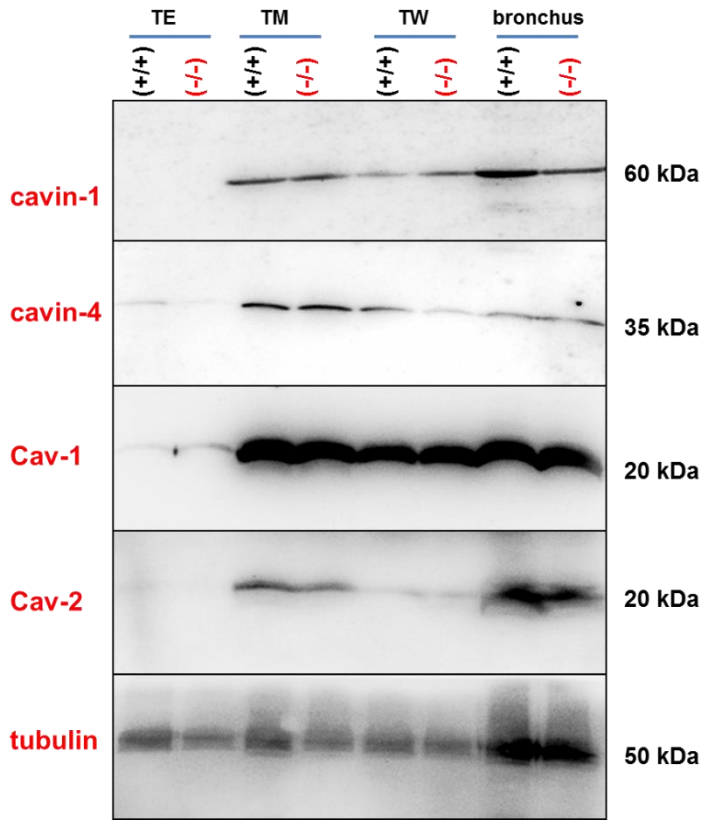

Fig. 3.16 Expression of Cav-1, cavin-1, cavin-4 and EHD-2 proteins in tracheal wall compartments and bronchus from Cav-3$^{+/+}$ and Cav-3$^{-/-}$ mice. Either cavin-1 or cavin-4 immunolabelling are present in the tracheal muscle (TM), bronchus and trachea without epithelium and smooth muscle (TW), while just cavin-4 antibody recognizes a single protein band in tracheal epithelium (TE). Cav-1 staining is strong in TM, TW and bronchus, while faint in TE. Cav-2 staining is distinct in TM and bronchus, while faint in TW. Tubulin-immunolabelling is observed in the preparations from Cav-3$^{+/+}$ and Cav-3$^{-/-}$ mice.

3.5.3 Immunohistochemistry

The polyclonal antibody to Cav-3 labelled tracheal SMC (arrowhead) and cardiomyocytes of the pulmonary vein (arrow) in Cav-3$^{+/+}$ mice (Fig. 3.17). This antibody did not show any labelling in tracheal SMC and cardiomyocytes of the pulmonary vein from Cav-3$^{-/-}$ mice (Fig. 3.17). The specificity of the Cav-3-antibody was further tested by Western blotting (see 3.4.4). Similar patterns of immunolabeling for Cav-1, cavin-1 and cavin-4 in tracheal muscle were observed in both Cav-3$^{-/-}$ and Cav-3$^{+/+}$ mouse strains (Fig. 3.17).

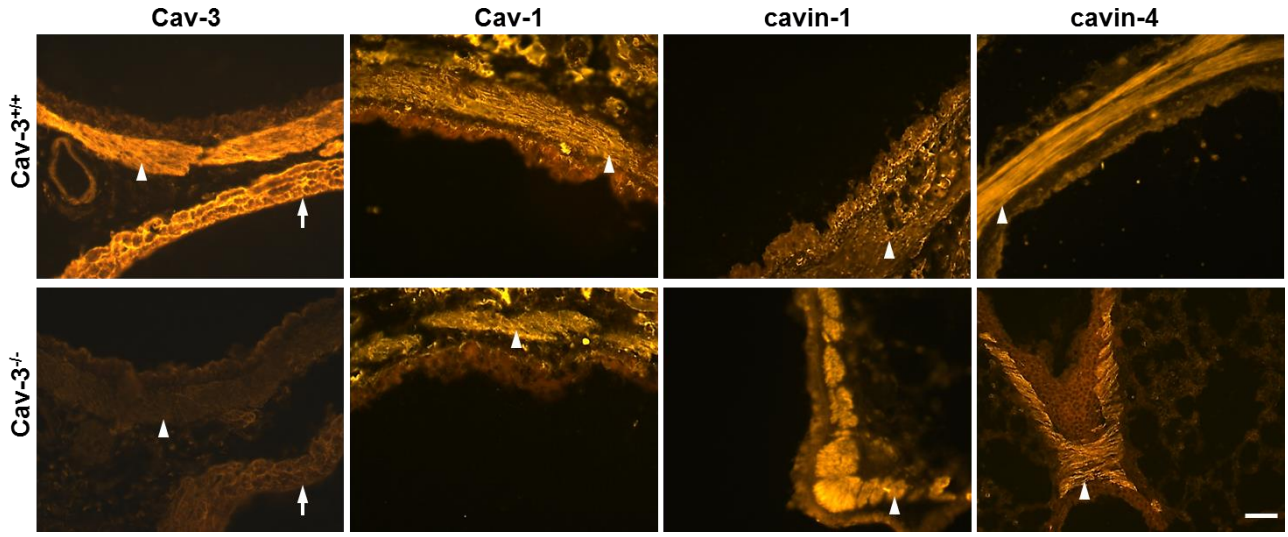

Fig. 3.17 Immunolabelling for Cav-3, Cav-1, cavin-1 and cavin-4 in Cav-3$^{+/+}$ and Cav-3$^{-/-}$ mice. Cav-3-immunoreactivity is seen in tracheal SMC (arrowhead) and cardiomyocytes of the pulmonary vein (arrow) in Cav-3$^{+/+}$ mice, but not in Cav-3$^{-/-}$ mice. Tracheal SMC are Cav-1-, cavin-1- and cavin-4-immunoreactive (arrowhead) in both mouse strains. Bar = 50 µm.

3.6 Interactions of caveolins and cavins

3.6.1 Cav-1 and Cav-3

Homogenized tissue lysates containing equal amounts of total protein were incubated with an anti-Cav-1-antibody. Antigen-antibody complexes were captured with agarose beads and bound proteins solubilized in a SDS sample buffer. Samples from co-immunoprecipitation (CO-IP) were resolved by 12% SDS-PAGE, transferred onto a PVDF membrane, and analyzed by probing with the antibody against Cav-3. No Cav-3-immunolabelling was present in samples from Cav-3$^{-/-}$ mice, while the antibody recognized a single 20 kDa band in samples from Cav-3$^{+/+}$ mice, confirming the specificity of the anti-Cav-3-antibody. Heart and skeletal muscle were used as CO-IP positive controls.

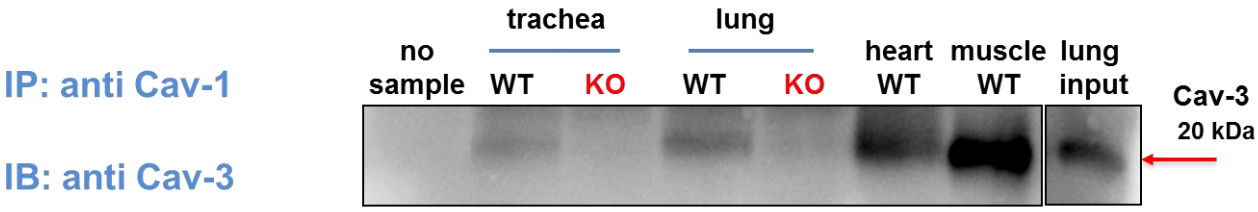

Fig. 3.18 CO-IP of Cav-1 and Cav-3 in Cav-3$^{+/+}$ (WT) and Cav-3$^{-/-}$ (KO) mice. Immunoprecipitates (IP) with Cav-1 are immunoblotted (IB) for Cav-3. Positive CO-IP controls include heart and skeletal muscle from Cav-3$^{+/+}$ mice. Lung input as intact protein lysate from Cav-3$^{+/+}$ mice is blotted and the expression level of Cav-3 protein is observed with longer exposure time. The negative control of CO-IP includes beads and antibody in the absence of lysate (no sample).

3.6.2 Cavin-1 and cavin-4

Homogenized tissue lysates containing equal amounts of total proteins were incubated with the anti-cavin-1-antibody. Samples from CO-IP were resolved by 10% SDS-PAGE, transferred onto a PVDF membrane, and analyzed by probing with an antibody against cavin-4. Cavin-4-immunolabelling was present in samples from the trachea, lung and skeletal muscle from Cav-$3^{+/+}$ mice. The antibody recognized a single 35 kDa protein band. In the lung input as intact protein lysate from Cav-$3^{+/+}$ mice, only a band at 65 kDa was detected (Fig. 3.19A). This could be because of a technical problem and shift of the band in lower molecular weights to the right side of the gel and exiting from the gel. Furthermore, we did Western blot from the intact protein lysates in a different blot to show cavin-4 expression level (Fig. 3.19B). The antibody recognized a 35 kDa protein band in lung input and pooled tracheal muscle from Cav-$3^{+/+}$ mice (Fig. 3.19B). In addition, in the highly concentrated lung lysate (60 µg/µl), an additional band at 65 kDa was detected which might represent a homodimer of cavin-4 (Fig. 3.19B).

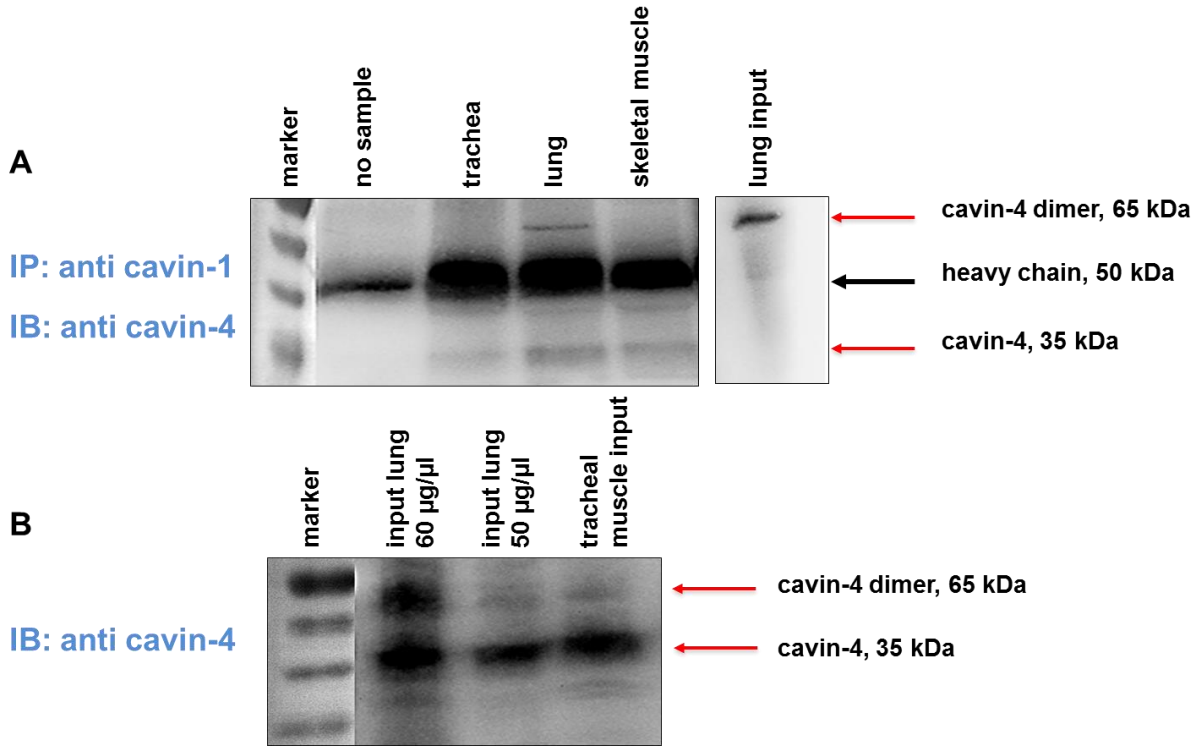

Fig. 3.19 CO-IP of cavin-1 and cavin-4 in Cav-$3^{+/+}$ mice. (A) Immunoprecipitates (IP) with cavin-1 are immunoblotted (IB) for cavin-4. Skeletal muscle serves as positive control. The negative control of CO-IP is done by running beads and antibody in the absence of lysate (no sample). In the lung input as intact protein lysate, the band at 65 kDa might represent a cavin-4 dimer. The presence of heavy chains of co-eluted antibody in the CO-IP products is observed. (B) Western blots of lysate without immunoprecipitation. The blot visible marker is merged and shown on the left using the fusion Fx program.

3.6.3 Cav-1 and cavin-1

Homogenized tissue lysates containing equal amounts of total proteins were incubated with the anti-Cav-1-antibody. Samples from CO-IP were resolved by 10% SDS-PAGE, transferred onto a PVDF membrane, and analyzed by probing with an antibody against cavin-1. Cavin-1-immunolabelling was present in the samples from Cav-3$^{-/-}$ and Cav-3$^{+/+}$ mice (Fig. 3.20). The antibody recognized a single 60 kDa protein band which was also detected in lysate from trachea and lung input of Cav-3$^{+/+}$ mice. The heart and skeletal muscle were used as positive controls. In the skeletal muscle, an additional band at 75 kDa was immunolabeled.

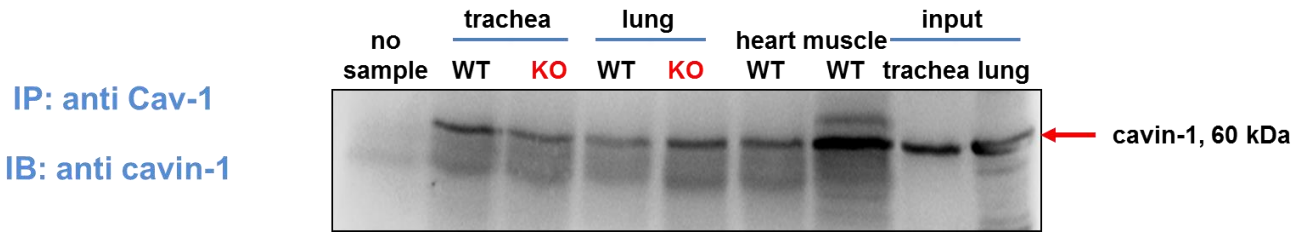

Fig. 3.20 CO-IP of Cav-1 and cavin-1 in the Cav-3$^{+/+}$ (WT) and Cav-3$^{-/-}$ (KO) mice. Immunoprecipitates (IP) with Cav-1 are immunoblotted (IB) for cavin-1. CO-IP, representing Cav-1-cavin-1 interaction in all tissue homogenates of Cav-3$^{+/+}$ and Cav-3$^{-/-}$ mice. The positive CO-IP controls include heart and skeletal muscle from Cav-3$^{+/+}$ mice. The negative control of CO-IP includes beads and antibody in the absence of lysate (no sample). The trachea and lung input as intact protein lysate are blotted to show the cavin-1 expression level.

3.6.4 Cav-3 and cavin-1

Homogenized tissue lysates from Cav-3$^{+/+}$ mice containing equal amounts of total proteins were incubated with the anti-Cav-3-antibody. Samples from CO-IP were resolved by 10% SDS-PAGE, transferred onto a PVDF membrane, and analyzed by probing with the antibody against cavin-1. Cavin-1-immunolabelling was present in lung and trachea samples. The antibody recognized a single 60 kDa protein band (Fig. 3.21). No cavin-1 labeling was present in Cav-3-precipitates from skeletal muscle. The lung input as intact protein lysate was blotted to show the expression level of cavin-1 protein.

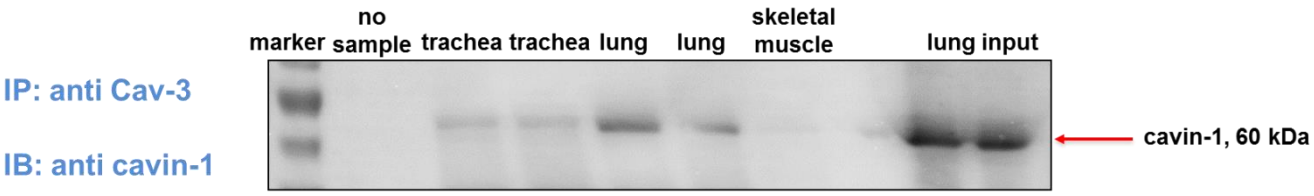

Fig. 3.21 CO-IP of Cav-3 and cavin-1 in the Cav-3$^{+/+}$ mice. Immunoprecipitates (IP) with Cav-3 are immunoblotted (IB) for cavin-1. CO-IP, representing Cav-3-cavin-1 interaction in trachea and lung homogenates. In skeletal muscle no interaction of Cav-3 and cavin-1 proteins is observed. The negative control

of CO-IP includes beads and antibody in the absence of lysate (no sample). The lung input as intact protein lysate is blotted to show the cavin-1 expression level. The blot visible marker is merged and shown on the left using the fusion Fx program.

3.6.5 Cav-3 and cavin-4

Homogenized tissue lysates containing equal amounts of total proteins were incubated with the anti-Cav-3-antibody. Samples from CO-IP were resolved by 10% SDS-PAGE, transferred onto a PVDF membrane, and analyzed by probing with an antibody against cavin-4. Cavin-4-immunolabelling was present in Cav-$3^{+/+}$ mice samples. The antibody recognized a single 35 kDa protein band. Cavin-4-immunolabelling was present in the trachea, lung and very faintly in skeletal muscle samples (Fig. 3.22). In the lung lysate, only a band at 65 kDa was detected. This could be because of a technical problem and shift of the band in lower molecular weights to the right side of the gel and exiting from the gel.

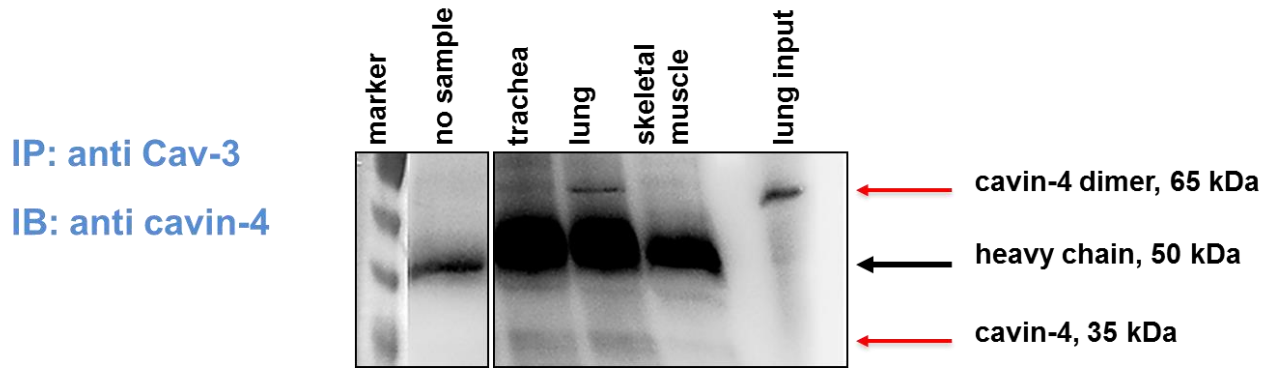

Fig. 3.22 CO-IP of Cav-3 and cavin-4 in the Cav-$3^{+/+}$ mice. Immunoprecipitates (IP) with Cav-3 are immunoblotted (IB) for cavin-4. CO-IP is representing Cav-3-cavin-4 interaction in all tissue homogenates of Cav-$3^{+/+}$ mice. The positive CO-IP control includes skeletal muscle which very faintly shows this interaction. The negative control of CO-IP includes beads and antibody in the absence of lysate (no sample). In the lung input, the band at 65 kDa might represent a cavin-4 dimer. The presense of heavy chains of co-eluted antibody in the CO-IP products is observed. The blot visible marker is merged and shown on the left using the fusion Fx program.

3.7 Role of Cav-3 for muscarine- and 5-HT-induced constriction in murine extrapulmonary airways

3.7.1 Muscarine-induced constriction

All segments of extrapulmonary airways, form cranial trachea to main bronchus, exhibited a concentration-dependent muscarinic contraction. Neither in absolute force nor in reactivity related to KCl-induced contraction (Figs. 3.23-3.26) nor in EC50 (Tab. 3.3), a significant difference between airways taken from Cav-$3^{-/-}$ and Cav-$3^{+/+}$ mice was observed. In both

strains, the contraction evoked by 10^{-5} M muscarine was not significantly enhanced further at higher concentrations in all segments.

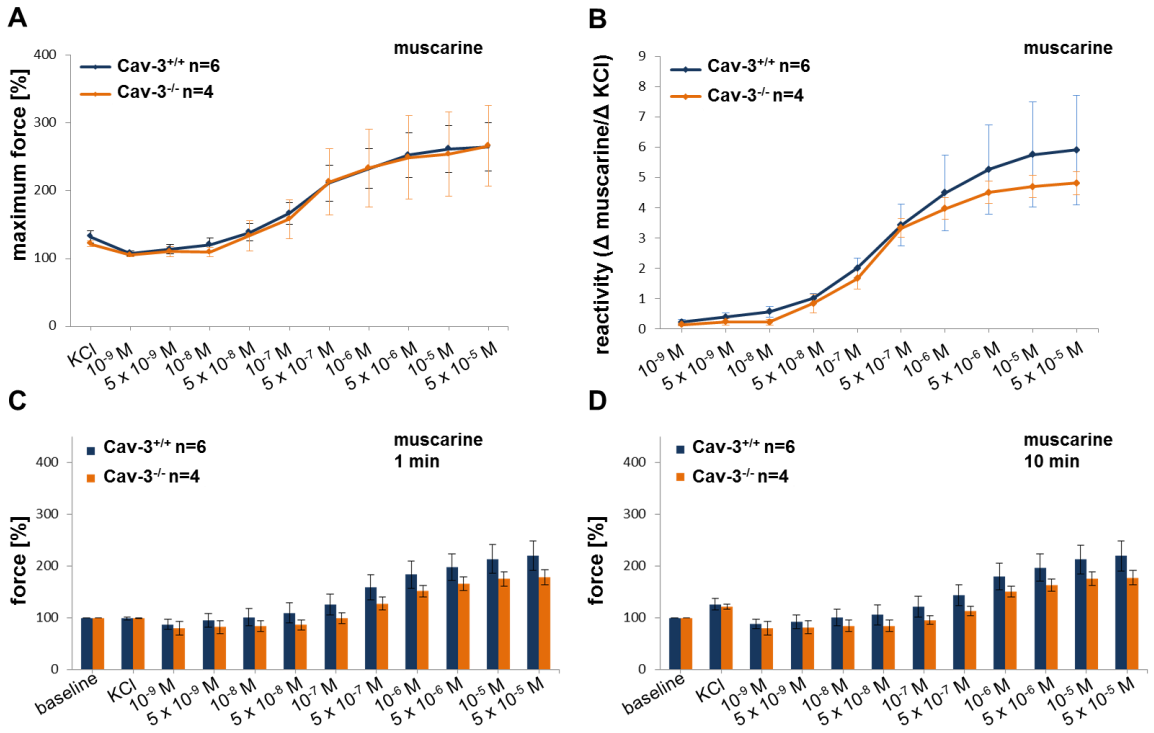

Fig. 3.23 Muscarine-induced contraction of cranial trachea from Cav-$3^{+/+}$ and Cav-$3^{-/-}$ mice in organ bath experiments. Concentration-dependent responses are shown as maximum reaction in force (A) and reactivity related to KCl-induced contraction (B), and as force developed 1 min (C) and 10 min (D) after application of muscarine. KCl (60 mM) was applied as a viability control for 5 min, and the prestimulus value was set as 100%. Data are presented as mean ± SEM. In neither parameter, a significant difference between samples from Cav-$3^{+/+}$ and Cav-$3^{-/-}$ mice was observed (Mann-Whitney *U*-test).

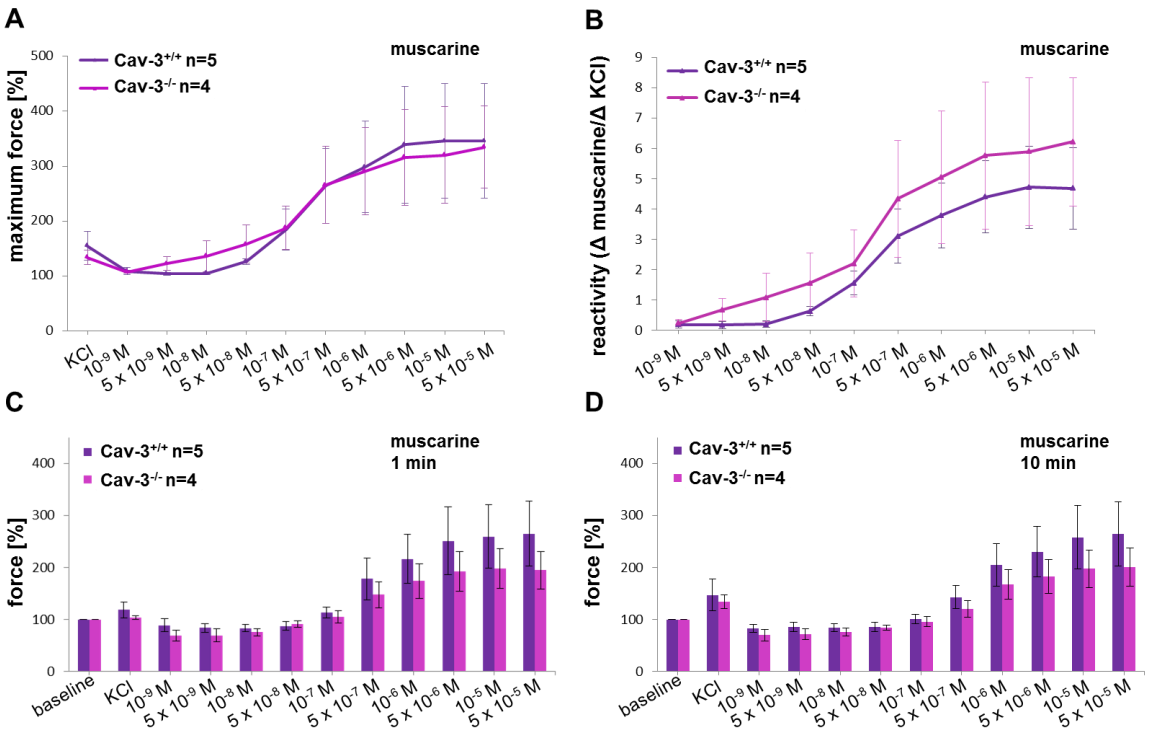

Fig. 3.24 Muscarine-induced contraction of middle trachea from Cav-3$^{+/+}$ and Cav-3$^{-/-}$ mice in organ bath experiments. Concentration-dependent responses are shown as maximum reaction in force (A) and reactivity related to KCl-induced contraction (B), and as force developed 1 min (C) and 10 min (D) after application of muscarine. KCl (60 mM) was applied as a viability control for 5 min, and the prestimulus value was set as 100%. Data are presented as mean ± SEM. In neither parameter, a significant difference between samples from Cav-3$^{+/+}$ and Cav-3$^{-/-}$ mice was observed (Mann-Whitney *U*-test).

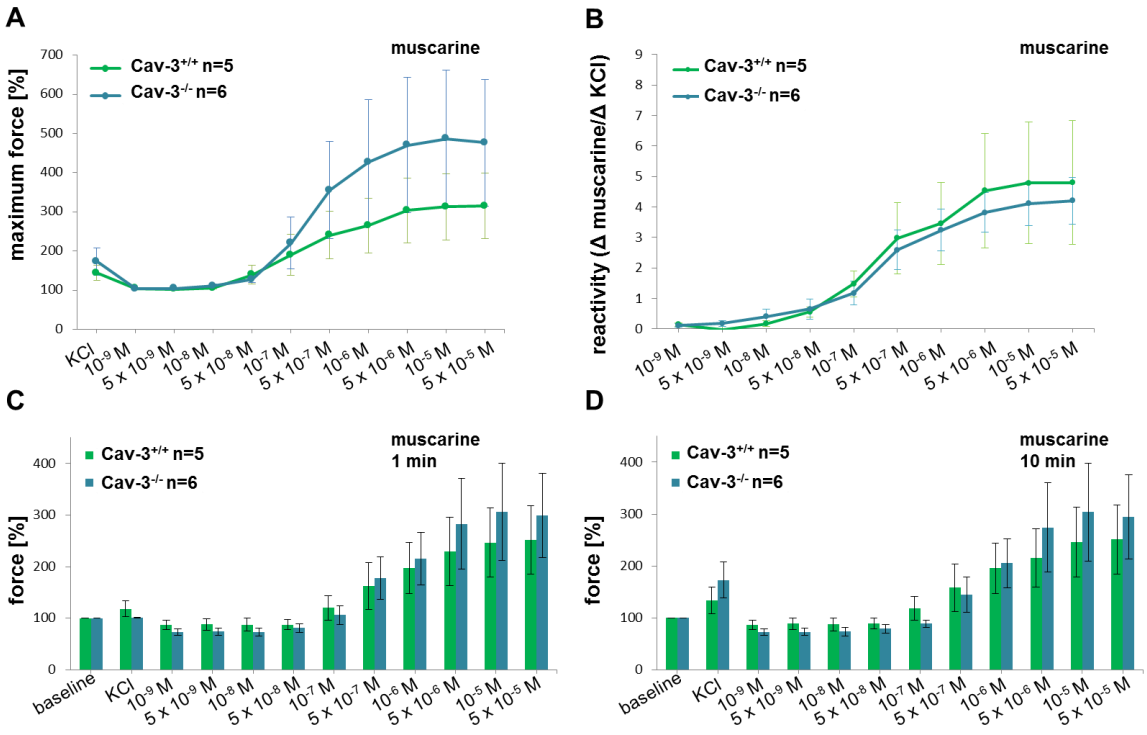

Fig. 3.25 Muscarine-induced contraction of caudal trachea from Cav-3$^{+/+}$ and Cav-3$^{-/-}$ mice in organ bath experiments. Concentration-dependent responses are shown as maximum reaction in force (A) and reactivity related to KCl-induced contraction (B), and as force developed 1 min (C) and 10 min (D) after application of muscarine. KCl (60 mM) was applied as a viability control for 5 min, and the prestimulus value was set as 100%. Data are presented as mean ± SEM. In neither parameter, a significant difference between samples from Cav-3$^{+/+}$ and Cav-3$^{-/-}$ mice was observed (Mann-Whitney *U*-test).

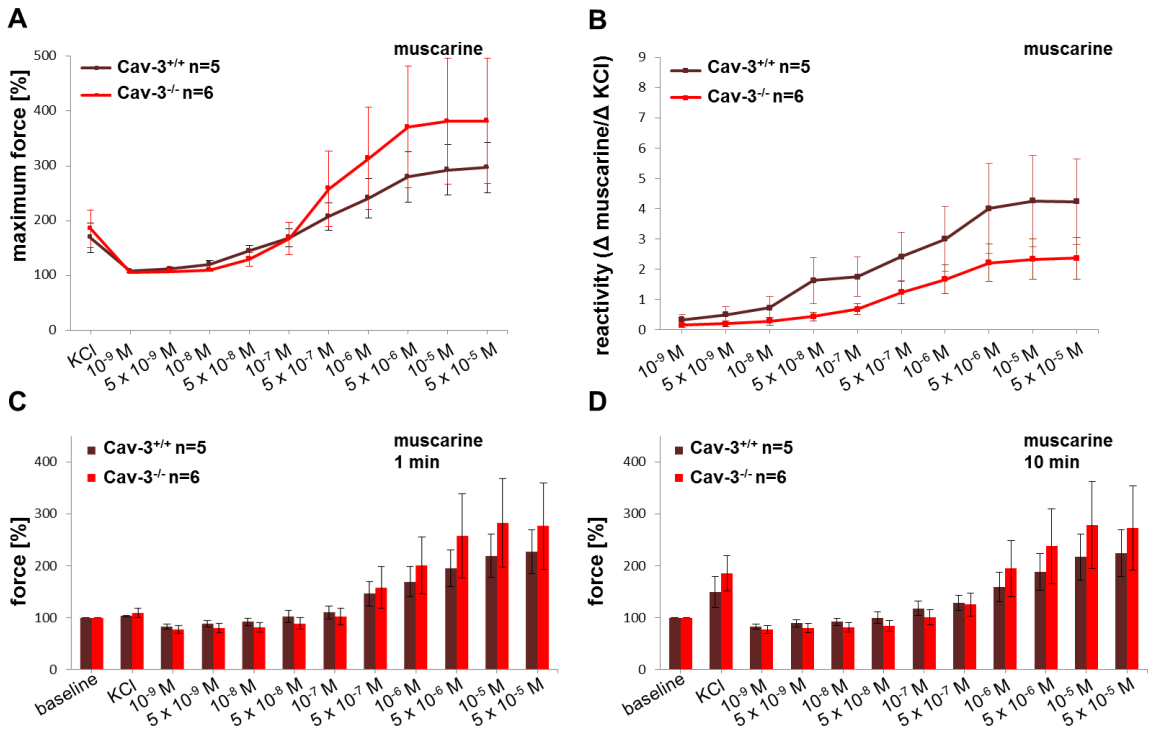

Fig. 3.26 Muscarine-induced contraction of main bronchus from Cav-3$^{+/+}$ and Cav-3$^{-/-}$ mice in organ bath experiments. Concentration-dependent responses are shown as maximum reaction in force (A) and reactivity related to KCl-induced contraction (B), and as force developed 1 min (C) and 10 min (D) after application of muscarine. KCl (60 mM) was applied as a viability control for 5 min, and the prestimulus value was set as 100%. Data are presented as mean ± SEM. In neither parameter, a significant difference between samples from Cav-3$^{+/+}$ and Cav-3$^{-/-}$ mice was observed (Mann-Whitney *U*-test).

3.7.2 5-HT-induced constriction

All segments of trachea in Cav-3$^{+/+}$ mice, form cranial to caudal part, exhibited a concentration-dependent 5-HT-induced contraction. In Cav-3$^{-/-}$ mice, higher concentrations of 5-HT were needed to induce a response in the cranial trachea (Figs. 3.23). This response was significantly lower than in Cav-3$^{+/+}$ mice at a concentration of (10^{-5} M) in reactivity level. Both in absolute force and in reactivity related to KCl-induced contraction, there was practically no 5-HT-induced response in tracheal middle, caudal and main bronchus in Cav-3$^{-/-}$ mice (Figs. 3.24-3.26). The main bronchus from Cav-3$^{+/+}$ mice showed high variability in the 5-HT-induced response and this variation caused a big deviation.

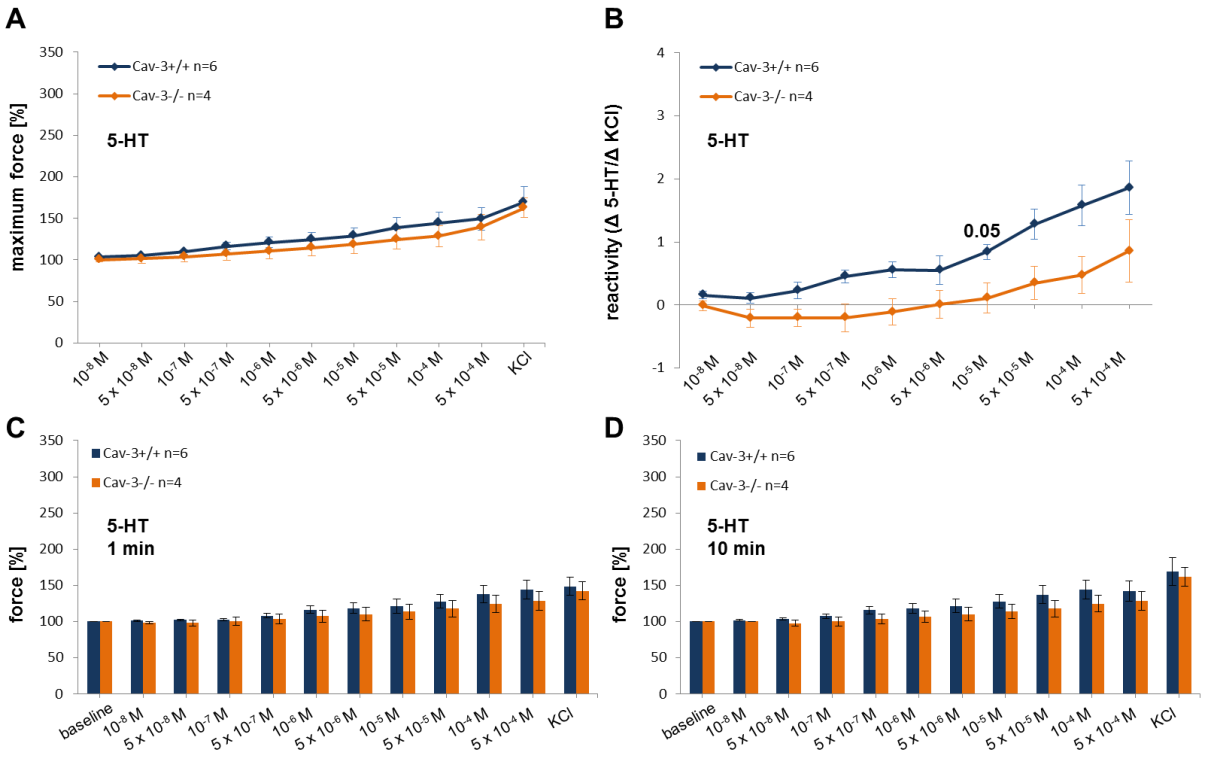

Fig. 3.27 5-HT-induced contraction of cranial trachea from Cav-3$^{+/+}$ and Cav-3$^{-/-}$ mice in organ bath experiments. Concentration-dependent responses are shown as maximum reaction in force (A) and reactivity related to KCl-induced contraction (B), and as force developed 1 min (C) and 10 min (D) after application of 5-HT. KCl (60 mM) was applied as a viability control for 5 min, and the prestimulus value was set as 100%. Data are presented as mean ± SEM. There was no 5-HT-induced response in Cav-3$^{-/-}$ mice measured in force recording. In the reactivity parameter, a significant difference between samples from Cav-3$^{+/+}$ and Cav-3$^{-/-}$ mice was observed. Mann-Whitney *U*-test conducted after Kruskal-Wallis test with $p \leq 0.05$, p values indicated in B.

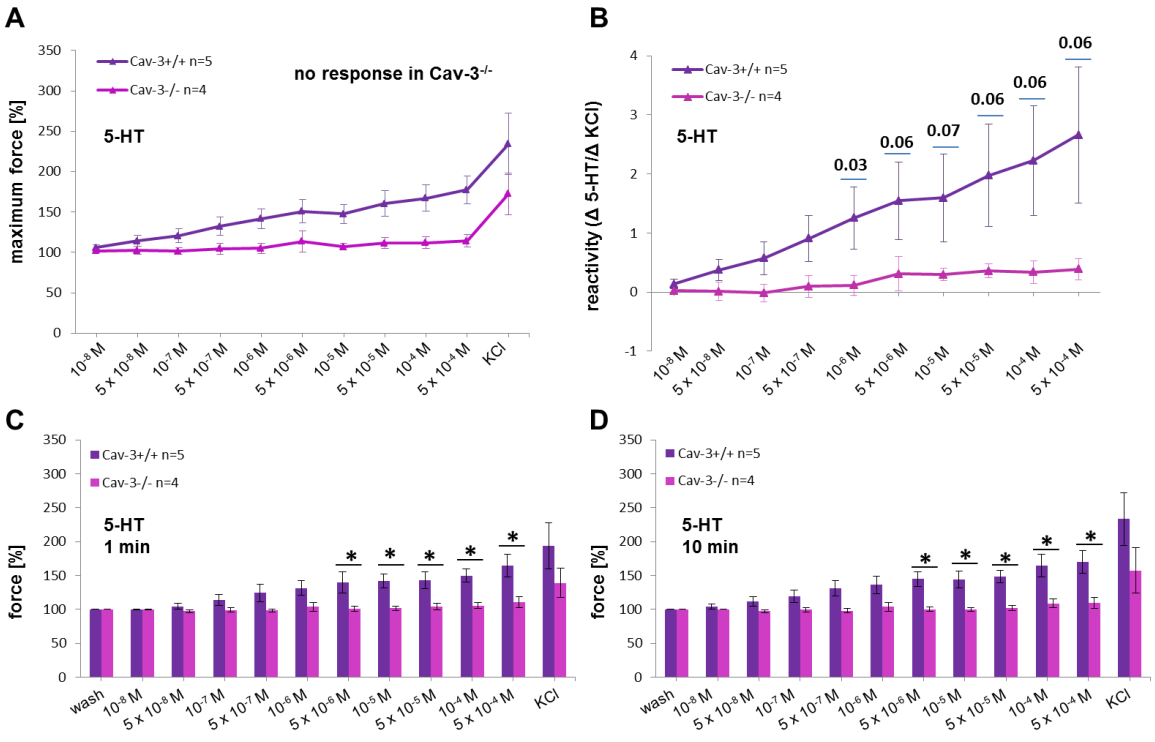

Fig. 3.28 5-HT-induced contraction of middle trachea from Cav-3$^{+/+}$ and Cav-3$^{-/-}$ mice in organ bath experiments. Concentration-dependent responses are shown as maximum reaction in force (A) and reactivity related to KCl-induced contraction (B), and as force developed 1 min (C) and 10 min (D) after application of 5-HT. KCl (60 mM) was applied as a viability control for 5 min, and the prestimulus value was set as 100%. Data are presented as mean ± SEM. There was no clear 5-HT-induced response in Cav-3$^{-/-}$ mice measured in force recording. In the reactivity parameter, a significant difference between samples from Cav-3$^{+/+}$ and Cav-3$^{-/-}$ mice was observed. Mann-Whitney *U*-test conducted after Kruskal-Wallis test with $p \leq 0.05$, p values indicated in B; C and D, * $p \leq 0.05$.

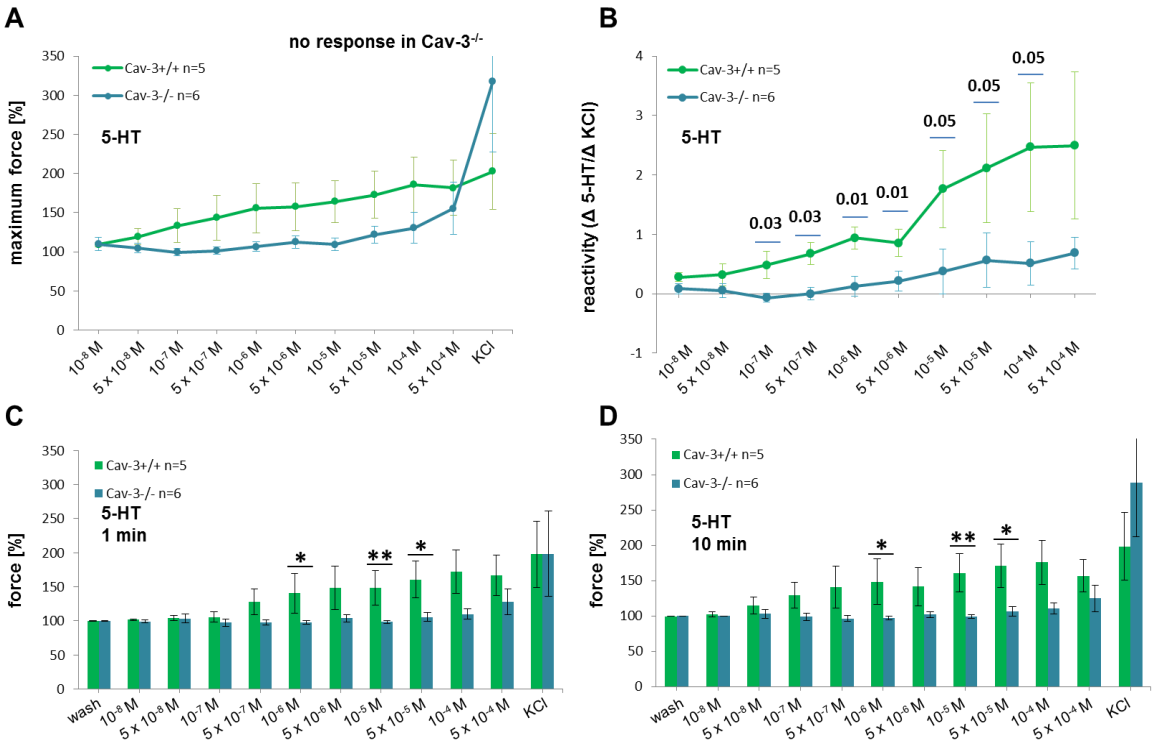

Fig. 3.29 5-HT-induced contraction of caudal trachea from Cav-3$^{+/+}$ and Cav-3$^{-/-}$ mice in organ bath experiments. Concentration-dependent responses are shown as maximum reaction in force (A) and reactivity related to KCl-induced contraction (B), and as force developed 1 min (C) and 10 min (D) after application of 5-HT. KCl (60 mM) was applied as a viability control for 5 min, and the prestimulus value was set as 100%. Data are presented as mean ± SEM. There was no clear 5-HT-induced response in Cav-3$^{-/-}$ mice measured in force recording. In the reactivity parameter, a significant difference between samples from Cav-3$^{+/+}$ and Cav-3$^{-/-}$ mice was observed. Mann-Whitney *U*-test conducted after Kruskal-Wallis test with $p \leq 0.05$, p values indicated in B; C and D, * $p \leq 0.05$, ** $p \leq 0.01$.

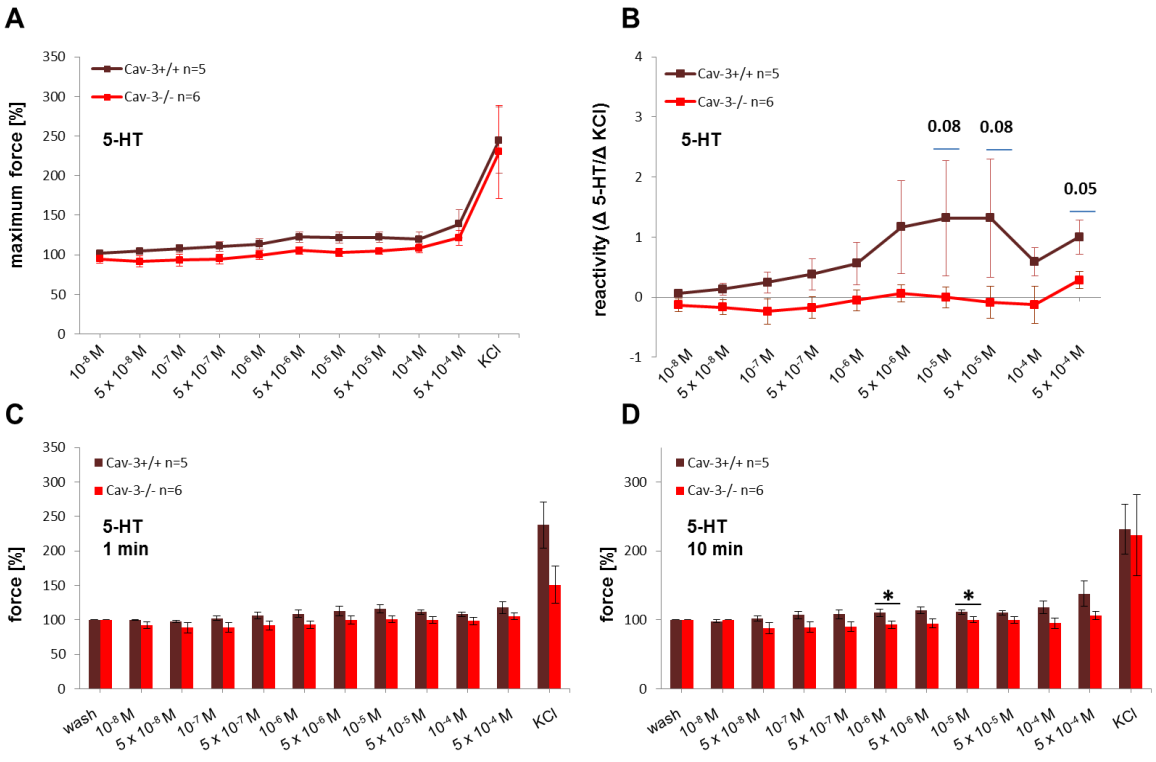

Fig. 3.30 5-HT-induced contraction of main bronchus from Cav-3$^{+/+}$ and Cav-3$^{-/-}$ mice in organ bath experiments. Concentration-dependent responses are shown as maximum reaction in force (A) and reactivity related to KCl-induced contraction (B), and as force developed 1 min (C) and 10 min (D) after application of 5-HT. KCl (60 mM) was applied as a viability control for 5 min, and the prestimulus value was set as 100%. Data are presented as mean ± SEM. There was no 5-HT-induced response in Cav-3$^{-/-}$ mice measured in force recording. In the reactivity parameter, a significant difference between samples from Cav-3$^{+/+}$ and Cav-3$^{-/-}$ mice was observed. Mann-Whitney *U*-test conducted after Kruskal-Wallis test with $p \leq 0.05$, p values indicated in B; D, * $p \leq 0.05$.

Muscarine	Cav-3$^{+/+}$		Cav-3$^{-/-}$	
	EC50 [nM]		EC50 [nM]	
samples	Mean	SEM	Mean	SEM
Cranial trachea	210.73	50.51	269.71	116.18
Middle trachea	182.96	9.40	465.42	276.13
Caudal trachea	230.09	43.65	323.17	83.72
Main bronchus	382.54	181.41	366.45	78.66

5-HT	Cav-3$^{+/+}$		Cav-3$^{-/-}$	
	EC50 [µM]		EC50 [µM]	
samples	Mean	SEM	Mean	SEM
Cranial trachea	14.35	8.52	26.12	15.31
Middle trachea	6.08	4.02	-	-
Caudal trachea	1.87	1.61	-	-
Main bronchus	46.93	28.26	-	-

Tab. 3.3 EC50 of muscarine- and 5-HT-induced contraction in Cav-3$^{+/+}$ and Cav-3$^{-/-}$ mice. EC50 values were estimated by using nonlinear regression sigmoidal curve analysis for responses to muscarine and 5-HT, respectively. No significant difference between samples from Cav-3$^{+/+}$ and Cav-3$^{-/-}$ mice in response to muscarine was observed (Mann-Whitney *U*-test). 5-HT-induced responses are fully abrogated in bronchus, middle and caudal trachea from the Cav-3$^{-/-}$ strain.

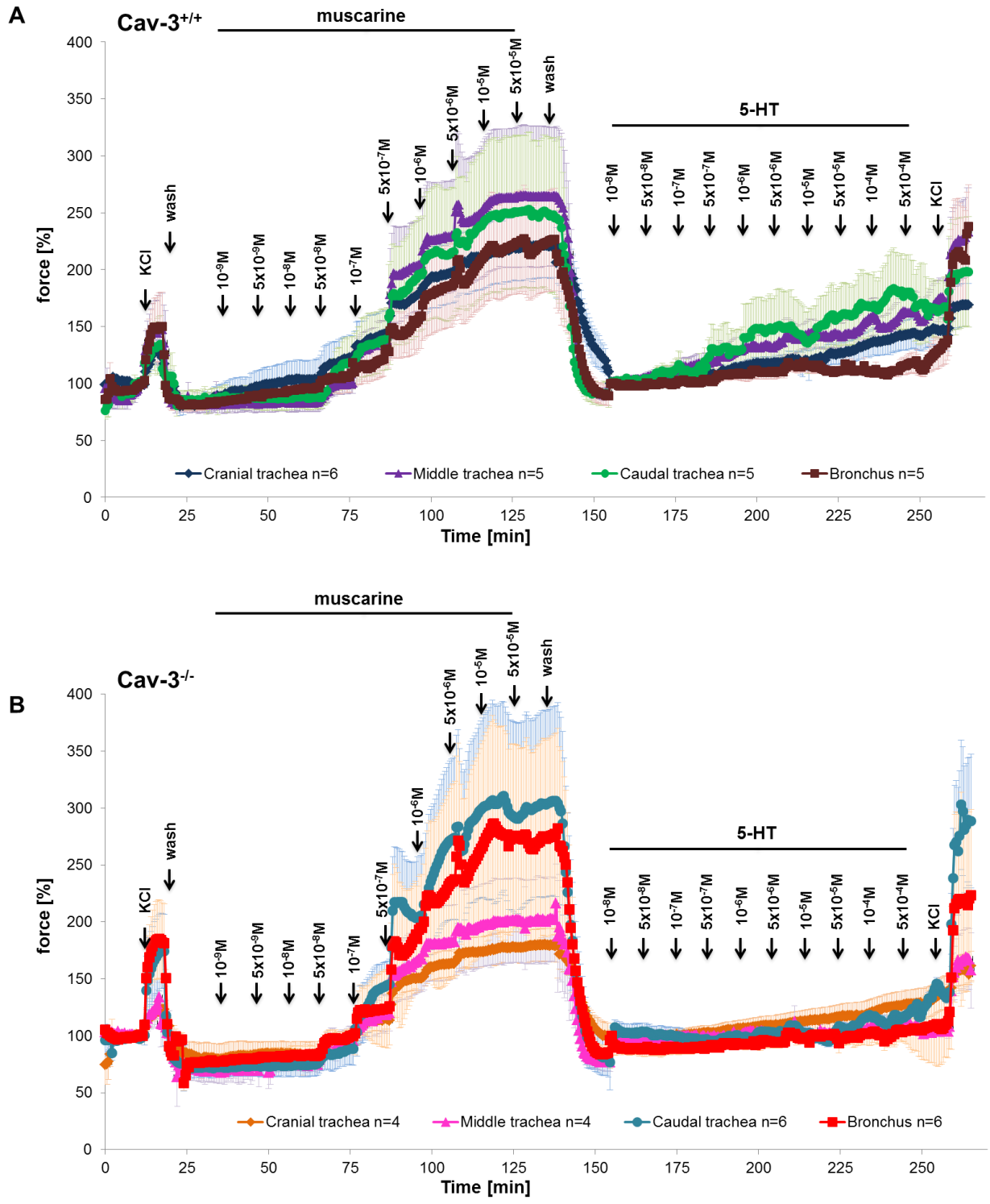

Fig. 3.31 Muscarine- and 5-HT-induced contraction in extrapulmonary airways of Cav-3$^{+/+}$ and Cav-3$^{-/-}$ mice in organ bath experiments. Concentration-dependent responses are shown in force of Cav-3$^{+/+}$ (A) and Cav-3$^{-/-}$ mice (B), after cumulative application of muscarine and 5-HT. These curves also illustrate the basis of the Figs. 3.23-3.30. KCl (60 mM) was applied as a viability control for 5 min, and the prestimulus value was set as 100%. Data are presented as mean ± SEM. In neither mouse strain, a significant difference between samples from different segments was observed (Mann-Whitney *U*-test).

3.8 Role of Cav-3 for muscarine- and 5-HT-induced constriction in murine intrapulmonary airways

3.8.1 Muscarine-induced constriction

Intrapulmonary bronchi exhibited a concentration-dependent muscarinic contraction measured as decrease in luminal airway area (Fig. 3.32A, B). The muscarine-induced constriction started at 10^{-8} M (p=0.02) in Cav-$3^{+/+}$ mice and at 5×10^{-8} M (p=0.02) in Cav-$3^{-/-}$ mice. However, compared with bronchi from wild-type animals (EC50: 1.14 ± 1.11 µM), Cav-3 deficiency (EC50: 0.038 ± 0.02 µM) caused an increase in the muscarine-induced bronchoconstriction at concentrations of 5×10^{-6} M - 5×10^{-5} M (Fig. 3.32C-D). In Cav-$3^{+/+}$ and Cav-$3^{-/-}$ mice, the contraction evoked by 5×10^{-7} M and 5×10^{-6} M (p=0.04) muscarine, respectively were not significantly enhanced further at higher concentrations (Fig. 3.32B-D).

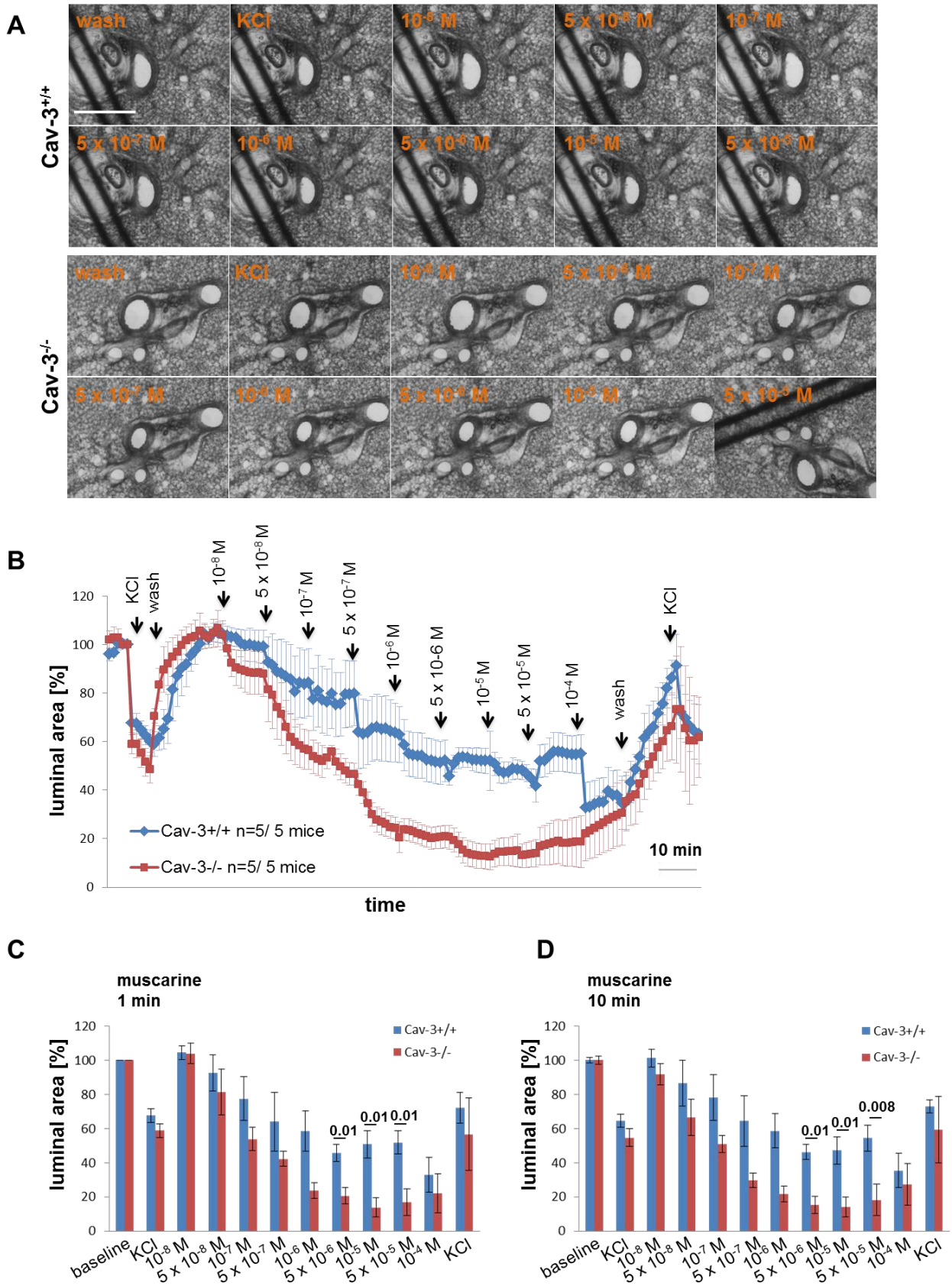

Fig. 3.32 Muscarine-induced constriction of intrapulmonary bronchi from Cav-3$^{+/+}$ and Cav-3$^{-/-}$ mice in video morphometry experiments. Concentration-dependent responses are shown as maximum reduction in the luminal area of mouse peripheral airways (A-B) and as luminal area at 1 min (C) and 10 min (D) after

application of muscarine. KCl (60 mM) was applied as a viability control for 5 min, and the prestimulus value was set as 100%. Data are presented as mean ± SEM. A significant difference between samples from Cav-$3^{+/+}$ and Cav-$3^{-/-}$ mice was observed (*p*-value calculated by Mann-Whitney *U*-test conducted after Kruskal-Wallis test with $p \leq 0.05$). Bar in (A) = 500 µm.

3.8.2 5-HT-induced constriction

To test for a desensitizing effect of 5-HT during cumulative application, three different application schedules were chosen. Intrapulmonary bronchi exhibited a concentration-dependent contraction in response to stimulation with gradually increasing concentrations (10^{-7}-10^{-3} M in half logarithmic mode) of 5-HT (Fig. 3.33A-B). The 5-HT-induced constriction started at 10^{-7} M in both Cav-$3^{+/+}$ mice (p=0.02) and in Cav-$3^{-/-}$ mice (p=0.05). The contraction evoked by 10^{-5} M in Cav-$3^{+/+}$ (EC50: 0.025 ± 0.006 µM, p=0.04) and in Cav-$3^{-/-}$ mice (EC50: 0.1 ± 0.03 µM, p=0.01) was not significantly enhanced further at higher concentrations. However, compared with bronchi from wild-type animals, Cav-3 deficiency had no effect on the 5-HT-induced bronchoconstriction (Fig. 3.32B-D).

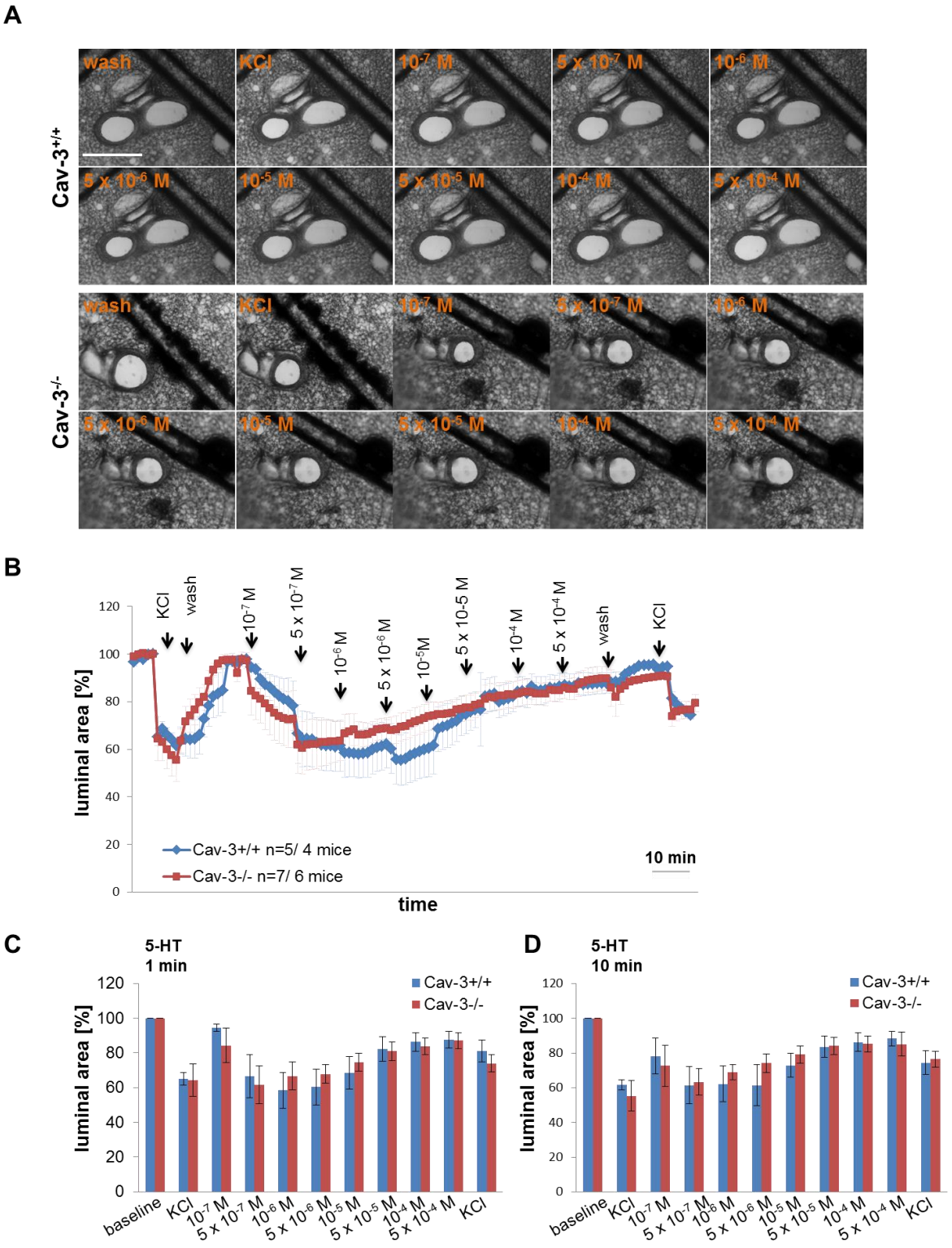

Fig. 3.33 5-HT-induced constriction of intrapulmonary bronchi from Cav-3$^{+/+}$ and Cav-3$^{-/-}$ mice in video morphometry experiments. Concentration-dependent responses are shown as maximum reduction in the luminal area of mouse peripheral airways (A-B) and as luminal area at 1 min (C) and 10 min (D) after application of cumulative concentrations of 5-HT (10^{-7}-10^{-3} M). KCl (60 mM) was applied as a viability control for 5 min, and the prestimulus value was set as 100%. Data are presented as mean ± SEM. At neither time point, a significant difference between samples from Cav-3$^{+/+}$ and Cav-3$^{-/-}$ mice was observed (Mann-Whitney *U*-test). Bar in (A) = 500 µm.

Intrapulmonary bronchi also exhibited a concentration-dependent contraction in response to stimulation with less repetitive 5-HT stimulation (10^{-6}-10^{-4} M) (Fig. 3.34A-B). Compared with bronchi from wild-type animals, Cav-3 deficiency had no effect on the 5-HT-induced bronchoconstriction (Fig. 3.34C-D).

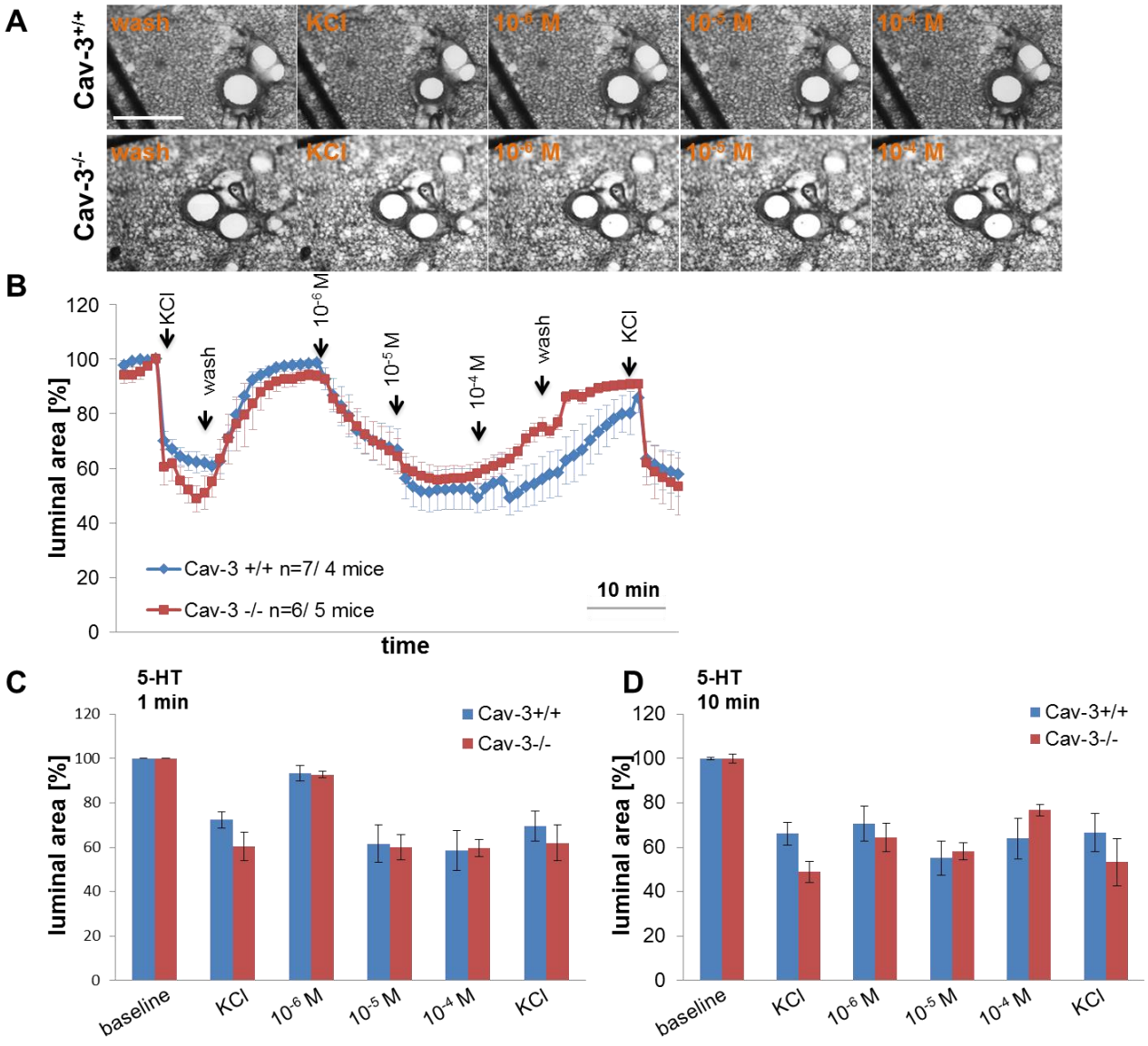

Fig. 3.34 5-HT-induced constriction of intrapulmonary bronchi from Cav-3$^{+/+}$ and Cav-3$^{-/-}$ mice in video morphometry experiments. Concentration-dependent responses are shown as maximum reduction in the luminal area of mouse peripheral airways (A-B) and as luminal area at 1 min (C) and 10 min (D) after application of 5-HT (10^{-6}-10^{-5}-10^{-4} M). KCl (60 mM) was applied as a viability control for 5 min, and the prestimulus value was set as 100%. Data are presented as mean ± SEM. At neither time point, a significant difference between samples from Cav-3$^{+/+}$ and Cav-3$^{-/-}$ mice was observed (Mann-Whitney *U*-test). Bar in (A) = 500 µm.

Stimulation with 10^{-4} M 5-HT followed by application of supramaximal concentration of 5-HT, 10^{-3} M also resulted in a concentration-dependent contraction (Fig. 3.35A-B). Intrapulmonary bronchi responded to 10^{-4} M 5-HT with an initial rapid constriction (p=0.01) in both mouse strains and with a sustained constriction at 10^{-3} M. Compared with bronchi from wild-type animals, Cav-3 deficiency had no effect on the 5-HT-induced bronchoconstriction (Fig. 3.35B-D).

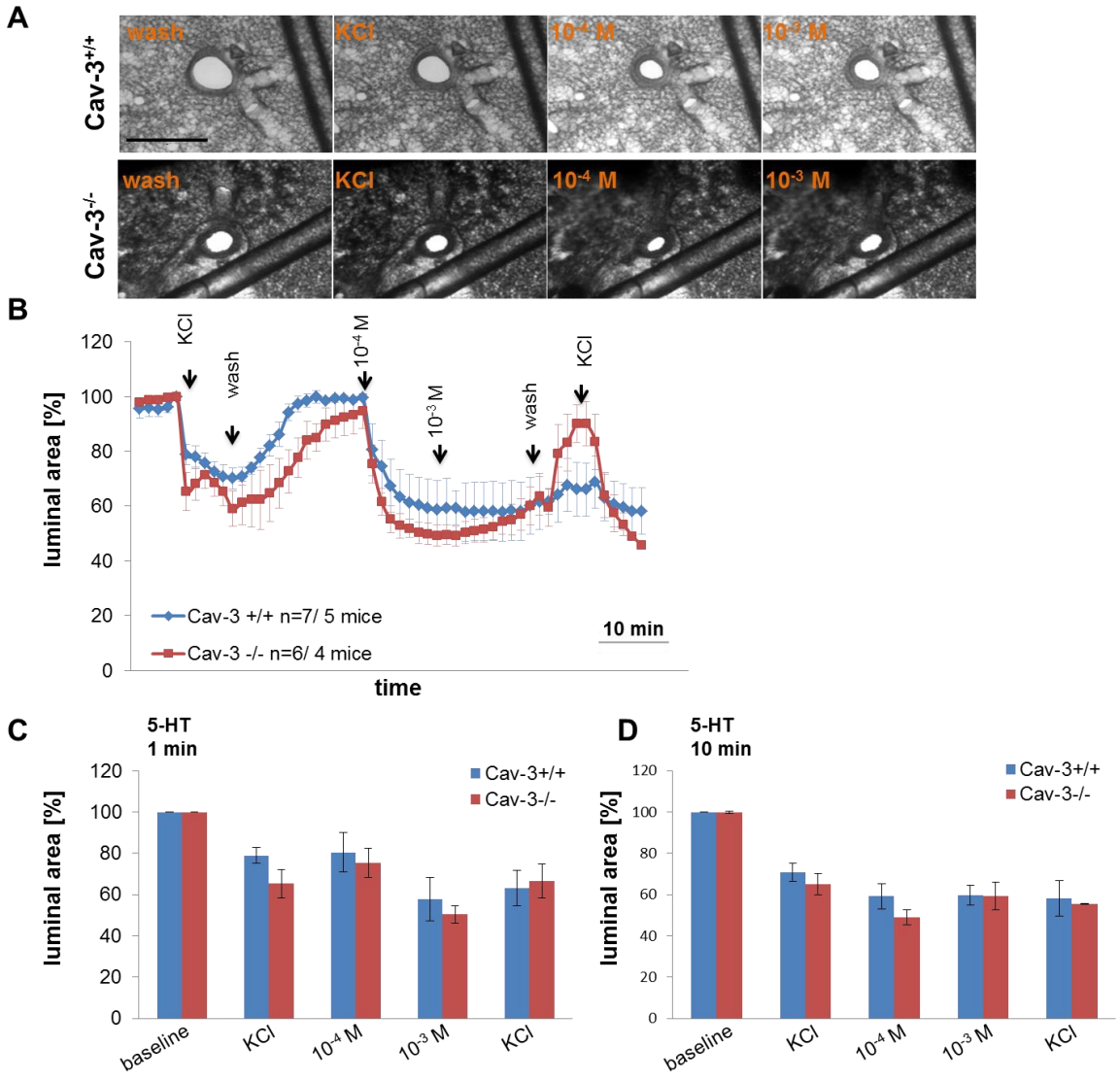

Fig. 3.35 5-HT-induced constriction of intrapulmonary bronchi from Cav-$3^{+/+}$ and Cav-$3^{-/-}$ mice in video morphometry experiments. Concentration-dependent responses are shown as maximum reduction in the luminal area of mouse peripheral airways (A-B) and as luminal area at 1 min (C) and 10 min (D) after application of cumulative concentrations of 5-HT (10^{-4}-10^{-3} M). KCl (60 mM) was applied as a viability control for 5 min, and the prestimulus value was set as 100%. Data are presented as mean ± SEM. At neither time point, a significant difference between samples from Cav-$3^{+/+}$ and Cav-$3^{-/-}$ mice was observed (Mann-Whitney *U*-test). Bar in (A) = 500 µm.

4 Discussion

4.1 Caveolae and the caveolar compartment structure

Caveolae are defined by a set of core protein ingredients, Cav, which govern their structure and function [59]. Although the presence of at least one of the caveolin family members, Cav-1 and Cav-3, is indispensable for caveolae formation in mammalian cells [8, 11-19, 22, 23], recent data suggest that certain accessory molecules, cavins, are necessary for stabilizing Cav-1 or Cav-3 functions and to form a caveola [8, 58]. Caveolins and cavins can be purified as a single species of protein complex named the caveolar coat complex [149]. The discovery of the cavin family as regulators of caveolae formation and stabilization has provided new insights to understand the role of muscle caveolae.

4.1.1 Cavin-1 and -4 distribution patterns indicate their involvement in Cav-1- and Cav-3-dependent caveolae formation

The present data show the expression of all four cavin proteins in murine trachea and lung, suggesting an important role in these tissues. Accordingly, Govender et al. [150] have noted pronounced alterations in pulmonary homeostasis after targeted deletion of cavin-1. They detected cavin-1 in alveolar macrophages, endothelial cells and type I pneumocytes. Deletion of cavin-1 led to a complex lung phenotype including marked hypercellularity, increased elastance and deposition of extracellular matrix as well as decreased levels of granulocyte-monocyte colony-stimulating factor (GM-CSF) which is critical for surfactant phospholipid catabolism and the clearance of pathogens from the lung [150].

In agreement with the findings of Govender et al. [150], we did not observe cavin-1-immunoreacitvity of the bronchial epithelium, but noted expression of both cavin-1 and -2 in the tracheal epithelium. Immunohistochemistry showed that cavin-1 is restricted to basal cells in the tracheal epithelium which explains the absence of cavin-1 from the bronchial epithelium which does not contain basal cells in the mouse. Real-time PCR demonstrated that the tracheal SM expresses all cavin isoforms, cavin-1 to -4. Bastiani et al. showed a dominant presence of cavin-4 in cardiac and skeletal muscles and clearly lower level of cavin-4 expression in other cell types [58]. Our observations also indicate that cavin family members, key components of caveolae, show a tissue-specific expression. Cavin-1 expression was higher than cavin-4 in the lung and tracheal wall compartments. Among the cavins, cavin-1 is required for caveolae formation in various cell types including epithelium, SM, and skeletal muscle [58, 68, 71]. This need for cavin-1 might explain its higher expression compared to that of cavin-4 in tracheal wall compartments and the lung.

In view of the tissue-specific expression of cavin proteins and their dependency on caveolins for membrane association, we assessed the localization of these two protein families in thoracic organs that contain Cav-dependent caveolae. We found that Cav-1 and cavin-1 co-localize in the tracheal basal epithelium, tracheal and bronchial SMC and endothelial cells. In agreement with this observation, cavin-1 has been shown to co-localize with Cav-1 in primary rat and 3T3-L1 cultured adipocytes, and the cavin-1 level, like that of Cav-1, is sensitive to cholesterol depletion [151]. Animals lacking cavin-1 have no detectable caveolae in any cell type and have a diminished protein content of all caveolin isoforms while a normal or above normal level of caveolin mRNA expression is retained [71]. We here show cavin-4 and Cav-3 to be co-localized in cardiac muscle cells and SMC from trachea and bronchi consistent with previously reported co-expression of cavin-4 and Cav-3 in human and mouse rhabdomyosarcoma [79]. Since Cav-3-deficient muscles from dystrophic patients display a loss of cavin-4, Cav-3 and cavin-4 may co-operate in maintaining proper function in the skeletal muscle [58, 79].

Consistent with our findings in mice, expression of all cavins was observed in primary human bronchial SMC using RT-PCR. Immunohistochemistry confirmed the presence of cavin-1 and -4 proteins in human bronchial SMC. The functional role of cavins in human airways is still poorly understood. In isolated human ASM, knockdown of either cavin-1 or cavin-3 by siRNA reduced ADP ribosyl cyclase activity and the expression of CD38, a bifunctional enzyme involved in cyclic ADP ribose metabolism. This had consequences on airway contractility as it reduced the histamine-induced increase in $[Ca^{2+}]_i$ [152]. The relevance of this in vitro finding for overall bronchial functions still needs to be clarified, since patients with cavin-1 mutations present with lipodystrophy and signs of skeletal muscle dystrophy, but smooth muscle dysfunction has not been reported yet [21].

Confirming previous data from our group, Cav-1 and Cav-3 were identified in mouse and human ASM on mRNA and protein levels in the present study [16, 105]. In contrast, the absence of Cav-3 in isolated human ASM and freshly dissected trachealis muscle was reported by other groups [18, 102, 136]. This discrepancy might be due to the different antibodies used for the detection and/or to alteration of Cav-3 expression by isolation of ASM. While functional data on the role of Cav-3 are still missing for human ASM, the present study revealed a functional impact of Cav-3 deficiency on murine airway contractility, thereby supporting the presence of Cav-3 in ASM.

4.1.2 Caveolae abundance and cavin expression are not reduced in airways of Cav-3$^{-/-}$ mice

Cav-3 is important for the transition from synthetic to contractile phenotype in vascular SMC [41, 153]. With this context in mind and in view of the dominant expression of Cav-3 in other muscle cells (cardiac and skeletal), we reasoned that Cav-3 might also organize caveolar coat complex and structure in ASM. To address this issue directly, we created a caveolin-3-deficient (Cav-3$^{-/-}$) mouse model, using *loxP*/*Cre* technology. This strategy gives the option to generate cell type-specific knockouts by expressing *Cre* under the control of cell type-specific promotors. Here, we first generated a global Cav-3 deficient mouse strain by cross-breeding with a *Cre*-deleter mouse line, in which *Cre* expression is driven in every cell type under the control of the adenovirus EIIa promoter. Previous studies also have generated Cav-3$^{-/-}$ mice using standard homologous recombination techniques [45, 154]. All Cav-3$^{-/-}$ mice generated so far, including ours and those reported by Galbiati et al. and Hagiwara et al. [45, 154], are designed by targeting exon-2 of the Cav-3 gene which encodes the bulk of the Cav-3 protein with all of its functional domains. These mice are viable, fertile and exhibit normal growth under normal conditions even into old age. The most notable pathological findings in Cav-3 deficiency reported by Hagiwara were muscle fiber necrosis in muscular dystrophies and pathological lesions mainly in the soleus muscle and the diaphragm [45]. Galbiati et al. showed mild myopathic changes in Cav-3 null mice which were similar in severity to those seen in patients with limb girdle muscular dystrophy caused by mutations within the coding sequence of the exon-2 of the Cav-3 gene [77, 154]. Ultra-structural analysis of skeletal muscle from our Cav-3$^{-/-}$ mice, which was done by M. Skill in our group, also revealed mild myopathic changes with variability in the size of necrotic fibers in the cytoskeletal architecture of muscle tissue that is characteristic of muscular dystrophy [submitted].

RT-PCR, Western blotting, and immunohistochemistry of a range of tissues confirmed that the Cav-3 mRNA and protein are indeed absent in the Cav-3$^{-/-}$ mice. Cav-1 deficiency leads to Cav-2 destabilization in the Cav-1-dominated caveolae so that, despite normal Cav-2 mRNA expression, Cav-2 protein is no longer detectable in the lung [155]. Such an effect was not observed for the newly generated Cav-3 deficient mouse line. The expression of all other caveolins and peripheral caveolar components was maintained in all investigated airway and lung compartments as assessed by Western blot and real-time PCR. The only alteration which we observed was a significant reduction in Cav-1 mRNA level which, however, did not translate into detectable changes in Cav-1 protein. There was no alteration in other caveolin and peripheral caveolar coat complex mRNA expression in Cav-3$^{-/-}$ animals as assessed by real-time PCR. Although Cav-3 and cavin-4 are co-localized and interact in murine airways,

there was no detectable change in cavin-4 when Cav-3 is deleted indicating that Cav-3 is dispensable for stabilization of cavin-4 in ASM. In contrast, Ogata et al. showed diminished membrane localization of cavin-4 in cardiomyocytes when Cav-3 was knocked down [156] pointing towards cell-type specific interaction patterns governing trafficking and stabilization.

Although cavins are dependent on caveolins for membrane association, we were able to detect cavin-1, cavin-4 and Cav-1 in both Cav-$3^{-/-}$ and Cav-$3^{+/+}$ mice by immunohistochemistry and Western blotting, suggesting that the caveolar coat complex is not dependent on Cav-3 in ASM. Our quantitative data on the caveolar abundance marker, EHD-2, imply that Cav-3 does not contribute to the abundancy of ASM caveolae, and caveolae are still present in Cav-$3^{-/-}$ mice. This is corroborated by electron microscopic analysis of tracheal SMC by M. Skill in our group, revealing no alteration in caveolae numbers in Cav-$3^{-/-}$ mice [submitted]. In contrast, Cav-3 as shown in previous studies regulates caveolar formation in cardiac and skeletal muscle cells, indicating that the Cav-3 deficiency leads to decreased numbers or the absence of caveolar structures, with associated T-tubular disorganization and dramatic cardiomyopathy [45, 46, 154, 157, 158]. In addition, several studies using transgenic mice overexpressing Cav-3 revealed an increased number of sarcolemmal muscle cell caveolae in skeletal muscle fibers and cardiomyocytes [146, 159]. Thus, there are obvious differences between smooth and striated muscle, and it is expected that specific aspects of caveolar function rather than caveolar abundancy are dependent on the expression of Cav-3 in tracheal SMC. In addition to Cav-3, Cav-1 is also expressed in ASM. Since we recently observed a decreased number of caveolae in tracheal SMC in Cav-$1^{-/-}$ mice in ultra-structural analysis [submitted], Cav-1 appears to be crucial for caveolae abundancy and caveolar morphogenesis in tracheal SMC.

4.1.3 Cav-3 interacts with Cav-1, cavin-1 and cavin-4 in ASM

Double-labelling immunohistochemistry demonstrated the occurrence of multiple Cav and cavin isoforms in ASM, suggesting interaction in multimeric complexes. This issue was further addressed by CO-IP experiments, centering on the role of Cav-3. Cav-1/Cav-3 hetero-oligomeric complexes have previously been observed in rat and mouse cardiomyocytes, mouse myoblasts and skeletal muscle of Cav-1-overexpressing mice [39, 40]. Accordingly, both caveolins were co-immunoprecipitated also in extracts from lung and trachea in the present study. This corroborates earlier findings from our group showing interaction of Cav-1 and Cav-3 by antibody based FRET (fluorescence resonance energy transfer) analysis by confocal laser scanning microscopy [16]. Similarly, cavin-4 has been shown to localize in

cardiomyocyte caveolae and to associate with other caveolae-associated proteins, including Cav-3 [65, 156]. This interaction appears not to be restricted to cardiac muscle since we observed Cav-3/cavin-4 CO-IP also in lung and trachea in the present study. It is likely that Cav-3/cavin-4 also interact in skeletal muscle since they are co-expressed in large quantity, and cavin-4 mislocalizes in skeletal muscle fibers from patients with caveolopathies [58], but this still needs to be demonstrated directly.

A newly recognized interaction under physiological conditions was noted for Cav-3 and cavin-1, which previously had been noted only after plasmid transfection [156]. Since cavin-1 mRNA was much more abundant than cavin-4 mRNA in ASM, cavin-1 might be the dominant interaction partner of Cav-3 in this tissue. Also, cavin-1 has previously been shown to be essential for caveolae formation and organization and to associate with Cav-1 or Cav-3 to drive caveolae formation in non-muscle and muscle cells, respectively [68, 151]. Accordingly, cavin-1 mutations lead to muscular dystrophy and cardiac dysfunction [20], and overexpression of this caveolae-associated protein rescues membrane repair defects in dystrophic muscle [160].

Since Cav-3 co-immunoprecipitated and co-localized with Cav-1, cavin-1 and cavin-4 in ASM, multimeric complexes consisting of all these caveolar coat complex proteins appeared to be likely. We directly addressed this question by CO-IP experiments. Equivocal findings have previously been reported for Cav-1/cavin-1 interaction. Liu et al. failed to see a direct interaction between Cav-1 and cavin-1 by CO-IP suggesting no direct interaction or weak interaction between them in adipocytes [151]. On the other hand, cavin-1 strongly interacts with Cav-1 in transfected Hela cell line to stabilize Cav-1 oligomers [149]. Upon overexpression of cavin-1 in the HEK293 cell line, Cav-1 recruitment into lipid raft fractions was apparently increased, and upon knockdown of cavin-1, Cav-1 was downregulated in 3T3-L1 cell lysates [151]. In lung and trachea, we detected distinct cavin-1/Cav-1 interaction, pointing towards cell-type specific interaction patterns. This interaction was similarly seen by CO-IP in the trachea and lung of both Cav-$3^{-/-}$ and Cav-$3^{+/+}$ mice, suggesting that the complex formation is not dependent on Cav-3, albeit both also co-immunoprecipitated with Cav-3.

Lastly, CO-IP revealed that the heteromeric protein complex in lung and trachea also contained both cavin-1 and cavin-4 proteins. However, despite the individual abilities of both cavin-1 and -4 to shape heteromeric complex in the cytoplasm prior to association with caveolin on the plasma membrane [59], further studies with caveolae buoyant fractions are required to test if this cavin complex is inserted into the membrane in this composition.

4.2 Role of Cav-3 in airway smooth muscle constriction

A wide range of contractile stimuli are acting either directly on ASM or indirectly through neural pathways leading to airway hyperreactivity [84]. Several GPCR including 5-HT and MR are aggregated at caveolae structures [14, 82]. Dysregulation of caveolae and caveolins is assumed to be involved in the pathogenesis of diseases associated with airway hyperreactivity [161]. In the past, a large number of signaling molecules were co-purified with Cav-3 suggesting that Cav-3 containing caveolae are involved in intracellular signaling [162], and Cav-3 has recently also identified in ASM [16]. Thus, knowing the regulatory role of Cav-3 in the constrictor response to contractile stimuli may provide an opportunity to modulate bronchial hyperreactivity.

4.2.1 Muscarine-induced constriction is enhanced in intrapulmonary airways of Cav-3$^{-/-}$ mice

ACh is the major physiological bronchoconstrictor and its effect is mediated primarily through the M3R and, to a lesser extent, through the M2R receptor subtype [89]. Several evidences accumulated that this muscarinic bronchoconstriction involves caveolae as signaling platforms. In murine intrapulmonary airways, muscarine-induced bronchoconstriction is largely reduced by pretreatment with the cholesterol depleting agent MCD which causes ultrastructural disappearance of caveolae from bronchial ASM [16]. Interactions of the M3R with caveolins appear likely but could not be directly investigated in ASM due to the lack of M3R specific antibodies as demonstrated using tissues from M3R knockout mice [163, 164]. The M2R directly interacts with Cav-3, but not Cav-1 in murine ASM, as shown by antibody based confocal FRET analysis [16]. On this background, the generation of a Cav-3 gene deficient mouse was initiated, and the prediction was that muscarinic bronchoconstriction will be diminished in this condition.

In contrast to this expectation, the response of all extrapulmonary airway segments (cranial to caudal trachea, extrapulmonary bronchus; assessed in organ bath recordings) to muscarine was indistinguishable in Cav-3$^{-/-}$ from Cav-3$^{+/+}$ mice, regardless whether EC50, force or reactivity was considered. In intrapulmonary bronchi, assessed by videomorphometry of PCLS, however, our findings show a considerable increase rather than decrease in muscarinic bronchoconstriction in Cav-3$^{-/-}$ mice. This demonstrates an unexpected inhibitory regulatory role of Cav-3 in cholinergic bronchoconstriction. In agreement with this finding, overactivity of SM was also reported in the rat urinary bladder with age and ascribed to a reduction in Cav-3 protein expression [144, 165]. The direct association between M2R and Cav-3 in murine bronchial SMC [16] suggests that this inhibition targets the M2R signaling pathway. The underlying molecular pathways are still unclear and cannot be finally deduced from the

present data. Cav-3 may inhibit MR function by direct interaction, or organize MR-independent inhibitory signaling. Findings on other cellular systems point to a link to nitrergic signaling. Using FRET analysis, we have previously demonstrated a direct association of Cav-3 and eNOS in rat airway epithelial cells [105]. In cardiac myocytes and in transfected COS cells co-expressing the M2R and eNOS, stimulation with carbachol leads to NO production [166-168]. In this setup, Cav-3 suppresses basal eNOS activity but is indispensable for cholinergic activation of eNOS. The disruption of the inhibitory eNOS-Cav-3 complex, e.g. with an oligopeptide corresponding to the Cav-3 scaffolding domain, completely abrogates cholinergic stimulation of eNOS with subsequent elevation of cGMP levels [166, 167]. In ASM, NO is a bronchodilator acting through cGMP-dependent and -independent mechanisms [169], and NO production by ASM itself can be stimulated by the cholinergic agonist carbachol at low concentration acting via the M2R [170]. Hence, it seems to be a plausible scenario that cholinergic stimulation of ASM not only activates a strong constrictor pathway but also an inhibitory component involving M2R-Cav-3-eNOS coupling. In such a setting, selectively removing Cav-3, as it is the case in Cav-3 deficient mice, would abrogate the inhibitory component, resulting in enhanced cholinergic constriction, whereas disruption of the entire signaling platform by MCD treatment would also affect the constrictor component, as reported earlier [16]. This would imply that Cav-3 is either not involved at all in this constrictor response or at least dispensable and its function might be compensated by Cav-1 in this pathway. Indeed, we also observed a hetero-oligomeric complex of Cav-1 and Cav-3 in trachea and lung by CO-IP. Cav-1/Cav-3 hetero-oligomeric complexes were also observed in rat and mouse myocytes of Cav-1-overexpressing mice [39, 40]. Several proteins binding to Cav-3 are also able to interact with Cav-1 [36, 171], suggesting that Cav-3 might be exchangeable with Cav-1. Considering the dependency of muscarinic constriction on intact caveolae, further functional studies with Cav-1/Cav-3-deficient mice or cavin-1-deficient mice which exhibit phenotypes reminiscent of Cav-1 and Cav-3-deficient mice [172] are necessary to solve this.

Notably, this augmentation of cholinergic bronchoconstriction in Cav-3 deficiency was not noted in organ bath recordings from extrapulmonary airways. This difference to intrapulmonary airways in PCLS may be due to different receptor coupling in extra- versus intrapulmonary airways. In support of this assumption, the total densities of several receptors, including both MR and β-AR, vary considerably along the airway tree from the trachea to the distal lung [89]. M3R-ligand binding density decreased from the segmental to subsegmental bronchus whereas the M2R subtype was distributed ubiquitously, and β2-AR increased along

the airways towards the periphery [89]. Of course, it also cannot be excluded that the different methodological approaches to record ASM constriction - force recording in organ bath versus videomorphometry of PCLS - may have contributed substantially to this difference.

4.2.2 5-HT-induced constriction is largely dependent on Cav-3 in extrapulmonary airway

The effects of 5-HT on ASM tone are complex, and both constrictor and relaxant actions have been reported depending on species and concentrations used. In humans, bronchoconstriction is ascribed to 5-HT2A receptors and bronchodilation to 5-HT1A receptors on smooth muscle [112]. Since free 5-HT levels in plasma are increased in asthma, it has been linked to pathophysiology of this disease [112, 113]. In mice, different modes of action of 5-HT have been reported for extra- and intrapulmonary airways, respectively. In the trachea, 5-HT is assumed to cause the release of ACh either from epithelial cells [173] or from cholinergic nerve fibers [174, 175] which then, in turn, causes airway constriction. In intrapulmonary airways, however, serotonergic bronchoconstriction is independent from the presence of M3R receptors and, therefore, not indirectly mediated via ACh [107].

Similarly, marked differences between extra- and intrapulmonary airways were also noted in the present study, in that the 5-HT-mediated constriction was equally strong in intrapulmonary airways of knockout and wild-type mice while it was absent in extrapulmonary airways of Cav-$3^{-/-}$ mice. Serotonergic airway constriction in murine extrapulmonary is considered to be indirectly mediated through ACh release from epithelial cells or nerve fibers [173-175]. Since muscarinic constriction of extrapulmonary airways was unaffected in Cav-$3^{-/-}$ mice, the cholinergic component of this indirect effect shall not be responsible for the abrogated serotonergic effect. Among the suspected immediate targets of 5-HT, cholinergic neurons and epithelial cells, there is no clear evidence for Cav-3 expression in autonomic neurons, although our group has previously reported Cav-3 expression in sensory neurons [176]. However, we here directly observed Cav-3 in tracheal epithelial cells, consistent with earlier reports of our group in rat [155]. Notably, we did not observe Cav-3-immunoreactivity in the epithelium of intrapulmonary bronchi, which correlates with the unaffected serotonergic response at this airway level.

In intrapulmonary bronchi, a large portion of the reaction to 5-HT is due to direct action upon the smooth muscle. In a parallel study we showed expression of the 5-HT receptor subtypes 5-HT1B, 5-HT2A, 5-HT6 and 5-HT7 in murine lung, and the 5-HT2A receptor inhibitor ketanserine inhibited 5-HT-induced constriction in murine PCLS [submitted]. Also, in other species the 5-HT2A receptor has been linked to direct serotonergic smooth muscle

constriction [112, 123]. The 5-HT2A receptor was shown to be located in caveolar and non-caveolar fractions in bovine ASM and in cardiomyocytes. In cardiomyocytes, Cav-3 regulates its shift between caveolar and lipid raft membrane compartments [114, 120, 162]. There, it associates with the 5-HT2A receptor and negatively regulates hypertrophic response of cardiomyoblasts and neonatal cardiomyocytes to 5-HT [120]. Despite this known interaction of Cav-3 with 5-HT2A receptors, Cav-3 deficiency did not affect serotonergic intrapulmonary bronchoconstriction in this study, whereas disruption of the entire signaling platform by MCD treatment entirely abrogated it, as reported earlier [16]. This implies that a cholesterol-rich membrane domain, most likely a caveola is needed for serotonergic bronchoconstriction, but Cav-3 is not involved at all in this response or at least dispensable.

Although Cav-3 expression in rat tracheal epithelium or murine sensory neurons was previously observed [155, 176] or its expression in apical membrane of epithelial cells in this study support Cav-3 role in indirect, ACh induced, serotonergic response.

4.3 Conclusions

The present study identifies Cav-3 as a member of the caveolar coat complex in the airways which determines specific functions in this signaling platform albeit being dispensable for structural maintenance of this compartment. Its role in regulating cholinergic airway constriction is restricted to intrapulmonary bronchi. Here, it exerts an inhibitory role, probably through its interaction with M2R-eNOS coupling in ASM. In contrast to its rather subtle role in modulation of cholinergic bronchoconstriction, Cav-3 is crucial for serotonergic constriction of extrapulmonary airways, where it is also expressed by epithelial cells. These epithelial cells are assumed to mediate serotonergic constriction of the trachea. The absence of Cav-3 from epithelial cells of intrapulmonary bronchi correlates with unaltered serotonergic response of these airways in Cav-$3^{-/-}$ mice. Potentially, these data warrant consideration during pharmacological modulation of the cholinergic and serotonergic responses and provide an opportunity to modulate airway hyperreactivity.

5 Summary

Acetylcholine (ACh) and serotonin are bronchoconstrictors clinically relevant in airway diseases associated with airway hyperreactivity. Their receptors are incorporated in membrane signaling platforms termed caveolae. These are Ω-shaped invaginations of the plasma membrane with a caveolar coat protein complex consisting of caveolins (Cav-1, -2 and -3) and cytoplasmic adapter proteins (cavin-1 to -4). There is evidence that Cav-3 might organize this caveolar coat complex in airway smooth muscle (ASM). To address this issue, we generated Cav-3-deficient mice to address the functional role of Cav-3 in ASM constriction using organ bath recording from extrapulmonary and videomicroscopy of precision cut-lung slices from intrapulmonary airways. Immunofluorescence, RT-PCR, real-time PCR, Western blotting and co-immunoprecipitation served to address the distribution and molecular composition of the caveolar coat complex in murine and human airways. Cav-3 was found in tracheal epithelium and ASM and was associated with Cav-1, cavin-1 and cavin-4. Cav-3 deficiency neither had impact on protein expression of caveolar coat complex members nor on EHD-2 expression, a caveolae abundancy marker. Thus, specific aspects of caveolar function rather than caveolar abundancy are dependent on the expression of Cav-3. The response of extrapulmonary airway to muscarine was not altered in Cav-$3^{-/-}$ mice, whereas a considerable increase in muscarinic bronchoconstriction was observed in Cav-$3^{-/-}$ intrapulmonary bronchi. This demonstrates an inhibitory regulatory role of Cav-3 in cholinergic bronchoconstriction. Cav-3 was previously found to interact with the muscarinic receptor subtype 2 (M2R) in bronchial SM, and in cardiac myocytes it couples M2R stimulation with endothelial NO synthase (eNOS) activation. Thus, the depletion of Cav-3 might cause an increased muscarine-induced bronchoconstriction through disruption of M2R-Cav-3-eNOS. Cav-3 deficiency fully abrogated serotonin-induced constriction of extrapulmonary airways while leaving intrapulmonary airways unaffected. Serotonergic airway constriction in murine extrapulmonary is considered to be indirectly mediated through ACh release from epithelial cells or nerve fibers. Since muscarinic constriction of extrapulmonary airways was unaffected in Cav-3-/- mice, the cholinergic component of this indirect effect shall not be responsible for the abrogated serotonergic effect. The selective expression of Cav-3 in epithelial cells – present in tracheal but not in intrapulmonary bronchial epithelial cells – might explain the differential effects of Cav-3 deficiency on serotonergic ASM constriction. Potentially, these data warrant consideration during pharmacological modulation of the cholinergic and serotonergic responses and provide an opportunity to modulate airway hyperreactivity.

6 Zusammenfassung

Acetylcholin (ACh) und Serotonin sind Bronchokonstriktoren von hoher klinischer Relevanz bei Erkrankungen, die mit bronchialer Hyperreagibilität einhergehen. Ihre Rezeptoren sind in spezialisierten Membrandomänen, Caveolae, organisiert. Dies sind Ω-förmige Membraneinstülpungen mit einem Proteingerüst aus Caveolinen (Cav-1, -2 und -3) und zytoplasmatischen Adapterproteinen (cavin-1 bis -4). Es gibt Hinweise, dass Cav-3 diesen Proteinkomplex in der glatten Atemwegsmuskulatur (ASM) organisiert. In dieser Arbeit wurde ein Cav-3-defizienter Mausstamm generiert und die funktionelle Rolle von Cav-3 in der ASM Konstriktion in Organbaduntersuchungen extrapulmonaler und videomikroskopischen Untersuchungen intrapulmonaler Bronchi in lebenden Lungenschnitten ermittelt. Die Verteilung und molekulare Zusammensetzung des caveolären Proteinkomplexes wurde mittels Immunfluoreszenz, RT-PCR, real-time PCR, Western blotting und Ko-Immunpräzipitation in Atemwegen der Maus und des Menschen untersucht. Cav-3 fand sich im Trachealepithel sowie ASM und war mit Cav-1, cavin-1 und cavin-4 assoziiert. Cav-3-Defizienz hatte weder auf die Expression anderer Proteinkomplexmitglieder, noch auf die von EHD-2, ein Strukturmarker von Caveolae, Einfluss. Cav-3 determiniert daher zwar spezifische Aspekte der Caveolenfunktion, nicht aber die strukturelle Ausbildung von Caveolae. Die Reaktion extrapulmonaler Atemwege auf Muskarin war unverändert in Cav-$3^{-/-}$ Mäusen, während die muskarinergen Konstriktion intrapulmonaler Bronchi zunahm. Dies zeigt eine inhibitorische Regulation der cholinergen Bronchokonstriktion durch Cav-3. Für Cav-3 wurde bereits eine Interaktion mit dem muskarinischen Rezeptorsubtyp 2 (M2R) in bronchialen Glattmuskelzellen gezeigt, und es koppelt den M2R mit Aktivierung der endothelialen NO-Synthase (eNOS) in Kardiomyozyten. Der Verlust von Cav-3 könnte daher die muskarinerge Bronchokonstriktion durch Aufhebung der M2R-Cav-3-eNOS-Koppelung verstärken. Die serotonininduzierte Konstriktion extrapulmonaler Atemwege war bei Cav-3-Defizienz völlig aufgehoben, während die der intrapulmonalen Bronchi unverändert blieb. Bei der serotonergen Kontraktion der extrapulmonalen Atemwege der Maus wird von einer indirekten Wirkung auf das Epithel oder Nervenfasern mit folgender ACh-Freisetzung ausgegangen. Da die cholinerge Konstriktion der extrapulmonalen Atemwege in Cav-3-/-- Mäusen unverändert war, ist diese Komponente der indirekten Wirkung nicht für den Verlust der serotonergen Kontraktion verantwortlich. Die selektive Expression von Cav-3 in trachealen, aber nicht bronchialen Epithelzellen, könnte den differenziellen Effekt der Cav-3-Defizienz auf die serotonerge ASM Konstriktion der verschiedenen Abschnitte erklären.

Diese Daten sind bei der pharmakologischen Modulation der cholinergen und serotonergen Effekte zu berücksichtigen und könnten eine zusätzliche Möglichkeit zur Beeinflussung der Atemwegshyperreagibilität bieten.

7 References

1. Simons K, Ikonen E: **Functional rafts in cell membranes.** *Nature* 1997, **387:**569-572.
2. Pike LJ: **Lipid rafts: bringing order to chaos.** *J Lipid Res* 2003, **44:**655-667.
3. Galbiati F, Razani B, Lisanti MP: **Caveolae and caveolin-3 in muscular dystrophy.** *Trends Mol Med* 2001, **7:**435-441.
4. Hansen CG, Nichols BJ: **Molecular mechanisms of clathrin-independent endocytosis.** *J Cell Sci* 2009, **122:**1713-1721.
5. Murata M, Peranen J, Schreiner R, Wieland F, Kurzchalia TV, Simons K: **VIP21/caveolin is a cholesterol-binding protein.** *Proc Natl Acad Sci U S A* 1995, **92:**10339-10343.
6. Fra AM, Williamson E, Simons K, Parton RG: **De novo formation of caveolae in lymphocytes by expression of VIP21-caveolin.** *Proc Natl Acad Sci U S A* 1995, **92:**8655-8659.
7. Le PU, Guay G, Altschuler Y, Nabi IR: **Caveolin-1 is a negative regulator of caveolae-mediated endocytosis to the endoplasmic reticulum.** *J Biol Chem* 2002, **277:**3371-3379.
8. Parton RG, del Pozo MA: **Caveolae as plasma membrane sensors, protectors and organizers.** *Nat Rev Mol Cell Biol* 2013, **14:**98-112.
9. Pelkmans L, Zerial M: **Kinase-regulated quantal assemblies and kiss-and-run recycling of caveolae.** *Nature* 2005, **436:**128-133.
10. Richter T, Floetenmeyer M, Ferguson C, Galea J, Goh J, Lindsay MR, Morgan GP, Marsh BJ, Parton RG: **High-resolution 3D quantitative analysis of caveolar ultrastructure and caveola-cytoskeleton interactions.** *Traffic* 2008, **9:**893-909.
11. Cohen AW, Hnasko R, Schubert W, Lisanti MP: **Role of caveolae and caveolins in health and disease.** *Physiol Rev* 2004, **84:**1341-1379.
12. Fujimoto T: **Calcium pump of the plasma membrane is localized in caveolae.** *J Cell Biol* 1993, **120:**1147-1157.
13. Fujimoto T, Nakade S, Miyawaki A, Mikoshiba K, Ogawa K: **Localization of inositol 1,4,5-trisphosphate receptor-like protein in plasmalemmal caveolae.** *J Cell Biol* 1992, **119:**1507-1513.
14. Razani B, Woodman SE, Lisanti MP: **Caveolae: from cell biology to animal physiology.** *Pharmacol Rev* 2002, **54:**431-467.
15. Bastiani M, Parton RG: **Caveolae at a glance.** *J Cell Sci* 2010, **123:**3831-3836.
16. Schlenz H, Kummer W, Jositsch G, Wess J, Krasteva G: **Muscarinic receptor-mediated bronchoconstriction is coupled to caveolae in murine airways.** *Am J Physiol Lung Cell Mol Physiol* 2010, **298:**L626-636.
17. Ostrom RS, Insel PA: **The evolving role of lipid rafts and caveolae in G protein-coupled receptor signaling: implications for molecular pharmacology.** *Br J Pharmacol* 2004, **143:**235-245.
18. Gosens R, Stelmack GL, Dueck G, Mutawe MM, Hinton M, McNeill KD, Paulson A, Dakshinamurti S, Gerthoffer WT, Thliveris JA, et al: **Caveolae facilitate muscarinic receptor-mediated intracellular Ca2+ mobilization and contraction in airway smooth muscle.** *Am J Physiol Lung Cell Mol Physiol* 2007, **293:**L1406-1418.
19. Lee J, Schmid-Schonbein GW: **Biomechanics of skeletal muscle capillaries: hemodynamic resistance, endothelial distensibility, and pseudopod formation.** *Ann Biomed Eng* 1995, **23:**226-246.
20. Rajab A, Straub V, McCann LJ, Seelow D, Varon R, Barresi R, Schulze A, Lucke B, Lutzkendorf S, Karbasiyan M, et al: **Fatal cardiac arrhythmia and long-QT syndrome in a new form of congenital generalized lipodystrophy with muscle rippling (CGL4) due to PTRF-CAVIN mutations.** *PLoS Genet* 2010, **6:**e1000874.
21. Hayashi YK, Matsuda C, Ogawa M, Goto K, Tominaga K, Mitsuhashi S, Park YE, Nonaka I, Hino-Fukuyo N, Haginoya K, et al: **Human PTRF mutations cause secondary deficiency of caveolins resulting in muscular dystrophy with generalized lipodystrophy.** *J Clin Invest* 2009, **119:**2623-2633.

22. Kurzchalia TV, Dupree P, Parton RG, Kellner R, Virta H, Lehnert M, Simons K: **VIP21, a 21-kD membrane protein is an integral component of trans-Golgi-network-derived transport vesicles.** *J Cell Biol* 1992, **118:**1003-1014.
23. Tagawa A, Mezzacasa A, Hayer A, Longatti A, Pelkmans L, Helenius A: **Assembly and trafficking of caveolar domains in the cell: caveolae as stable, cargo-triggered, vesicular transporters.** *J Cell Biol* 2005, **170:**769-779.
24. Gratton JP, Bernatchez P, Sessa WC: **Caveolae and caveolins in the cardiovascular system.** *Circ Res* 2004, **94:**1408-1417.
25. Sargiacomo M, Scherer PE, Tang Z, Kubler E, Song KS, Sanders MC, Lisanti MP: **Oligomeric structure of caveolin: implications for caveolae membrane organization.** *Proc Natl Acad Sci U S A* 1995, **92:**9407-9411.
26. Patel HH, Tsutsumi YM, Head BP, Niesman IR, Jennings M, Horikawa Y, Huang D, Moreno AL, Patel PM, Insel PA, Roth DM: **Mechanisms of cardiac protection from ischemia/reperfusion injury: a role for caveolae and caveolin-1.** *FASEB J* 2007, **21:**1565-1574.
27. Head BP, Patel HH, Roth DM, Murray F, Swaney JS, Niesman IR, Farquhar MG, Insel PA: **Microtubules and actin microfilaments regulate lipid raft/caveolae localization of adenylyl cyclase signaling components.** *J Biol Chem* 2006, **281:**26391-26399.
28. Robenek H, Weissen-Plenz G, Severs NJ: **Freeze-fracture replica immunolabelling reveals caveolin-1 in the human cardiomyocyte plasma membrane.** *J Cell Mol Med* 2008, **12:**2519-2521.
29. Song KS, Scherer PE, Tang Z, Okamoto T, Li S, Chafel M, Chu C, Kohtz DS, Lisanti MP: **Expression of caveolin-3 in skeletal, cardiac, and smooth muscle cells. Caveolin-3 is a component of the sarcolemma and co-fractionates with dystrophin and dystrophin-associated glycoproteins.** *J Biol Chem* 1996, **271:**15160-15165.
30. Wang XM, Zhang Y, Kim HP, Zhou Z, Feghali-Bostwick CA, Liu F, Ifedigbo E, Xu X, Oury TD, Kaminski N, Choi AM: **Caveolin-1: a critical regulator of lung fibrosis in idiopathic pulmonary fibrosis.** *J Exp Med* 2006, **203:**2895-2906.
31. Bernatchez PN, Bauer PM, Yu J, Prendergast JS, He P, Sessa WC: **Dissecting the molecular control of endothelial NO synthase by caveolin-1 using cell-permeable peptides.** *Proc Natl Acad Sci U S A* 2005, **102:**761-766.
32. Murata T, Lin MI, Stan RV, Bauer PM, Yu J, Sessa WC: **Genetic evidence supporting caveolae microdomain regulation of calcium entry in endothelial cells.** *J Biol Chem* 2007, **282:**16631-16643.
33. Bauer PM, Yu J, Chen Y, Hickey R, Bernatchez PN, Looft-Wilson R, Huang Y, Giordano F, Stan RV, Sessa WC: **Endothelial-specific expression of caveolin-1 impairs microvascular permeability and angiogenesis.** *Proc Natl Acad Sci U S A* 2005, **102:**204-209.
34. Yu J, Bergaya S, Murata T, Alp IF, Bauer MP, Lin MI, Drab M, Kurzchalia TV, Stan RV, Sessa WC: **Direct evidence for the role of caveolin-1 and caveolae in mechanotransduction and remodeling of blood vessels.** *J Clin Invest* 2006, **116:**1284-1291.
35. Garcia-Cardena G, Martasek P, Masters BS, Skidd PM, Couet J, Li S, Lisanti MP, Sessa WC: **Dissecting the interaction between nitric oxide synthase (NOS) and caveolin. Functional significance of the nos caveolin binding domain in vivo.** *J Biol Chem* 1997, **272:**25437-25440.
36. Venema VJ, Ju H, Zou R, Venema RC: **Interaction of neuronal nitric-oxide synthase with caveolin-3 in skeletal muscle. Identification of a novel caveolin scaffolding/inhibitory domain.** *J Biol Chem* 1997, **272:**28187-28190.
37. Biederer CH, Ries SJ, Moser M, Florio M, Israel MA, McCormick F, Buettner R: **The basic helix-loop-helix transcription factors myogenin and Id2 mediate specific induction of caveolin-3 gene expression during embryonic development.** *J Biol Chem* 2000, **275:**26245-26251.
38. Parton RG, Way M, Zorzi N, Stang E: **Caveolin-3 associates with developing T-tubules during muscle differentiation.** *J Cell Biol* 1997, **136:**137-154.
39. Capozza F, Cohen AW, Cheung MW, Sotgia F, Schubert W, Battista M, Lee H, Frank PG, Lisanti MP: **Muscle-specific interaction of caveolin isoforms: differential complex**

formation between caveolins in fibroblastic vs. muscle cells. *Am J Physiol Cell Physiol* 2005, **288:**C677-691.

40. Volonte D, McTiernan CF, Drab M, Kasper M, Galbiati F: **Caveolin-1 and caveolin-3 form heterooligomeric complexes in atrial cardiac myocytes that are required for doxorubicin-induced apoptosis.** *Am J Physiol Heart Circ Physiol* 2008, **294:**H392-401.
41. Gutierrez-Pajares JL, Iturrieta J, Dulam V, Wang Y, Pavlides S, Malacari G, Lisanti MP, Frank PG: **Caveolin-3 Promotes a Vascular Smooth Muscle Contractile Phenotype.** *Front Cardiovasc Med* 2015, **2:**27.
42. Le Lay S, Kurzchalia TV: **Getting rid of caveolins: phenotypes of caveolin-deficient animals.** *Biochim Biophys Acta* 2005, **1746:**322-333.
43. Alvarez-Santos M, Ramos-Ramirez P, Gutierrez-Aguilar F, Sanchez-Hernandez S, Lascurain R, Olmos-Zuniga R, Jasso-Victoria R, Bobadilla NA, Bazan-Perkins B: **Antigen-induced airway hyperresponsiveness and obstruction is related to caveolin-1 expression in airway smooth muscle in a guinea pig asthma model.** *Clin Transl Allergy* 2015, **5:**14.
44. Bains SN, Tourkina E, Atkinson C, Joseph K, Tholanikunnel B, Chu HW, Riemer EC, Martin R, Hoffman S: **Loss of caveolin-1 from bronchial epithelial cells and monocytes in human subjects with asthma.** *Allergy* 2012, **67:**1601-1604.
45. Hagiwara Y, Sasaoka T, Araishi K, Imamura M, Yorifuji H, Nonaka I, Ozawa E, Kikuchi T: **Caveolin-3 deficiency causes muscle degeneration in mice.** *Hum Mol Genet* 2000, **9:**3047-3054.
46. Woodman SE, Park DS, Cohen AW, Cheung MW, Chandra M, Shirani J, Tang B, Jelicks LA, Kitsis RN, Christ GJ, et al: **Caveolin-3 knock-out mice develop a progressive cardiomyopathy and show hyperactivation of the p42/44 MAPK cascade.** *J Biol Chem* 2002, **277:**38988-38997.
47. Crossman DJ, Ruygrok PN, Soeller C, Cannell MB: **Changes in the organization of excitation-contraction coupling structures in failing human heart.** *PLoS One* 2011, **6:**e17901.
48. Hayashi T, Arimura T, Ueda K, Shibata H, Hohda S, Takahashi M, Hori H, Koga Y, Oka N, Imaizumi T, et al: **Identification and functional analysis of a caveolin-3 mutation associated with familial hypertrophic cardiomyopathy.** *Biochem Biophys Res Commun* 2004, **313:**178-184.
49. Minetti C, Bado M, Broda P, Sotgia F, Bruno C, Galbiati F, Volonte D, Lucania G, Pavan A, Bonilla E, et al: **Impairment of caveolae formation and T-system disorganization in human muscular dystrophy with caveolin-3 deficiency.** *Am J Pathol* 2002, **160:**265-270.
50. Rybin VO, Xu X, Steinberg SF: **Activated protein kinase C isoforms target to cardiomyocyte caveolae : stimulation of local protein phosphorylation.** *Circ Res* 1999, **84:**980-988.
51. Rybin VO, Xu X, Lisanti MP, Steinberg SF: **Differential targeting of beta -adrenergic receptor subtypes and adenylyl cyclase to cardiomyocyte caveolae. A mechanism to functionally regulate the cAMP signaling pathway.** *J Biol Chem* 2000, **275:**41447-41457.
52. Rybin VO, Pak E, Alcott S, Steinberg SF: **Developmental changes in beta2-adrenergic receptor signaling in ventricular myocytes: the role of Gi proteins and caveolae microdomains.** *Mol Pharmacol* 2003, **63:**1338-1348.
53. Moren B, Shah C, Howes MT, Schieber NL, McMahon HT, Parton RG, Daumke O, Lundmark R: **EHD2 regulates caveolar dynamics via ATP-driven targeting and oligomerization.** *Mol Biol Cell* 2012, **23:**1316-1329.
54. Stoeber M, Stoeck IK, Hanni C, Bleck CK, Balistreri G, Helenius A: **Oligomers of the ATPase EHD2 confine caveolae to the plasma membrane through association with actin.** *EMBO J* 2012, **31:**2350-2364.
55. Henley JR, Krueger EW, Oswald BJ, McNiven MA: **Dynamin-mediated internalization of caveolae.** *J Cell Biol* 1998, **141:**85-99.
56. Oh P, McIntosh DP, Schnitzer JE: **Dynamin at the neck of caveolae mediates their budding to form transport vesicles by GTP-driven fission from the plasma membrane of endothelium.** *J Cell Biol* 1998, **141:**101-114.

57. Hansen CG, Shvets E, Howard G, Riento K, Nichols BJ: **Deletion of cavin genes reveals tissue-specific mechanisms for morphogenesis of endothelial caveolae.** *Nat Commun* 2013, **4:**1831.
58. Bastiani M, Liu L, Hill MM, Jedrychowski MP, Nixon SJ, Lo HP, Abankwa D, Luetterforst R, Fernandez-Rojo M, Breen MR, et al: **MURC/Cavin-4 and cavin family members form tissue-specific caveolar complexes.** *J Cell Biol* 2009, **185:**1259-1273.
59. Kovtun O, Tillu VA, Ariotti N, Parton RG, Collins BM: **Cavin family proteins and the assembly of caveolae.** *J Cell Sci* 2015, **128:**1269-1278.
60. Rahman A, Sward K: **The role of caveolin-1 in cardiovascular regulation.** *Acta Physiol (Oxf)* 2009, **195:**231-245.
61. Fairn GD, Schieber NL, Ariotti N, Murphy S, Kuerschner L, Webb RI, Grinstein S, Parton RG: **High-resolution mapping reveals topologically distinct cellular pools of phosphatidylserine.** *J Cell Biol* 2011, **194:**257-275.
62. Jansa P, Mason SW, Hoffmann-Rohrer U, Grummt I: **Cloning and functional characterization of PTRF, a novel protein which induces dissociation of paused ternary transcription complexes.** *EMBO J* 1998, **17:**2855-2864.
63. Gustincich S, Schneider C: **Serum deprivation response gene is induced by serum starvation but not by contact inhibition.** *Cell Growth Differ* 1993, **4:**753-760.
64. Izumi Y, Hirai S, Tamai Y, Fujise-Matsuoka A, Nishimura Y, Ohno S: **A protein kinase Cdelta-binding protein SRBC whose expression is induced by serum starvation.** *J Biol Chem* 1997, **272:**7381-7389.
65. Ogata T, Ueyama T, Isodono K, Tagawa M, Takehara N, Kawashima T, Harada K, Takahashi T, Shioi T, Matsubara H, Oh H: **MURC, a muscle-restricted coiled-coil protein that modulates the Rho/ROCK pathway, induces cardiac dysfunction and conduction disturbance.** *Mol Cell Biol* 2008, **28:**3424-3436.
66. Tagawa M, Ueyama T, Ogata T, Takehara N, Nakajima N, Isodono K, Asada S, Takahashi T, Matsubara H, Oh H: **MURC, a muscle-restricted coiled-coil protein, is involved in the regulation of skeletal myogenesis.** *Am J Physiol Cell Physiol* 2008, **295:**C490-498.
67. Hansen CG, Nichols BJ: **Exploring the caves: cavins, caveolins and caveolae.** *Trends Cell Biol* 2010, **20:**177-186.
68. Hill MM, Bastiani M, Luetterforst R, Kirkham M, Kirkham A, Nixon SJ, Walser P, Abankwa D, Oorschot VM, Martin S, et al: **PTRF-Cavin, a conserved cytoplasmic protein required for caveola formation and function.** *Cell* 2008, **132:**113-124.
69. Breen MR, Camps M, Carvalho-Simoes F, Zorzano A, Pilch PF: **Cholesterol depletion in adipocytes causes caveolae collapse concomitant with proteosomal degradation of cavin-2 in a switch-like fashion.** *PLoS One* 2012, **7:**e34516.
70. Sinha B, Koster D, Ruez R, Gonnord P, Bastiani M, Abankwa D, Stan RV, Butler-Browne G, Vedie B, Johannes L, et al: **Cells respond to mechanical stress by rapid disassembly of caveolae.** *Cell* 2011, **144:**402-413.
71. Liu L, Brown D, McKee M, Lebrasseur NK, Yang D, Albrecht KH, Ravid K, Pilch PF: **Deletion of Cavin/PTRF causes global loss of caveolae, dyslipidemia, and glucose intolerance.** *Cell Metab* 2008, **8:**310-317.
72. Foster LJ, De Hoog CL, Mann M: **Unbiased quantitative proteomics of lipid rafts reveals high specificity for signaling factors.** *Proc Natl Acad Sci U S A* 2003, **100:**5813-5818.
73. Voldstedlund M, Vinten J, Tranum-Jensen J: **cav-p60 expression in rat muscle tissues. Distribution of caveolar proteins.** *Cell Tissue Res* 2001, **306:**265-276.
74. Cao H, Alston L, Ruschman J, Hegele RA: **Heterozygous CAV1 frameshift mutations (MIM 601047) in patients with atypical partial lipodystrophy and hypertriglyceridemia.** *Lipids Health Dis* 2008, **7:**3.
75. Woodman SE, Cheung MW, Tarr M, North AC, Schubert W, Lagaud G, Marks CB, Russell RG, Hassan GS, Factor SM, et al: **Urogenital alterations in aged male caveolin-1 knockout mice.** *J Urol* 2004, **171:**950-957.
76. McNally EM, de Sa Moreira E, Duggan DJ, Bonnemann CG, Lisanti MP, Lidov HG, Vainzof M, Passos-Bueno MR, Hoffman EP, Zatz M, Kunkel LM: **Caveolin-3 in muscular dystrophy.** *Hum Mol Genet* 1998, **7:**871-877.

77. Minetti C, Sotgia F, Bruno C, Scartezzini P, Broda P, Bado M, Masetti E, Mazzocco M, Egeo A, Donati MA, et al: **Mutations in the caveolin-3 gene cause autosomal dominant limb-girdle muscular dystrophy.** *Nat Genet* 1998, **18:**365-368.
78. McMahon KA, Zajicek H, Li WP, Peyton MJ, Minna JD, Hernandez VJ, Luby-Phelps K, Anderson RG: **SRBC/cavin-3 is a caveolin adapter protein that regulates caveolae function.** *EMBO J* 2009, **28:**1001-1015.
79. Faggi F, Codenotti S, Poliani PL, Cominelli M, Chiarelli N, Colombi M, Vezzoli M, Monti E, Bono F, Tulipano G, et al: **MURC/cavin-4 is co-expressed with caveolin-3 in rhabdomyosarcoma tumors and its silencing prevents myogenic differentiation in the human embryonal RD cell line.** *PLoS One* 2015, **10:**e0130287.
80. Vatta M, Ackerman MJ, Ye B, Makielski JC, Ughanze EE, Taylor EW, Tester DJ, Balijepalli RC, Foell JD, Li Z, et al: **Mutant caveolin-3 induces persistent late sodium current and is associated with long-QT syndrome.** *Circulation* 2006, **114:**2104-2112.
81. Rock JR, Randell SH, Hogan BL: **Airway basal stem cells: a perspective on their roles in epithelial homeostasis and remodeling.** *Dis Model Mech* 2010, **3:**545-556.
82. Wess J, Han SJ, Kim SK, Jacobson KA, Li JH: **Conformational changes involved in G-protein-coupled-receptor activation.** *Trends Pharmacol Sci* 2008, **29:**616-625.
83. Pierce KL, Premont RT, Lefkowitz RJ: **Seven-transmembrane receptors.** *Nat Rev Mol Cell Biol* 2002, **3:**639-650.
84. Long JW, Yang XD, Cao L, Lu SM, Cao YX: **Alteration of airway responsiveness mediated by receptors in ovalbumin-induced asthmatic E3 rats.** *Acta Pharmacol Sin* 2009, **30:**965-972.
85. Struckmann N, Schwering S, Wiegand S, Gschnell A, Yamada M, Kummer W, Wess J, Haberberger RV: **Role of muscarinic receptor subtypes in the constriction of peripheral airways: studies on receptor-deficient mice.** *Mol Pharmacol* 2003, **64:**1444-1451.
86. Mak JC, Barnes PJ: **Autoradiographic visualization of muscarinic receptor subtypes in human and guinea pig lung.** *Am Rev Respir Dis* 1990, **141:**1559-1568.
87. Cheng JB, Townley RG: **Comparison of muscarinic and beta adrenergic receptors between bovine peripheral lung and tracheal smooth muscles: a striking difference in the receptor concentration.** *Life Sci* 1982, **30:**2079-2086.
88. Eglen RM, Hegde SS, Watson N: **Muscarinic receptor subtypes and smooth muscle function.** *Pharmacol Rev* 1996, **48:**531-565.
89. Ikeda T, Anisuzzaman AS, Yoshiki H, Sasaki M, Koshiji T, Uwada J, Nishimune A, Itoh H, Muramatsu I: **Regional quantification of muscarinic acetylcholine receptors and beta-adrenoceptors in human airways.** *Br J Pharmacol* 2012, **166:**1804-1814.
90. Roffel AF, Elzinga CR, Zaagsma J: **Muscarinic M3 receptors mediate contraction of human central and peripheral airway smooth muscle.** *Pulm Pharmacol* 1990, **3:**47-51.
91. Mitchelson F: **Muscarinic receptor differentiation.** *Pharmacol Ther* 1988, **37:**357-423.
92. Grandordy BM, Cuss FM, Sampson AS, Palmer JB, Barnes PJ: **Phosphatidylinositol response to cholinergic agonists in airway smooth muscle: relationship to contraction and muscarinic receptor occupancy.** *J Pharmacol Exp Ther* 1986, **238:**273-279.
93. Meurs H, Timmermans A, Van Amsterdam RG, Brouwer F, Kauffman HF, Zaagsma J: **Muscarinic receptors in human airway smooth muscle are coupled to phosphoinositide metabolism.** *Eur J Pharmacol* 1989, **164:**369-371.
94. Hirshman CA, Lande B, Croxton TL: **Role of M2 muscarinic receptors in airway smooth muscle contraction.** *Life Sci* 1999, **64:**443-448.
95. Wang YX, Dhulipala PD, Li L, Benovic JL, Kotlikoff MI: **Coupling of M2 muscarinic receptors to membrane ion channels via phosphoinositide 3-kinase gamma and atypical protein kinase C.** *J Biol Chem* 1999, **274:**13859-13864.
96. Jones CA, Madison JM, Tom-Moy M, Brown JK: **Muscarinic cholinergic inhibition of adenylate cyclase in airway smooth muscle.** *Am J Physiol* 1987, **253:**C97-104.
97. Sankary RM, Jones CA, Madison JM, Brown JK: **Muscarinic cholinergic inhibition of cyclic AMP accumulation in airway smooth muscle. Role of a pertussis toxin-sensitive protein.** *Am Rev Respir Dis* 1988, **138:**145-150.

98. Stengel PW, Gomeza J, Wess J, Cohen ML: **M(2) and M(4) receptor knockout mice: muscarinic receptor function in cardiac and smooth muscle in vitro.** *J Pharmacol Exp Ther* 2000, **292:**877-885.
99. Stengel PW, Yamada M, Wess J, Cohen ML: **M(3)-receptor knockout mice: muscarinic receptor function in atria, stomach fundus, urinary bladder, and trachea.** *Am J Physiol Regul Integr Comp Physiol* 2002, **282:**R1443-1449.
100. Lai HH, Boone TB, Yang G, Smith CP, Kiss S, Thompson TC, Somogyi GT: **Loss of caveolin-1 expression is associated with disruption of muscarinic cholinergic activities in the urinary bladder.** *Neurochem Int* 2004, **45:**1185-1193.
101. Somara S, Gilmont RR, Martens JR, Bitar KN: **Ectopic expression of caveolin-1 restores physiological contractile response of aged colonic smooth muscle.** *Am J Physiol Gastrointest Liver Physiol* 2007, **293:**G240-249.
102. Prakash YS, Thompson MA, Vaa B, Matabdin I, Peterson TE, He T, Pabelick CM: **Caveolins and intracellular calcium regulation in human airway smooth muscle.** *Am J Physiol Lung Cell Mol Physiol* 2007, **293:**L1118-1126.
103. Sharma P, Ryu MH, Basu S, Maltby SA, Yeganeh B, Mutawe MM, Mitchell RW, Halayko AJ: **Epithelium-dependent modulation of responsiveness of airways from caveolin-1 knockout mice is mediated through cyclooxygenase-2 and 5-lipoxygenase.** *Br J Pharmacol* 2012, **167:**548-560.
104. Feron O, Smith TW, Michel T, Kelly RA: **Dynamic targeting of the agonist-stimulated m2 muscarinic acetylcholine receptor to caveolae in cardiac myocytes.** *J Biol Chem* 1997, **272:**17744-17748.
105. Krasteva G, Pfeil U, Filip AM, Lips KS, Kummer W, Konig P: **Caveolin-3 and eNOS colocalize and interact in ciliated airway epithelial cells in the rat.** *Int J Biochem Cell Biol* 2007, **39:**615-625.
106. Bai Y, Zhang M, Sanderson MJ: **Contractility and Ca2+ signaling of smooth muscle cells in different generations of mouse airways.** *Am J Respir Cell Mol Biol* 2007, **36:**122-130.
107. Kummer W, Wiegand S, Akinci S, Wessler I, Schinkel AH, Wess J, Koepsell H, Haberberger RV, Lips KS: **Role of acetylcholine and polyspecific cation transporters in serotonin-induced bronchoconstriction in the mouse.** *Respir Res* 2006, **7:**65.
108. Ikawati Z, Hayashi M, Nose M, Maeyama K: **The lack of compound 48/80-induced contraction in isolated trachea of mast cell-deficient Ws/Ws rats in vitro: the role of connective tissue mast cells.** *Eur J Pharmacol* 2000, **402:**297-306.
109. Davis C, Kannan MS, Jones TR, Daniel EE: **Control of human airway smooth muscle: in vitro studies.** *J Appl Physiol Respir Environ Exerc Physiol* 1982, **53:**1080-1087.
110. Wohlsen A, Uhlig S, Martin C: **Immediate allergic response in small airways.** *Am J Respir Crit Care Med* 2001, **163:**1462-1469.
111. Cushley MJ, Wee LH, Holgate ST: **The effect of inhaled 5-hydroxytryptamine (5-HT, serotonin) on airway calibre in man.** *Br J Clin Pharmacol* 1986, **22:**487-490.
112. Cazzola I, Matera MG: **5-HT modifiers as a potential treatment of asthma.** *Trends Pharmacol Sci* 2000, **21:**13-16.
113. Lechin F, van der Dijs B, Orozco B, Lechin M, Lechin AE: **Increased levels of free serotonin in plasma of symptomatic asthmatic patients.** *Ann Allergy Asthma Immunol* 1996, **77:**245-253.
114. Sommer B, Montano LM, Carbajal V, Flores-Soto E, Ortega A, Ramirez-Oseguera R, Irles C, El-Yazbi AF, Cho WJ, Daniel EE: **Extraction of membrane cholesterol disrupts caveolae and impairs serotonergic (5-HT2A) and histaminergic (H1) responses in bovine airway smooth muscle: role of Rho-kinase.** *Can J Physiol Pharmacol* 2009, **87:**180-195.
115. Dreja K, Voldstedlund M, Vinten J, Tranum-Jensen J, Hellstrand P, Sward K: **Cholesterol depletion disrupts caveolae and differentially impairs agonist-induced arterial contraction.** *Arterioscler Thromb Vasc Biol* 2002, **22:**1267-1272.
116. Shakirova Y, Bonnevier J, Albinsson S, Adner M, Rippe B, Broman J, Arner A, Sward K: **Increased Rho activation and PKC-mediated smooth muscle contractility in the absence of caveolin-1.** *Am J Physiol Cell Physiol* 2006, **291:**C1326-1335.

117. Akopov SE, Zhang L, Pearce WJ: **Regulation of Ca2+ sensitization by PKC and rho proteins in ovine cerebral arteries: effects of artery size and age.** *Am J Physiol* 1998, **275:**H930-939.
118. Masu K, Saino T, Kuroda T, Matsuura M, Russa AD, Ishikita N, Satoh Y: **Regional differences in 5-HT receptors in cerebral and testicular arterioles of the rat as revealed by Ca2+ imaging of real-time confocal microscopy: variances by artery size and organ specificity.** *Arch Histol Cytol* 2008, **71:**291-302.
119. Nuno DW, England SK, Lamping KG: **RhoA localization with caveolin-1 regulates vascular contractions to serotonin.** *Am J Physiol Regul Integr Comp Physiol* 2012, **303:**R959-967.
120. Mialet-Perez J, D'Angelo R, Villeneuve C, Ordener C, Negre-Salvayre A, Parini A, Vindis C: **Serotonin 5-HT2A receptor-mediated hypertrophy is negatively regulated by caveolin-3 in cardiomyoblasts and neonatal cardiomyocytes.** *J Mol Cell Cardiol* 2012, **52:**502-510.
121. Bhatnagar A, Sheffler DJ, Kroeze WK, Compton-Toth B, Roth BL: **Caveolin-1 interacts with 5-HT2A serotonin receptors and profoundly modulates the signaling of selected Galphaq-coupled protein receptors.** *J Biol Chem* 2004, **279:**34614-34623.
122. Dupont LJ, Pype JL, Demedts MG, De Leyn P, Deneffe G, Verleden GM: **The effects of 5-HT on cholinergic contraction in human airways in vitro.** *Eur Respir J* 1999, **14:**642-649.
123. Van Nueten JM, Leysen JE, Vanhoutte PM, Janssen PA: **Serotonergic responses in vascular and non-vascular tissues.** *Arch Int Pharmacodyn Ther* 1982, **256:**331-334.
124. Buckner CK, Dea D, Liberati N, Krell RD: **A pharmacologic examination of receptors mediating serotonin-induced bronchoconstriction in the anesthetized guinea pig.** *J Pharmacol Exp Ther* 1991, **257:**26-34.
125. Segura P, Vargas MH, Cordoba-Rodriguez G, Chavez J, Arreola JL, Campos-Bedolla P, Ruiz V, Garcia-Hernandez LM, Mendez C, Montano LM: **Role of 5-HT2A, 5-HT4 and 5-HT7 receptors in the antigen-induced airway hyperresponsiveness in guinea-pigs.** *Clin Exp Allergy* 2010, **40:**327-338.
126. Rizzo CA, Kreutner W, Chapman RW: **5-HT3 receptors augment neuronal, cholinergic contractions in guinea pig trachea.** *Eur J Pharmacol* 1993, **234:**109-112.
127. Tolloczko B, Jia YL, Martin JG: **Serotonin-evoked calcium transients in airway smooth muscle cells.** *Am J Physiol* 1995, **269:**L234-240.
128. Webber SE, Salonen RO, Widdicombe JG: **Receptors mediating the effects of 5-hydroxytryptamine on the tracheal vasculature and smooth muscle of sheep.** *Br J Pharmacol* 1990, **99:**21-26.
129. Bergdahl A, Gomez MF, Dreja K, Xu SZ, Adner M, Beech DJ, Broman J, Hellstrand P, Sward K: **Cholesterol depletion impairs vascular reactivity to endothelin-1 by reducing store-operated Ca2+ entry dependent on TRPC1.** *Circ Res* 2003, **93:**839-847.
130. El-Yazbi AF, Cho WJ, Boddy G, Daniel EE: **Caveolin-1 gene knockout impairs nitrergic function in mouse small intestine.** *Br J Pharmacol* 2005, **145:**1017-1026.
131. Lee YH, Hwang MK, Morgan KG, Taggart MJ: **Receptor-coupled contractility of uterine smooth muscle: from membrane to myofilaments.** *Exp Physiol* 2001, **86:**283-288.
132. Gosens R, Stelmack GL, Bos ST, Dueck G, Mutawe MM, Schaafsma D, Unruh H, Gerthoffer WT, Zaagsma J, Meurs H, Halayko AJ: **Caveolin-1 is required for contractile phenotype expression by airway smooth muscle cells.** *J Cell Mol Med* 2011, **15:**2430-2442.
133. Weiss N, Couchoux H, Legrand C, Berthier C, Allard B, Jacquemond V: **Expression of the muscular dystrophy-associated caveolin-3(P104L) mutant in adult mouse skeletal muscle specifically alters the Ca(2+) channel function of the dihydropyridine receptor.** *Pflugers Arch* 2008, **457:**361-375.
134. Franzini-Armstrong C: **Simultaneous maturation of transverse tubules and sarcoplasmic reticulum during muscle differentiation in the mouse.** *Dev Biol* 1991, **146:**353-363.
135. Vassilopoulos S, Oddoux S, Groh S, Cacheux M, Faure J, Brocard J, Campbell KP, Marty I: **Caveolin 3 is associated with the calcium release complex and is modified via in vivo triadin modification.** *Biochemistry* 2010, **49:**6130-6135.
136. Gosens R, Mutawe M, Martin S, Basu S, Bos ST, Tran T, Halayko AJ: **Caveolae and caveolins in the respiratory system.** *Curr Mol Med* 2008, **8:**741-753.

137. Munoz P, Rosemblatt M, Testar X, Palacin M, Zorzano A: **Isolation and characterization of distinct domains of sarcolemma and T-tubules from rat skeletal muscle.** *Biochem J* 1995, **307 (Pt 1):**273-280.
138. Tang Z, Scherer PE, Okamoto T, Song K, Chu C, Kohtz DS, Nishimoto I, Lodish HF, Lisanti MP: **Molecular cloning of caveolin-3, a novel member of the caveolin gene family expressed predominantly in muscle.** *J Biol Chem* 1996, **271:**2255-2261.
139. Segal SS, Brett SE, Sessa WC: **Codistribution of NOS and caveolin throughout peripheral vasculature and skeletal muscle of hamsters.** *Am J Physiol* 1999, **277:**H1167-1177.
140. Shanahan CM, Weissberg PL: **Smooth muscle cell heterogeneity: patterns of gene expression in vascular smooth muscle cells in vitro and in vivo.** *Arterioscler Thromb Vasc Biol* 1998, **18:**333-338.
141. Sterk PJ, Fabbri LM, Quanjer PH, Cockcroft DW, O'Byrne PM, Anderson SD, Juniper EF, Malo JL: **Airway responsiveness. Standardized challenge testing with pharmacological, physical and sensitizing stimuli in adults. Report Working Party Standardization of Lung Function Tests, European Community for Steel and Coal. Official Statement of the European Respiratory Society.** *Eur Respir J Suppl* 1993, **16:**53-83.
142. Grootendorst DC, Rabe KF: **Mechanisms of bronchial hyperreactivity in asthma and chronic obstructive pulmonary disease.** *Proc Am Thorac Soc* 2004, **1:**77-87.
143. Fryer AD, Jacoby DB: **Muscarinic receptors and control of airway smooth muscle.** *Am J Respir Crit Care Med* 1998, **158:**S154-160.
144. Kim SO, Song SH, Lee SC, Cho KA, Park JS, Kwon D, Park K: **Altered expression of caveolin 2 and 3 in smooth muscle of rat urinary bladder by 17beta-estradiol.** *BMC Urol* 2013, **13:**44.
145. Halayko AJ, Tran T, Gosens R: **Phenotype and functional plasticity of airway smooth muscle: role of caveolae and caveolins.** *Proc Am Thorac Soc* 2008, **5:**80-88.
146. Wright PT, Nikolaev VO, O'Hara T, Diakonov I, Bhargava A, Tokar S, Schobesberger S, Shevchuk AI, Sikkel MB, Wilkinson R, et al: **Caveolin-3 regulates compartmentation of cardiomyocyte beta2-adrenergic receptor-mediated cAMP signaling.** *J Mol Cell Cardiol* 2014, **67:**38-48.
147. Macdougall DA, Agarwal SR, Stopford EA, Chu H, Collins JA, Longster AL, Colyer J, Harvey RD, Calaghan S: **Caveolae compartmentalise beta2-adrenoceptor signals by curtailing cAMP production and maintaining phosphatase activity in the sarcoplasmic reticulum of the adult ventricular myocyte.** *J Mol Cell Cardiol* 2012, **52:**388-400.
148. Martin C, Uhlig S, Ullrich V: **Videomicroscopy of methacholine-induced contraction of individual airways in precision-cut lung slices.** *Eur Respir J* 1996, **9:**2479-2487.
149. Ludwig A, Howard G, Mendoza-Topaz C, Deerinck T, Mackey M, Sandin S, Ellisman MH, Nichols BJ: **Molecular composition and ultrastructure of the caveolar coat complex.** *PLoS Biol* 2013, **11:**e1001640.
150. Govender P, Romero F, Shah D, Paez J, Ding SY, Liu L, Gower A, Baez E, Aly SS, Pilch P, Summer R: **Cavin1; a regulator of lung function and macrophage phenotype.** *PLoS One* 2013, **8:**e62045.
151. Liu L, Pilch PF: **A critical role of cavin (polymerase I and transcript release factor) in caveolae formation and organization.** *J Biol Chem* 2008, **283:**4314-4322.
152. Sathish V, Thompson MA, Sinha S, Sieck GC, Prakash YS, Pabelick CM: **Inflammation, caveolae and CD38-mediated calcium regulation in human airway smooth muscle.** *Biochim Biophys Acta* 2014, **1843:**346-351.
153. Doyle DD, Upshaw-Earley J, Bell E, Palfrey HC: **Expression of caveolin-3 in rat aortic vascular smooth muscle cells is determined by developmental state.** *Biochem Biophys Res Commun* 2003, **304:**22-25.
154. Galbiati F, Engelman JA, Volonte D, Zhang XL, Minetti C, Li M, Hou H, Jr., Kneitz B, Edelmann W, Lisanti MP: **Caveolin-3 null mice show a loss of caveolae, changes in the microdomain distribution of the dystrophin-glycoprotein complex, and t-tubule abnormalities.** *J Biol Chem* 2001, **276:**21425-21433.
155. Krasteva G, Pfeil U, Drab M, Kummer W, Konig P: **Caveolin-1 and -2 in airway epithelium: expression and in situ association as detected by FRET-CLSM.** *Respir Res* 2006, **7:**108.

156. Ogata T, Naito D, Nakanishi N, Hayashi YK, Taniguchi T, Miyagawa K, Hamaoka T, Maruyama N, Matoba S, Ikeda K, et al: **MURC/Cavin-4 facilitates recruitment of ERK to caveolae and concentric cardiac hypertrophy induced by alpha1-adrenergic receptors.** *Proc Natl Acad Sci U S A* 2014, **111:**3811-3816.
157. Horikawa YT, Panneerselvam M, Kawaraguchi Y, Tsutsumi YM, Ali SS, Balijepalli RC, Murray F, Head BP, Niesman IR, Rieg T, et al: **Cardiac-specific overexpression of caveolin-3 attenuates cardiac hypertrophy and increases natriuretic peptide expression and signaling.** *J Am Coll Cardiol* 2011, **57:**2273-2283.
158. Tsutsumi YM, Horikawa YT, Jennings MM, Kidd MW, Niesman IR, Yokoyama U, Head BP, Hagiwara Y, Ishikawa Y, Miyanohara A, et al: **Cardiac-specific overexpression of caveolin-3 induces endogenous cardiac protection by mimicking ischemic preconditioning.** *Circulation* 2008, **118:**1979-1988.
159. Galbiati F, Volonte D, Chu JB, Li M, Fine SW, Fu M, Bermudez J, Pedemonte M, Weidenheim KM, Pestell RG, et al: **Transgenic overexpression of caveolin-3 in skeletal muscle fibers induces a Duchenne-like muscular dystrophy phenotype.** *Proc Natl Acad Sci U S A* 2000, **97:**9689-9694.
160. Zhu H, Lin P, De G, Choi KH, Takeshima H, Weisleder N, Ma J: **Polymerase transcriptase release factor (PTRF) anchors MG53 protein to cell injury site for initiation of membrane repair.** *J Biol Chem* 2011, **286:**12820-12824.
161. Ozier A, Allard B, Bara I, Girodet PO, Trian T, Marthan R, Berger P: **The pivotal role of airway smooth muscle in asthma pathophysiology.** *J Allergy (Cairo)* 2011, **2011:**742710.
162. Head BP, Patel HH, Roth DM, Lai NC, Niesman IR, Farquhar MG, Insel PA: **G-protein-coupled receptor signaling components localize in both sarcolemmal and intracellular caveolin-3-associated microdomains in adult cardiac myocytes.** *J Biol Chem* 2005, **280:**31036-31044.
163. Jositsch G, Papadakis T, Haberberger RV, Wolff M, Wess J, Kummer W: **Suitability of muscarinic acetylcholine receptor antibodies for immunohistochemistry evaluated on tissue sections of receptor gene-deficient mice.** *Naunyn Schmiedebergs Arch Pharmacol* 2009, **379:**389-395.
164. Pradidarcheep W, Stallen J, Labruyere WT, Dabhoiwala NF, Michel MC, Lamers WH: **Lack of specificity of commercially available antisera against muscarinergic and adrenergic receptors.** *Naunyn Schmiedebergs Arch Pharmacol* 2009, **379:**397-402.
165. Lowalekar SK, Cristofaro V, Radisavljevic ZM, Yalla SV, Sullivan MP: **Loss of bladder smooth muscle caveolae in the aging bladder.** *Neurourol Urodyn* 2012, **31:**586-592.
166. Feron O, Dessy C, Opel DJ, Arstall MA, Kelly RA, Michel T: **Modulation of the endothelial nitric-oxide synthase-caveolin interaction in cardiac myocytes. Implications for the autonomic regulation of heart rate.** *J Biol Chem* 1998, **273:**30249-30254.
167. Feron O, Saldana F, Michel JB, Michel T: **The endothelial nitric-oxide synthase-caveolin regulatory cycle.** *J Biol Chem* 1998, **273:**3125-3128.
168. Sterin-Borda L, Echague AV, Leiros CP, Genaro A, Borda E: **Endogenous nitric oxide signalling system and the cardiac muscarinic acetylcholine receptor-inotropic response.** *Br J Pharmacol* 1995, **115:**1525-1531.
169. Ricciardolo FL: **Multiple roles of nitric oxide in the airways.** *Thorax* 2003, **58:**175-182.
170. Matera MG, Calzetta L, Passeri D, Facciolo F, Rendina EA, Page C, Cazzola M, Orlandi A: **Epithelium integrity is crucial for the relaxant activity of brain natriuretic peptide in human isolated bronchi.** *Br J Pharmacol* 2011, **163:**1740-1754.
171. Feron O, Belhassen L, Kobzik L, Smith TW, Kelly RA, Michel T: **Endothelial nitric oxide synthase targeting to caveolae. Specific interactions with caveolin isoforms in cardiac myocytes and endothelial cells.** *J Biol Chem* 1996, **271:**22810-22814.
172. Davalos A, Fernandez-Hernando C, Sowa G, Derakhshan B, Lin MI, Lee JY, Zhao H, Luo R, Colangelo C, Sessa WC: **Quantitative proteomics of caveolin-1-regulated proteins: characterization of polymerase i and transcript release factor/CAVIN-1 IN endothelial cells.** *Mol Cell Proteomics* 2010, **9:**2109-2124.
173. Moffatt JD, Cocks TM, Page CP: **Role of the epithelium and acetylcholine in mediating the contraction to 5-hydroxytryptamine in the mouse isolated trachea.** *Br J Pharmacol* 2004, **141:**1159-1166.

174. Eum SY, Norel X, Lefort J, Labat C, Vargaftig BB, Brink C: **Anaphylactic bronchoconstriction in BP2 mice: interactions between serotonin and acetylcholine.** *Br J Pharmacol* 1999, **126:**312-316.
175. Weigand LA, Myers AC, Meeker S, Undem BJ: **Mast cell-cholinergic nerve interaction in mouse airways.** *J Physiol* 2009, **587:**3355-3362.
176. Krasteva GT, Filip A-M, Kummer W: **Expression of the muscle specific caveolin-isoform, cav-3, in mouse sensory neurons.** *Autonomic Neuroscience: Basic and Clinical*, **135:**69.

8 Declaration

"I declare that I have completed this dissertation single-handedly without the unauthorized help of a second party and only with the assistance acknowledged therein. I have appropriately acknowledged and referenced all text passages that are derived literally from or are based on the content of published or unpublished work of others, and all information that relates to verbal communications. I have abided by the principles of good scientific conduct laid down in the charter of the Justus Liebig University of Giessen in carrying out the investigations described in the dissertation."

Giessen, 2016

_____

Maryam Keshavarz